STUDIA
UNIVERSITATIS BABEȘ-BOLYAI

PHYSICA

2

1989

CLUJ-NAPOCA

ANUL XXXIV 1989

STUDIA
UNIVERSITATIS BABEŞ-BOLYAI

PHYSICA

2

Redacţia: 3400 CLUJ-NAPOCA, str. M. Kogălniceanu, 1 ● Telefon 1 61 01

SUMAR — CONTENTS

STUDIA UNIV BABEŞ–BOLYAI, PHYSICA, XXXIV, 2, 1989

DIELECTRIC PROPERTIES OF SOME RUTILE CERAMIC MATERIALS

AL. NICULA* and LIANA SANDRU**

Received June 6, 1989

ABSTRACT. — By modifying the percentage of ZrO_2 and SnO_2 in rutile ceramic material composition, variation curves $\varepsilon = \varepsilon(f)$ and $\mathrm{tg}\,\delta = \mathrm{tg}\,\delta(f)$ are obtained, and they have a more complicated behaviour because of the relaxation phenomena. The theoretical deductions, greatly doublet by experimental determinations proved the existence of some unique optimum values of the correlation for each sample type.

1. **General Considerations.** Technical literature presents a very wide range of problems destined for the study of a great veriety of ceramic materials beginning with those having a very high strength and finishing with those being the most sensitive to receiving and transmitting electrical signals [1, 4].

High frequency current operation of electronic devices increased the researchers' interest in obtaining new substances having dielectric constants corresponding to the condenser capacitance increase and to other practical property improvement [1, 2, 5, 6, 8].

2. **Experimental Methods.** Ceramic materials with dielectric properties were obtained from synthesis raw materials: oxides (30% TiO_2 rutile, 40.1% TiO_2 anatase, 31% ZrO_2 natural haddeleyite or 31% ZrO_2 synthetic, 13% SnO_2, 3% ZnO), alkaline-earth carbonates ($BaCO_3$) and 8% zettlicz kaolin ($12\,Al_2O_3 \cdot 2\,SiO_4 \cdot 2\,H_2O$). After sample preparation and calcination and sintering treatment, new substances resulted: $BaZrO_3$, $\beta-SiO_2$, $BaTiO_3$, $ZnTiO_3$, $\delta-Al_2O_3$ and $ZrTiO_4$.

By obtaining ceramic samples, it was intended to esetablish the influence of SnO_2 and ZrO_2 on dielectric constant and losses and some technological factors of rutile ceramic material preparation.

The influence of ZrO_2 and SnO_2 on dielectric constant and losses was studied in the following sample versions:

a_M, b_M and C_M respectively a_{1M}, b_{1M} and C_{1N}

a_A, b_A and C_A respectively a_{1A}, b_{1A} and C_{1A}

a_n, b_n and C_n respectively a_{1n}, b_{1n} and C_{1n}

The samples a_M and b_M have a similar composition (the difference is of 2.19% in comparison with TiO_2 rutile and ZrO_2). There are differences between these two samples and the sample C_M of about 11 3% in comparison with ZrO_2 and 13% in comparison with SnO_2

The difference between the samples a, b and C and the samples a_1, b_1 and C_1, both version having n, m and A subscripts, consists of using ZrO_2 n h for the first three versions and ZrO_2 synthetic for the other three versions (n represents uncalcined samples, M — samples ground in porcelain mortar and A — samples ground in agate mortar).

During the sample preparing process, some versions were not calcined and others were calcined to 1 050°C and then thermally treated for sintering to 1.280°C. Samples were worked in accordance with the techniques presented in technical literature [8]. For the measurements destined for the calculations of dielectric constant ε and dielectric losses $\mathrm{tg}\,\delta$, Q-meters were used and their frequency f was modified between 1—30 MHz and 30—135 MHz.

* University of Cluj-Napoca, Department of Physics, 3400 Cluj-Napoca, Romania
** IPG — Ploieşti, Department of PEA, 2000 Ploieşti, Romania

The calculation relations for the experimental results processing, after the measurements of dielectric constant, loss resistance R, quality factor Q and dielectric losses tg δ, were those presented in technical literature [2, 8].

3. Experimental Results Intepretatiron. Using the experimental data obtained after the measurements of the samples mentioned above, Fig. 1 presents the variation curves of constant $\varepsilon = \varepsilon(f)$ for samples a_M, b_M and c_M

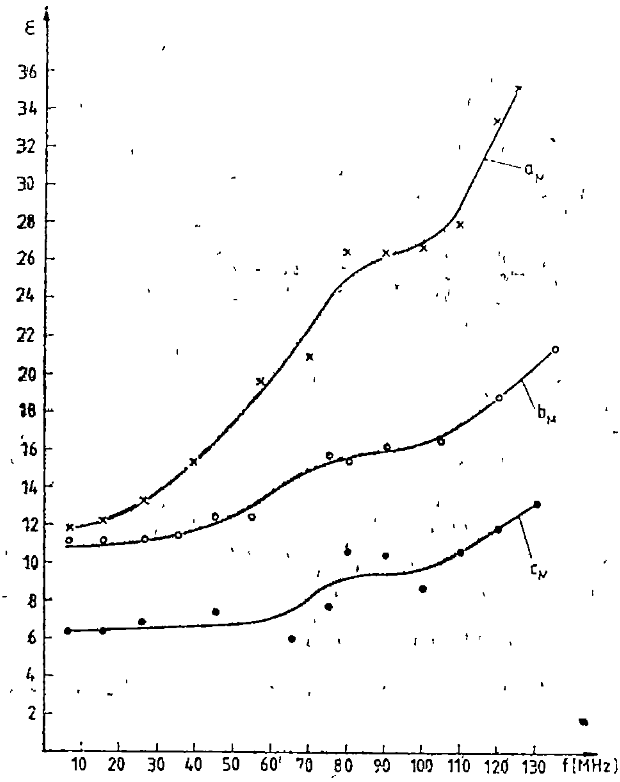

Fig. 1. Variation curves $\varepsilon = \varepsilon(f)$.

In the first group of samples, with M subscripts, both versions have about the same variations of constant $\varepsilon = \varepsilon(f)$. Analysing the shape of curves in Fig. 1, it was established that they represented the cubic polynomial, i.e

$$\varepsilon = A_0 f^3 + A_1 f^2 + A_2 f + A_3$$

Based on the least squares principle, the system of normal equations is written as follows:

$$nA_0 + A_1 \sum_{i=1}^{n} f_i + A_2 \sum_{i=1}^{n} f_i^2 + \ldots + A_m \sum_{i=1}^{n} f_i^m = \sum_{i=1}^{n} f_i$$

$$A_0 \sum_{i=1}^{n} f_i + A_1 \sum_{i=1}^{n} f_i^2 + A_2 \sum_{i=1}^{n} f_i^3 + \ldots + A_m \sum_{i=1}^{n} f_i^{m+1} = \sum_{i=1}^{n} f_i \, i$$

$$A_0 \sum_{i=1}^{n} f_i^2 + A_1 \sum_{i=1}^{n} f_i^3 + A_2 \sum_{i=1}^{n} f_i^4 + \ldots + A_m \sum_{i=1}^{n} f_i^{m+2} = \sum_{i=1}^{n} f_i^2 i \quad (1.1)$$

$$A_0 \sum_{i=1}^{n} f_i^m + A_1 \sum_{i=1}^{n} f_i^{m+1} + A_2 \sum_{i=1}^{n} f_i^{m+2} + \ldots + A_m \sum_{i=1}^{n} f_i^{2m} = \sum_{i=1}^{n} f_i^m i$$

By solving the system of m independent linear equations, the optimum values for the coefficients A_j, $j \in [1, m]$ are determined. As the function *fprm* was arbitrarily considered, the way in which the obtained data reflect the real process is checked.

By solving the system (1 1), the following regression relations were obtained corresponding to samples a_M, b_M, C_M and a_{1M}, b_{M1}, C_{1M}, respectively, i.e

$$\varepsilon_{a_M} = -4.590 \times 10^{-6} f^3 + 1\,29 \times 10^{-3} f^2 + 9\,01 \times 10^{-2} f + 10\,71$$

$$\varepsilon_{b_M} = -1.696 \times 10^{-6} f^3 + 8.53 \times 10^{-4} f^2 - 9.90 \times 10^{-3} f + 11.07$$

$$\varepsilon_{C_M} = 2.154 \times 10^{-6} f^3 + 1\,00 \times 10^{-5} f^2 + 1\,46 \times 10^{-2} f + 6\,24$$

$$\varepsilon_{a_{1M}} = 3\,290 \times 10^{-5} f^3 - 4.76 \times 10^{-3} f^2 + 3\,13 \times 10^{-1} f + 7.41$$

$$\varepsilon_{b_{1M}} = 2.334 \times 10^{-5} f^3 - 3.82 \times 10^{-3} f^2 + 2\,77 \times 10^{-1} f + 7.07$$

$$\varepsilon_{C_{1M}} = 8\,200 \times 10^{-6} f^3 - 9\,47 \times 10^{-4} f^2 + 1\,28 \times 10^{-1} f + 7.34$$

The following conclusions are attained by studying the connecting function variation in Fig 1 between the analysed parameters ($\varepsilon = \varepsilon(f)$):

— The maximum value of curve ε_{a_M} corresponds to frequency $f = 217\,453$ MHz and then, for higher frequencies, the value of the constant decreases;

— The maximum value of curve ε_{b_M} is obtained at a frequency of $f = 329\,391$ MHz and then, at higher frequencyes, the value of the constant decreases,

— At curve ε_{C_M}, it comes out that ε increasingly depends on frequency f, a peak value of the dielectric constant failing to be analitically attained.

It results from the study of the $\varepsilon = \varepsilon(f)$ connecting function variation for samples $\varepsilon_{a_{1M}}$, $\varepsilon_{b_{1M}}$ and $\varepsilon_{C_{1M}}$ that this dependence increases, a peak value of the dielectric constant failing to be analytically attained.

Technical literature [2] explains some phenomena referring to variation $\varepsilon = \varepsilon(f)$ In static field ($\omega = 0$) and for high frequencies ($\omega - \infty$), the dielectric constant is a real value The Debye dispersion relations of the dielectric constant demonstrate that dielectric dispersion occurs within a wide frequency range. In the case of substances whose molecules present, beside electronic relaxation, a phenomenon of bipolar relaxation, a Debye dispersion phenomenon must occur, based on the hypothesis that all the molecules have the same relaxation times, what is not verified in the case of many substances

The description of relaxation phenomena by means of Debye relation is quite simplifying and, consequently, the existence of a continuous distribution of relaxation times within the range $[0, \infty]$ is assumed. In these cases, the mathematical relations for the phenomenon description are quite complicated.

It comes out that the absence of SnO_2 in sample C_M results in decreasing constant ε. Zirconia ZrO_2, during thermal treatment, reduces the tendency to non-stoichiometry of TiO_2. Sample dosage with ZrO_2 results in increasing ceramic material porosity, determining dielectric constant decreasing By increasing the percentage of ZrO_2 n.h. in sample $a_M = 31\%$ to sample $C_M = 40.7\%$, dielectric constant value decreases according to a_M and C_M curve behaviour in Fig. 1.

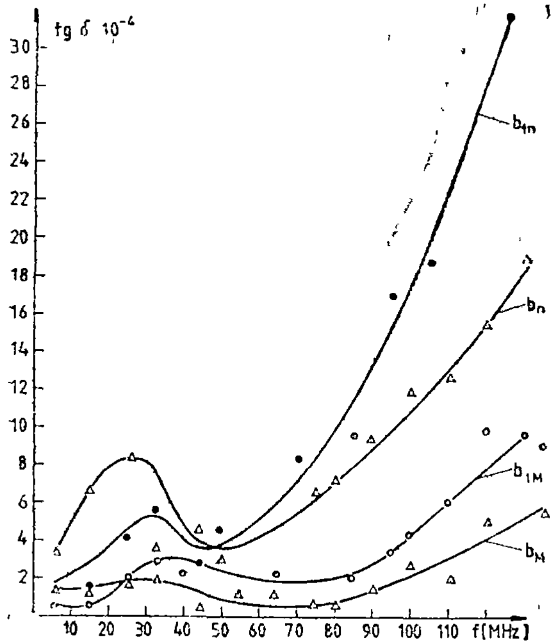

Fig. 2. Variation curves tg δ = tg δ(f).

On the other hand, ZrO_2 contributes to liquid solution formation by isomorph integration of cations Zr^{4+} Sample C_M has a lower dielectric constant value because the quantity of ZrO_2 and SnO_2 is too high.

The experimental results of ZrO_2 influence un rutile ceramic material composition ranges among other researchers' preocupations and results. Thus it is mentioned [7] that, for $BaZrO_3$ ceramic material obtained from $BaCO_3$ and ZrO_2 with an additive of 20% TiO_2, ε is maximum, then it decreases and increases again with an additive of over 30% TiO_2.

The curves $tg\delta = tg\delta(f)$ in Fig 2 have two distinct shapes of them belonging to a certain frequency range If it is written $tg\delta = t$ and the equation system (1 1) is used, for the curves in Fig. 2, the following regression correlations consisting of two parts are obtained·

$$t_{b_{1n}} = -6\,977 \times 10^{-8}f^3 + 4\,719 \times 10^{-6}f^2 - 7.622 \times 10^{-5}f + 4\,48 \times 10^{-4},$$
for $f \in [1,\ 44]$ and
$$4.052 \times 10^{-7}f^2 - 3.560 \times 10^{-5}f + 1\,25 \times 10^{-3}$$
for $f \in [50,\ 125]$

$$t_{b_n} = -6.608 \times 10^{-7}f^2 + 3\,372 \times 10T^{-5}f + 2.27 \times 10^{-7},$$
for $\in [1, 50)$ and
$$6.132 \times 10^{-9}f^3 - 1\,768 \times 10^{-6}f^2 + 1.873 \times 10^{-4}f - 6.05 \times 10^{-3}$$
for $f \in [50, 130]$

$$t_{b_{1M}} = -9.298 \times 10^{-8}f^2 + 1\,041 \times 10^{-5}f - 1.45 \times 10^{-5},$$
for $f \in [1, 85]$ and

$- 5\,585 \times 10^{-8}f^3 + 1.863 \times 10^{-5}f^2 - 2.083 \times 10^{-3}f + 7.37 \times 10^{-2}$ for $f \in [95, 130]$

$$t_{b_M} = \begin{cases} 7.950 \times 10^{-10}f^3 - 1.633 \times 10^{-7}f^2 + 7\,771 \times 10^{-6}f + 7.52 \times 10^{-5} & \text{for } f \in [1^4\ 75] \text{ and} \\ 9.368 \times 10^{-6}f - 7\,02 \times 10^{-4}, & \text{for } f \in [90, 135]. \end{cases}$$

The following conclusions result from the variation analysis of polynomial functions representing the curves in Fig. 2·

— The maximum of the concave curve $t_{b_{1n}}$ within the range $f \in [1, 44]$ is obtained for $f = 34\ 55$ and then it decreases around $f \in [34\ 55\ 43\ 93]$. The minimum of the first part of curve $t_{b_{1n}}$ corresponding to frequency $f = 43.93$ also represents the beginning of the second part of the curve, when the function is convexly increasing.

— The maximum of the concave curve t_{b_n} within the range $f \in [1, 50]$ is obtained for $f = 25\ 51$ MHz. Within the range $f \in [1, 25\ 51]$, the function is increasing, then it decreases within the range $f \in [25\ 51, 50]$ For frequencies exceeding 50 MHz, the function is increasing and convex to frequencies of 130 MHz

— The maximum of the concave curve $t_{b_{1m}}$ within the range $f \in [1, 70]$ is obtained for $f = 53$ MHz Within the range $f \in [1, 53]$, the function is increasing and then it decreases to $f = 85$ MHz For frequencies at which $f \in [85, 130]$, the curve is convexly increasing.

— The maximum of the concave curve t_{b_M} within the range $f \in [1, 75]$, the function is concavely increasing and then it decreases to $f = 75$ MHz. Within the frequency range 75—135 MHz, the function is straightly increasing

It results from the comparative analysis of curves in Fig 2 that the highest dielectric losses occur at curves b_{1n} and then decrease in decreasing order for samples b_n, b_{1m} and b_M.

On the first part of the polynomial functions, the curve behaviour is generally concave, their maximum occurs at frequencies of 34.55, 25 51, 53 and 30.65 MHz. On the latter part, the curve behaviour is convex and increasing.

It results, from the analysis of curve behaviour $\mathrm{tg}\delta \doteq \mathrm{tg}\delta(f)$ for the samples mentioned above, that, within the frequency range of 1 to about 70 MHz, maximum losses are recorded, next they reach a minimum and then dielectric losses increase very much.

The polarization mechanism of the studied ceramic materials differs from the other polarization phenomena because of the possibility of charge migration and accumulation in the polycrystal grain separating layers — interfacial polarization [2, 6].

In the case of a dielectric ceramic material, the difference $\mathrm{tg}\delta = \mathrm{tg}\delta(f)$ is more complicated because the relaxation phenomena depend on the frequency range. Instead of one relaxation time, a series of relaxation times must be used, what complicates the mathematical model

4. Conclusions. The sample composition, whose percentage of ZrO_2 and SnO_2 was modified, influenced the dielectric constant and loss values The absence of SnO_2 in the samples results in decreasing constant ε and ZrO_2 reduces the tendency to non-stoichiometry of TiO_2 during thermal treatments.

Variations $\varepsilon = \varepsilon(f)$ and $tg\delta = tg\delta(f)$ for the studied samples are more complicated because of the relaxation phenomena dependent on the frequency range. The correlations established for dielectric constant and losses demonstrate the correctness of curve tracing and the accuracy of experimental result interpretation.

The theoretical deductions, greatly doublet by experimental determinations, proved the existence of some unique optimum values of the correlation for each sample type The equations used for determining the coefficients A_j to establish polynomials, solved by computer, certify the correlation between experimental results and calculated results.

The dielectric losses for samples having n subscipts are higher than those for samples having M and A subscipts This fact is explained by higher porosity of uncalcined samples

REFERENCES

1. M. Cantogrel, *Amer Ceram. Soc Bull.*, **65**, 9 (1986).
2. Al. Nicula, F. Pușcaș, *Dielectrici și feroelectrici*, Ed. Scrisul Românesc, Craiova, 1982.
3. Al. Nicula, L. Sandru, *Progrese în fizică*, București, 1987.
4. S. Nishigaki, H. Kato, S. Yano, M. Kamimura, *Amer. Ceram Soc Bull*, **66**, 9 (1987).
5. B S. Rawal, M. Kahn, W R. Buessern, *Grain Boundary Phenom. Electron Symp 82-nd Amm. Mact Amer. Ceram Soc. Chicago 1891.*
6. P. Sixon, P Dansas, G Nuzillat, R. Arnoult, *RGE* nr. 4, 1987
7. M. M. Sekkina, D M Nemedu, *Indian. Ceramic*, **29**, 9 (1986)
8. Liana Sandru, *Buletinul I.P.G.*, vol. XXXVII, nr. 1–2, Ploiești.

STUDIA UNIV. BABEŞ–BOLYAI, PHYSICA, XXXIV, 2, 1989

DEDUCTION OF HIGHER ORDER ACCELERATIONS BY THE METHOD OF DIFFERENTIAL OPERATORS

CONSTANTIN TUDOSIE*

Received May 17, 1989

ABSTRACT. — In this paper we give a new method for the deduction of the higher order accelerations, existing in the linear differential equation of order n of very fast dynamical phenomena. The proposed method relies on certain "differential operators" and allows determination of the accelerations of any order $\sigma > n$.

1. **Introduction.** In a series of previously published papers [2], [3], [4], [5], [6], we have developed various methods for the determination of higher order accelerations, which exist or do not exist in the linear or nonlinear differential equations describing very fast dynamical phenomena. These methods rely on certain operators introduced by means of some unknown functions of time as independent variable

In the present paper we give a new method for determining the higher order accelerations by using certain "differential operators".

2. **The method.** Let be the linear differential equation of a very fast dynamical phenomenon

$$\sum_{i=0}^{n} a_i(t) \overset{(i)}{x}(t) = A(t), \tag{1}$$

with the initial conditions $\overset{(i)}{x}(0) = \overset{(i)}{x}_0$, $(i = 0, 1, 2, \ldots, n-1)$. The functions $A(t)$ and a_i, $(i = 0, 1, 2, \ldots, n)$ are continuous having continuous derivatives on $[0, a]$, $a > 0$ and $a_0(t) \neq 0$, $t \in [0, a]$

Introducing the "differential operator"

$$d \overset{(\sigma)}{x}(t), \ (\sigma = 0, 1, 2, \ldots, n+1),$$

and denoting

$$u_i(t) = a_i(t) \overset{(i)}{x}(t), \ (i = 0, 1, 2, \ldots, n), \tag{2}$$

equation (1) becomes

$$\sum_{i=0}^{n} u_i(t) \, d \overset{(\sigma)}{x}(t) = A(t) \, d \overset{(\sigma)}{x}(t), \tag{3}$$

$$(\sigma = 0, 1, 2, \ldots, n+1).$$

* Polytechnic Institute of Cluj-Napoca, 3400 Cluj-Napoca, Romania

Then, by integrating (3) and differentiating (2), it follows

$$
\begin{aligned}
&A(t)\overset{(\sigma)}{x}(t) - A(0)\overset{(\sigma)}{x}_0 - \int_0^t \dot{A}(s)\overset{(\sigma)}{x}(s)ds - \\
&- \sum_{i=0}^{n}\Big\{a_i(t)\cdot\overset{(i)}{x}(t)\cdot\overset{(\sigma)}{x}(t) - a_i(0)\cdot\overset{(i)}{x}_0\cdot\overset{(\sigma)}{x}_0 - \\
&- \int_0^t \overset{(\sigma)}{x}(s)\Big[a_i(s)\cdot\overset{(i)}{x}(s) + a_i(s)\cdot\overset{(i+1)}{x}(s)\Big]ds\Big\} = 0,
\end{aligned}
\tag{4}
$$

$$(\sigma = 0,\ 1,\ 2,\ \ldots,\ n+1)$$

The equations (4) constitute a system (S) of $n+2$ nonlinear integral equations with $n+2$ unknown quantities

$$\overset{(\sigma)}{x}(t),\ (\sigma = 0,\ 1,\ 2,\ \ldots,\ n+1)$$

3 Determination of the solution of the system *(S)* In order to determine the solution of the system (S), we will apply on the interval $[0, a]$, $a > 0$, a method similar to that of polygonal lines [2], [3]

Thus, using the quadrature formula

$$\int_0^{k\frac{a}{m}} f(s)ds \approx \frac{a}{m}\sum_{\nu=1}^{k} f\left(\nu\frac{a}{m}\right),\quad (k = 1,\ 2,\ 3,\ \ldots,\ m),$$

for the approximate evaluation of the integrals, we obtain, on the considered interval, a system of $m(n+2)$ algebraic nonlinear equations with $m(n+2)$ unknown quantities

$$
\begin{aligned}
&A\left(k\frac{a}{m}\right)\overset{(\sigma)}{x}\left(k\frac{a}{m}\right) - A(0)\overset{(\sigma)}{x}_0 - \frac{a}{m}\sum_{\nu=1}^{k}A\left(\nu\frac{a}{m}\right)\overset{(\sigma)}{x}\left(\nu\frac{a}{m}\right) - \\
&- \sum_{i=0}^{n}\Big\{a_i\left(k\frac{a}{m}\right)\cdot\overset{(i)}{x}\left(k\frac{a}{m}\right)\cdot\overset{(\sigma)}{x}\left(k\frac{a}{m}\right) - a_i(0)\cdot\overset{(i)}{x}_0\cdot\overset{(\sigma)}{x}_0 - \\
&- \frac{a}{m}\sum_{\nu=1}^{k}\overset{(\sigma)}{x}\left(\nu\frac{a}{m}\right)\Big[a_i\left(\nu\frac{a}{m}\right)\cdot\overset{(i)}{x}\left(\nu\frac{a}{m}\right) + a_i\left(\nu\frac{a}{m}\right)\overset{(i+1)}{x}\left(\nu\frac{a}{m}\right)\Big]\Big\} = 0,
\end{aligned}
\tag{5}
$$

$$(\sigma = 0,\ 1,\ 2,\ \ldots,\ n+1)$$

The values of the constants $\overset{(n)}{x}_0$ and $\overset{(n+1)}{x}_0$ follow from (1) for $t = 0$, either directly or by derivation

The diagrams of the variation of the variable quantities $\overset{(\sigma)}{x}$, ($\sigma = 0, 1, 2, \ldots, n + 1$), constructed through the points t_k, ($k = \overline{1, m}$), give the graphical approximation of the functions of the system (s), on the considered interval $[0, a]$, $a > 0$

The numerical solution of system (5) can be carried out, using the known methods [1]

The method presented here allows to determine accelerations $\overset{(\sigma)}{x}(t)$, for any $\sigma > n$.

REFERENCES

1 Démidovitch, B, Maron, I *Éléments de calcul numérique*, Éditions Mir, Moscou, 1973.

2 Tudosie, C, *Deduction of higher order accelerations by the method of associated angular velocity*, "Strojnicky Časopis", 34, č 3, pp 337–341, 1983

3 Tudosie, C, *Determination of higher order accelerations by a functional method.*, "Acta Technica", ČSAV, No. 2, pp. 218–224, 1983.

4 Tudosie, C., *A method for calculating the higher order accelerations*, "Mathematica", Tome 25 (48), No. 1, pp 69–74, 1983

5. Tudosie, C., *A method for determining linear accelerations and direct connexion functions of a dynamic system*, pp 61–65.
Determination of higher than second order accelerations by the method of direct connexion functions, pp. 66–70.
Buletinul ştiinţific al Institutului politehnic Cluj-Napoca, Seria Matematică, Mecanică aplicată, Construcţii de maşini, 28, 1985

6 Tudosie, C, On a product-type differential equation. "Babeş–Bolyai" University, Faculty of Mathematics and Physics, Research seminars, Seminar on Differential Equations, Preprint Nr. 8, pp. 37–42, 1988

STUDIA UNIV BABEŞ–BOLYAI, PHYSICA, XXXIV, 2, 1989

COMMENTS UPON THE SOLUTION OF SOME LINEAR AND NONLINEAR DIFFERENTIAL EQUATIONS OF CERTAIN KIND

CONSTANTIN TUDOSIE*

Received. May 8, 1989

ABSTRACT. — In this paper the higher order accelerations are determined for the case when the linear and nonlinear differential equations of certain kind describe phenomena having a very fast evolution In solving the proposed problems one uses linear and nonlinear operators, defined through the so-called "functions of direct or inverse connexion".

1. **Introduction.** By resorting to the so-called "functions of direct and inverse connexion" exhibiting linear operator character, we have developed in a series of previous published papers a method for constructing the solution of certain differential equations whose coefficients are function of time, evaluating in this way at the same time the higher order accelerations [2], [3], [4], [5], [6].

Actually, our aim in what follows is to determine the higher order accelerations, when the linear or nonlinear differential equations of certain kind describe phenomena having a very fast evolution

In solving the proposed problems we use linear and nonlinear operators, introduced — as we had made in the above cited papers — by means of the so-called "functions of direct and inverse connexion"

2 **The linear equation.** We will firstly consider the linear differential equation

$$\sum_{i=1}^{n} a_i(t) \overset{(i)}{x} = A(t), \tag{1}$$

together with the initial conditions $\overset{(i)}{x}(0) = \overset{(i)}{x}_0$, $(i = 1, 2, 3, \ldots, n-1)$, where the functions a_i, $(i = 1, 2, 3, \ldots, n)$ are continuous with continuous derivatives on $[0, a]$, A being also a continuous function of t in the same time interval

By integrating the equation (1), we obtain

$$\sum_{i=1}^{n} \left[a_i(t) \overset{(i-1)}{x}(t) - \int_0^t \overset{(i-1)}{x}(s) \dot{a}_i(s)\, ds \right] = K + \int_0^t A(s)\, ds, \quad K = \sum_{i=1}^{n} a_i(0) \overset{(i-1)}{x_0} \tag{2}$$

Then, the introduction of the so-called "functions of direct connexion" $\omega_{i,\, i-1}(t)$, $(i = 1, 2, \ldots, n)$, [4] leads to the equations

$$\overset{(i)}{x}(t) = \omega_{i,\, i-1}(t) \cdot \overset{(i-1)}{x}(t), \quad (i = 1, 2, 3, \ldots, n) \tag{3}$$

---

* *Polytechnic Institute of Cluj-Napoca, 3400 Cluj-Napoca, Romania*

Now, replacing (3) into (1), it follows

$$\sum_{i=1}^{n} a_i(t)\omega_{i,\,i-1}(t) \cdot \overset{(i-1)}{x}(t) = A(t). \tag{4}$$

Integrating both parts of (3) we get

$$\overset{(i-1)}{x}(t) = \overset{(i-1)}{x_0} \exp\left[\int_0^t \omega_{i,\,i-1}(s)\,ds\right], \tag{5}$$

$$(i = 1,\ 2,\ \ldots,\ n).$$

The equations (2), (3) and (5) constitute a system — denoted by us by (S) — of $2n + 1$ equations with $2n + 1$ unknown quantities

$$x,\ \overset{(i)}{x},\ \omega_{i,\,i-1},\ (i = 1,\ 2,\ \ldots,\ n).$$

3 **Determination of the solution of the system** *(S)*. We apply on the interval $[0,\ a]$, $a > 0$, a similar method to that of polygonal lines.

That is, we apply the following quadrature formula

$$\int_0^{t_k} f(s)\,ds \approx \delta \sum_{\nu=1}^{k} f(\nu\delta),\ \ (k = 1,\ 2,\ \ldots,\ m),$$

$$t_k = k\,\frac{a}{m} = k\delta,$$

in order to obtain an approximate evaluation of the encountered integrals, and we get, on the considered interval a system of $m(2n + 1)$ algebraic equations with $m(2n + 1)$ unknown quantities

$$\left\{\begin{aligned}
&K + \delta \sum_{\nu=1}^{k} A(\nu\delta) - \sum_{i=1}^{n}\left[a_i\,(k\delta) \cdot \overset{(i-1)}{x}(k\delta) - \delta \sum_{\nu=1}^{k} \overset{(i-1)}{x}(\nu\delta)\,\dot{a}_i\,(\nu\delta)\right] = 0,\\
&\overset{(i)}{x}(k\delta) - \omega_{i,\,i-1}(k\delta) \cdot \overset{(i-1)}{x}(k\delta) = 0,\\
&\overset{(i-1)}{x}(k\delta) - \overset{(i-1)}{x_0} \exp\left[\delta \sum_{\nu=1}^{k} \omega_{i,\,i-1}(\nu\delta)\right] = 0,\\
&(i = 1,\ 2,\ \ldots,\ n),\ (k = 1,\ 2,\ \ldots,\ m)
\end{aligned}\right. \tag{6}$$

The constant $\overset{(n)}{x_0}$ follows from (1), if we put there $t = 0$,

$$\overset{(n)}{x_0} = a_n^{-1}(0)\left[A(0) - \sum_{i=1}^{n-1} a_i(0) \cdot \overset{(i)}{x_0}\right]$$

On the other hand the constant values x_0 and $\omega_{i,\,i-1}(0)$, $(i = 1,\ 2,\ \ldots,\ n)$

follow by setting into the equations (3) and (4), $t = 0$, constructing in this way a system of $n + 1$ algebraic equations with $n + 1$ unknown quantities

$$\begin{cases} \overset{(i)}{x_0} - \omega_{i,\,i-1}(0) \cdot \overset{(i-1)}{x_0} = 0, \ (i = 1, 2, \ldots, n), \\ A(0) - \sum\limits_{i=1}^{n} a_i(0) \cdot \omega_{i,\,i-1}(0) \cdot \overset{(i-1)}{x_0} = 0 \end{cases}$$

With the purpose of determining the numerical solutions of system (6), one applies the well known methods [1]. The diagrams illustrating the variation of the functions x, $\overset{(i)}{x}$, $\omega_{i,\,i-1}$, $(i = 1, 2, \ldots, n)$ are constructed using points on the considered interval $[0, a]$, $a > 0$.

We observe, that the equation (2) in the system (S) may be replaced by the equation (4).

4. **The nonlinear equation.** Let be the nonlinear equation

$$\sum_{i=0}^{n} a_i(t) \left[\overset{(i)}{x}\right]^{i+j_i} = A(t), \tag{7}$$

together with the initial conditions $\overset{(i)}{x}(0) = \overset{(i)}{x_0}$, $(i = 0, 1, 2, \ldots, n-1)$, and $j_i \in \{2, 3, 4, \ldots\}$.

By resorting to the "functions of inverse connextion" [4] $\omega_{i,\,i+j_i}(t)$, $(i = 0, 1, 2, \ldots, n)$ we may write down the equations

$$\left[\overset{(i)}{x}\right]^{i+j_i-1} \overset{(i+1)}{x} = \omega_{i,i+j_i}(t), \ (i = 0, 1, 2, \ldots, n), \ j_i \in \{2, 3, 4, \ldots\} \tag{8}$$

Subsequently, multiplying (8) by $(i + j_i)dt$ and integrating afterwards we get

$$\left[\overset{(i)}{x}(t)\right]^{i+j_i} = \left[\overset{(i)}{x_0}\right]^{i+j_i} + (i + j_i) \int_0^t \omega_{i,\,i+j_i}(s)ds, \tag{9}$$

$$(i = 0, 1, 2, \ldots, n), \quad (j_i = 2, 3, 4, \ldots).$$

By substituting (9) into (7), we obtain

$$\sum_{i=0}^{n} a_i(t) \left\{\left[\overset{(i)}{x_0}\right]^{i+j_i} + (i + j_i) \int_0^t \omega_{i,\,i+j_i}(s)\, ds\right\} = A(t), \tag{10}$$

$$(i = 0, 1, 2, \ldots, n), \ (j_i = 2, 3, 4, \ldots)$$

Equations (8), (9) and (10) constitute a system (Q) of $2n + 3$ equations with $2n + 3$ unknown quantities

$$\overset{(i)}{x}, \ \overset{(i+1)}{x}, \ \omega_{i,\,i+j_i}, \ (i = 0, 1, 2, \ldots, n), \ (j_i = 2, 3, 4, \ldots)$$

In order to get a solution of the system (Q) we apply the same method as that we have used to solve system (S).

The constants $\overset{(n)}{x}_0$ and $\overset{(n+1)}{x}_0$ are determined from (7), directly and by derivations, for $t = 0$.

The constants $\omega_{i,i+j_i}(0)$ are determined from (8)

$$\omega_{i,i+j_i}(0) = \left[\overset{(i)}{x}_0\right]^{i+j_i-1} \cdot \overset{(i+1)}{x}_0, \quad (i = 0,\ 1,\ 2,\ \ldots,\ n),$$

$$(j_i = 2,\ 3,\ 4,\ \ldots).$$

5. **The second method.** We will write down now the equation (7) under the following form

$$a_\sigma(t)\left[\overset{(\sigma)}{x}\right]^{\sigma+j_\sigma} + \sum_{i=0}^{\sigma-1} a_i(t)\left[\overset{(i)}{x}\right]^{i+j_i} + \sum_{k=\sigma+1}^{n} a_k(t)\left[\overset{(k)}{x}\right]^{k+j_k} = A(t), \tag{11}$$

where the functions a_i, $(i = 0,\ 1,\ 2,\ \ldots,\ n)$ and A are continuous, with continuous derivatives on $[0,\ a]$, $a > 0$. By introducing the "functions of inverse connexion" for $i < \sigma$, and the "functions of direct connexion" for $k > \sigma$, that is

$$\varepsilon_{i,\sigma+j_\sigma}(t) \text{ and } \varepsilon_{k,\sigma+j_\sigma}(t),$$

$$(i = 0,\ 1,\ 2,\ \ldots,\ \sigma - 1),\ (k = \sigma + 1,\ \sigma + 2,\ \ldots,\ n),$$

we may write the following equations

$$\overset{(i)}{x}(t) = \varepsilon_{i,\sigma+j_\sigma}(t) \cdot \left[\overset{(\sigma)}{x}(t)\right]^{\sigma+j_\sigma}, \quad (i = 0,\ 1,\ 2,\ \ldots,\ \sigma - 1), \tag{12}$$

$$\overset{(k)}{x}(t) = \varepsilon_{k,\sigma+j_\sigma}(t)\left[\overset{(\sigma)}{x}(t)\right]^{\sigma+j_\sigma}, \quad (k = \sigma + 1,\ \sigma + 2,\ \ldots,\ n). \tag{13}$$

By substituting (12) and (13) into (11) we get

$$a_\sigma(t)\left[\overset{(\sigma)}{x}(t)\right]^{\sigma+j_\sigma} + \sum_{i=0}^{\sigma-1} a_i(t)\left\{\varepsilon_{i,\sigma+j_\sigma}(t)\left[\overset{(\sigma)}{x}(t)\right]^{\sigma+j_\sigma}\right\}^{i+j_i} +$$

$$+ \sum_{k=\sigma+1}^{n} a_k(t)\left\{\varepsilon_{k,\sigma+j_\sigma}(t)\left[\overset{(\sigma)}{x}(t)\right]^{\sigma+j_\sigma}\right\}^{k+j_k} = A(t). \tag{14}$$

Then, by resorting to the "functions of inverse connexion" $\varepsilon_{i+1,\sigma+j_\sigma}(t)$, $(i = 0, 1, 2, \ldots, \sigma - 1)$, we way write down the equations

$$\overset{(i+1)}{x}(t) = \varepsilon_{i+1,\sigma+j_\sigma}(t)\left[\overset{(\sigma)}{a}(t)\right]^{\sigma+j_\sigma}, \quad (i = 0, 1, 2, \ldots, \sigma - 1). \tag{15}$$

By integrating (12) and (15) we obtain

$$\overset{(i)}{x}(t) = \overset{(i)}{x}_0 \exp\left\{\int_0 [\varepsilon_{i+1,\sigma+j_\sigma}(s)]\,[\varepsilon_{i,\sigma+j_\sigma}(s)]^{-1}\,ds\right\}, \tag{16}$$

$$(i = 0, 1, 2, \ldots, \sigma - 1)$$

On the other hand, for $k = \sigma + e + 1$, and $k = \sigma + e$, $(e = 1, 2, 3, \ldots, n - \sigma)$, the equations (13) become

$$\overset{(\sigma+e+1)}{x}(t) = \varepsilon_{\sigma+e+1,\sigma+j_\sigma}(t)\left[\overset{(\sigma)}{x}(t)\right]^{\sigma+j_\sigma}, \tag{17}$$

$$\overset{(\sigma+e)}{x}(t) = \varepsilon_{\sigma+e,\sigma+j_\sigma}(t)\left[\overset{(\sigma)}{x}(t)\right]^{\sigma+j_\sigma}, \tag{18}$$

$$(e = 1, 2, 3, \ldots, n - \sigma).$$

Now, integrating (17) and (18), it results

$$\overset{(\sigma+e)}{x}(t) = \overset{(\sigma+e)}{x}_0 \exp\left\{\int_0^t [\varepsilon_{\sigma+e+1,\sigma+j_\sigma}(s)]\,[\varepsilon_{\sigma+e,\sigma+j_\sigma}(s)]^{-1}\,ds\right\}, \tag{19}$$

$$(e = 1, 2, 3, \ldots, n - \sigma).$$

For $k = n + 1$, the equation (13) becomes

$$\overset{(n+1)}{x}(t) = \varepsilon_{n+1,\sigma+j_\sigma}(t)\left[\overset{(\sigma)}{x}(t)\right]^{\sigma+j_\sigma}. \tag{20}$$

We obtain the function $\overset{(n+1)}{x}(t)$ by deriving the equation (11).

The equations (12), (13), (14), (16), (19) and (20) constitute a system (Q_σ) of $2(n + 1)$ equations with $2(n + 1)$ unknown quantities $\overset{(i)}{x}$, $\overset{(\sigma)}{x}$, $\overset{(k)}{x}$, $\varepsilon_{i,\sigma+j_\sigma}$, $\varepsilon_{k,\sigma+j_\sigma}$, $\varepsilon_{n+1,\sigma+j_\sigma}$,

$$(i = 0, 1, 2, \ldots, \sigma - 1), \quad (k = \sigma + 1, \sigma + 2, \ldots, n)$$

The constants $\overset{(n)}{x}_0$ and $\overset{(n+1)}{x}_0$ are determined directly from (7) and by deriving it, then setting $t = 0$

The value of the constants $\varepsilon_{i,\,\sigma+j_\sigma}(0)$, $\varepsilon_{k,\,\sigma+j_\sigma}(0)$ and $\varepsilon_{n+1,\,\sigma+j_\sigma}(0)$ follow from (12), (13) and (20), if we put there $t = 0$,

$$\begin{cases} \varepsilon_{i,\,\sigma+j_\sigma}(0) = \overset{(i)}{x_0} \cdot \left[\overset{(\sigma)}{x_0}\right]^{-(\sigma+j_\sigma)}, \quad \varepsilon_{k,\,\sigma+j_\sigma}(0) = \overset{(k)}{x_0}\left[\overset{(\sigma)}{x_0}\right]^{-(\sigma+j_\sigma)}, \\ \varepsilon_{n+1,\,\sigma+j_\sigma}(0) = \overset{(n+1)}{x_0}\left[\overset{(\sigma)}{x_0}\right]^{-(\sigma+j_\sigma)}, \quad (i = 0,\ 1,\ 2,\ \ldots,\ \sigma - 1), \end{cases}$$

$$(k = \sigma + 1, \quad \sigma + 2, \ \ldots, \ n)$$

The solution of the system (Q_σ) will be obtained by applying the same method as that used to solve the system (S).

REFERENCES

1. Démidovitch, B., Maron, I., *Éléments de calcul numérique*, Éditions Mir, Moscou, 1973.
2. Tudosie, C., *A method for determining linear accelerations and direct connexion functions of a dynamic system*, pp 61–65; *Determination of higher than second order accelerations by the method of direct connexion functions*, pp. 66–70. "Buletinul ştiinţific al Institutului politehnic Cluj-Napoca", Seria. Matematică, Mecanică aplicată, Construcţii de maşini, **28**, 1985.
3. Tudosie, C., *Deduction of higher order accelerations by the method of associated angular velocity*, "Strojnicky Časpois", **34**, č. 3, pp. 337–341, 1983.
4. Tudosie, C., *Determination of higher order accelerations by a functional method*, "Acta Technica", ČSAV, No 2, pp. 218–224, 1983.
5. Tudosie, C., *A method for calculating the higher order accelerations*, "Mathematica", Tome 25 (48), No 1, pp 69–74, 1983.
6. Tudosie, C., *On a product-type differential equation*. "Babeş–Bolyai" University, Faculty of Mathematics and Physics, Research seminars, Seminar on Differential Equations, Preprint Nr. 8, pp 37–42, 1988

STUDIA UNIV BABEŞ—BOLYAI, PHYSICA, XXXIV, 2, 1989

THE INFLUENCE OF CDW (SDW) ON T_c

L. MACARIE*

Received · June 6, 1989

ABSTRACT. — The model of the carriers in CuO_2 layers which are divided into two groups heavy and light holes, is used for a study of the influence of charge density wave, CDW (or of the spin density wave, SDW) on T_c. A calculation of T_c as a function of the excitonic gap W, is made using a phonon mechanism in the Cu—O planes.

1. **Introduction.** In high—T_c superconductors there is a competition between the superconductivity and a structural instability which is generally accompanied by charge density wave (CDW) formation In $BaPb_{1-x}Bi_xO_3$ there is a clear evidence for a CDW formation, but in La_2CuO_4 and $YBa_2Cu_3O_6$, there is evidence for an antiferromagnetic state, which could be a spin density wave (SDW) However, as the doping is varied the antiferromagnetic and superconducting states seem to be anticorrelated low doping favouring the antiferromagnetic, high doping the superconducting state

In a two-dimensional model, considering Cu—O planes, the plane band is a hybridized p—d band The CDW transition can be interpreted as a localization transition of the d-holes More accuratelly, it might be described as the formation of a covalent bond between the Cu and the O Such an interpretation of CDW formation has been discussed by Cohen and Anderson [1] and McMillan [2]. If we base on the papers of Hirsch and Scalapino [3] and Markiewicz [4], we will have that the CDW transition localize the d-holes and opens a gap near the high density of states parts of the Fermi surface ungapped. The holes are separated into two groups associated with high and low density of states regions of the Fermi surface heavy and light holes respectively Only the former are involved in CDW formation, while both can be involved in superconductivity.

The present two hole picture of the Fermi surface is in excellent agreement with recent photoemission experiments [5]

The transition to long range order may not occur at all for $T > T_c$ there may be only short range 2D CDW correlations present An analogous situation occurs in La_2CuO_4, where strong 2D spin density correlations are present for hundreds of degrees above the antiferromagnetic transition [6] This occurs because long range order cannot exist in a strictly 2D system the antiferomagnetic transition is driven by extremely weak interlayer correlations In the present case there is an interesting possibility that the superconductivity itself provides the interlayer correlations which cause the long-range CDW order

2 **Calculation of** T_c Starting from this model described, we can study the influence of CDW or SDW on T_c because the theory can also describe SDW

* University of Cluj-Napoca, Faculty of Mathematics and Physics, 3400 Cluj-Napoca, Romania

formation by a slight modification [7]. We use a Billbro—McMillan (BM) hamiltonian [8] which has already been used to interpret the superconductivity at $BaPb_{1-x}Bi_xO_3$ [9] and La—Sr—Cu—O [10], although, the model would probably overestimate the isotope effect in this material [11] (the model involves a purely phonon-induced pairing interaction). But, to explain the very high T_c's found in Y—Ba—Cu—O or the Tl and Bi compounds it is necessary to add an "excitonic" term H_x, to the BM hamiltonian

The density of states according to the two hole picture can be written

$$\rho(\varepsilon) = \begin{cases} \rho_1(\varepsilon) = N_1 \ln \frac{t_0}{\varepsilon}, \; N_1 = \frac{2}{\pi t_0 V_0}, & \text{associated with the heavy holes } (V_0 \text{ is the unit cell volume}) \\ \rho_2(\varepsilon) \cong N_2, & \text{associated with the light holes (away from the van Hove singularity)} \end{cases} \tag{1}$$

where $t_0 = \frac{E_B}{8}$ and E_B is the full band width

For a prevailing phonon mechanism ($H_x = 0$), the calculations from a BM hamiltonian lead to the superconducting gap Δ equation which can be written

$$\Delta = V_{BCS} \int_{-\omega_0}^{\omega_0} d\varepsilon \; \rho_1(\varepsilon) \frac{\Delta}{2\sqrt{\varepsilon^2 + \Delta^2 + w^2}} th \frac{\sqrt{\varepsilon^2 + \Delta^2 + w^2}}{2T} +$$

$$+ V_{BCS} \int_{-\omega_0}^{\omega_0} d\varepsilon \; \rho_2(\varepsilon) \frac{\Delta}{2\sqrt{\varepsilon^2 + \Delta^2}} th \frac{\sqrt{\varepsilon^2 + \Delta^2}}{2T} \tag{2}$$

where W is the excitonic gap, ω_0 is the BCS cutoff, V_{BCS} is the BCS attractive interaction.

The critical temperature T_c will be obtained from (2) taking $\Delta(T_c) = 0$ and the equation for T_c becomes

$$1 = V_{BCS} \int_0^{\omega_0} \frac{d\varepsilon \; \rho_1(\varepsilon)}{\sqrt{\varepsilon^2 + w^2}} th \frac{\sqrt{\varepsilon^2 + w^2}}{2T_c} + V_{BCS} \int_0^{\omega_0} \frac{\rho_2(\varepsilon)}{\varepsilon} th \frac{\varepsilon}{2T_c} d\varepsilon \tag{3}$$

Using the substitution $\varepsilon = \sqrt{y^2 - w^2}$ and the approximation $\frac{w^2}{y^2} \ll 1$, the first integral becomes

$$I_1 = \frac{1}{2} \int_W^{\sqrt{\omega_0^2 + W^2}} \frac{dy}{y} \left[\ln \left| \frac{t_0}{y + w} \right| + \ln \left| \frac{t_0}{y - w} \right| \right] th \frac{y}{2T_c} \tag{4}$$

If we introduce the notation : $x = \beta_c y$, where $\beta_c = \frac{1}{2T_c}$ and using the approximation $\beta W \to 0$, I_1 becomes :

$$I_1 = \int_{\beta_c W}^{\beta_c \sqrt{\omega_0^2+W^2}} \frac{dx}{x} \ln \beta_c t_0 \cdot thx - \int_{\beta_c W}^{\beta_c \sqrt{\omega_0^2+W^2}} \frac{dx}{x} \ln |x| \cdot thx \cong$$

$$\cong \ln \beta_c t_0 \cdot \ln \left(\beta_c \sqrt{\omega_0^2 + W^2}\right) + \alpha \ln \beta_c t_0 \tag{5}$$

where $\alpha = -\int_0^{\omega_0} \frac{\ln x}{ch^2 x} dx \cong 0\,818$ (the well-known integral from BCS theory)

In the same approximation, the second integral from (3) becomes :

$$I_2 = \int_0^{\omega_0} \frac{th \frac{\varepsilon}{2T_c}}{\varepsilon} d\varepsilon \cong \ln \left(\beta_c \sqrt{\omega_0^2 + w^2}\right) + \alpha \tag{6}$$

Eq. (5) can be transformed if we use an approximation for t_0 :

$$t_0 \simeq 10 \sqrt{\omega_0^2 + W^2}$$

The number before the square root results from the condition :

$$\lim_{W \to 0} t_0 \simeq 10\omega_0 \text{ because } t_0 \simeq 0\,5 \text{ eV}, \quad \omega_0 \simeq 0\,05 \text{ eV}$$

And eq (5) becomes :

$$I_1 \cong \ln^2 \left(\beta_c \sqrt{\omega_0^2 + W^2}\right) + (2 + \alpha) \ln \left(\beta_c \sqrt{\omega_0^2 + W^2}\right) + 2\alpha \tag{7}$$

Using the notation $\bar{N}_1 = N_1 \cdot V_{BCS}$

$$\bar{N}_2 = N_2 \cdot V_{BCS} \text{ and } X = \ln \left(\beta_c \sqrt{\omega_0^2 + W^2}\right)$$

and the Eq (6—7), we obtain from Eq (3)

$$\bar{N}_1 X^2 + X[\bar{N}_2 + \bar{N}_1(2 + \alpha)] + [\alpha \bar{N}_2 + 2\alpha \bar{N}_1 - 1] = 0 \tag{8}$$

From the solution $X^{\min}$ of this equation, we obtain the expression for T_c :

$$T_c \cong 0{,}50 \sqrt{\omega_0^2 + W^2} \exp \left\{ -\frac{\bar{N}_2 + \bar{N}_1(2 + \alpha)}{2\bar{N}_1} \left[1 - \frac{4\bar{N}_1(\alpha\bar{N}_2 + 2\alpha\bar{N}_1 - 1)}{[\bar{N}_2 + \bar{N}_1(2 + \alpha)]^2}\right]^{1/2} + \right.$$

$$\left. + \frac{\bar{N}_2 + \bar{N}_1(2 + \alpha)}{2\bar{N}_1} \right\} \tag{9}$$

This general form for T is hard to be interpreted. Anyhow, we can see that the presence of CDW (SDW) modifies T_c.

3 **Discussion.** We shall interpret the relation for T_c in a particular case: a) at the van Hove singularity, when CDW is absent $(W = 0)$:

$$T_c \cong 1\ 13\ \omega_0 \exp\left(-\frac{1}{\sqrt{\bar{N}_1}}\right) \tag{10}$$

b) when the CDW transition has occured, at the van Hove singularity $\bar{N}_2 = 0$) and:

$$T_c \cong 0\ 50 \sqrt{\omega_0^2 + W^2} \exp\left(-\frac{1}{\sqrt{\bar{N}_1}}\right) \tag{11}$$

where

$$\bar{N}_1 \cong \frac{1}{5\pi\ V_0} \cdot V_{BCS} \cdot \frac{1}{\sqrt{\omega_0^2 + W^2}} \tag{12}$$

Introducing (12) in (11) results:

$$T_c \cong 0\ 50 \sqrt{\omega_0^2 + W^2} \exp\left[-\frac{(\omega_0^2 + W^2)^{1/4}}{\sqrt{\frac{1}{5\pi V_0} \cdot V_{BCS}}}\right] \tag{13}$$

We see that, T_c decreases in the case $W = 0$ because the exponential term varies stronger than the factor $\sqrt{\omega_0^2 + W^2}$

4. **Conclusions.** Therefore, there is a competition between superconductivity and CDW or SDW transition. If CDW (SDW) transition does not occur, a superconducting transition can take place at a higher T_c, which could be explained by the large total density of states Once the CDW sets in, it opens a gap W for the heavy holes and the total density of states will be reduced As we can see from Eq (13), T_c will decrease according to reality

This model could be applied for the high$-T_c$ superconductors but we must take into considerations the contributions of the other parts of the systems, too (not only Cu—O planes) and the interactions between them In the same time, in Y—Ba—Cu—O or the Tl and Bi compounds it is necessary to take $H_x \neq 0$.

REFERENCES

1 M L Cohen, P W Anderson, *Superconductivity in d- and f-Band Metals*, (N Y 1972) p. 17

2 W L McMillan, *Phys Rev* **B 16**, 643 (1977)

3 J E Hirsch, D J Scalapino, *Phys Rev Lett*, **56**, 2732 (1986)

4 R S Markiewicz (preprint 1988).

5. Z. X Shen, K W Allen, J J Yeh, J S. Kong, W Ellis, W. Spicer, I. Lindau, M. B Maple, Y D Dalichaouch, M S. Torikachvili, J Z. Sun, T H Geballe, *Phys. Rev*, **B 36**, 8414 (1987).
6. G. Shirane, Y. Endoh, R J Birgeneau, M A Kastner, Y Hidaka, M. Oda, M Suzuki, T Murakami, *Phys. Rev Lett*, **59**, 1613 (1987)
7. A. M Gabovich, A S Shpigel, *J Phys*, **F 14**, 3031 (1984).
8. G. Bilbro, W. L McMillan, *Phys Rev*, **B 14**, 1887 (1976)
9. A M Gabovich, D. P. Moiseev, A S Shpigel, *J. Phys*, **C 15**, 1569 (1982).
10. T. H. Choy, H X He, *Phys Rev.*, **B 36**, 8807 (1987)
11. B. Batlogg, G Kourouklis, W Weber, R J Cava, A Jayaraman, A E. White, K. T Shon, L. W Rupp, E. A Rietman, *Phys Rev Lett*, **59**, 912 (1987).

STUDIA UNIV BABEŞ–BOLYAI, PHYSICA, XXXIV, 2, 1989

PARAMETRIC OSCILLATIONS OF A MAGNETIZED PLASMA IN AN ELLIPTICALLY POLARIZED ELECTRIC FIELD

S. COLDEA* and J. KARACSONY*

Received. July 4, 1989

ABSTRACT. — The parametric instabilities of a magnetized two-component cold plasma are studied in a left hand polarized electric field and in a hybrid pump field, by applying a method based on multitime scale perturbation. The growth rates of instabilities are calculated for the dipole approximation.

1. Introduction. Parametric excitation of plasma waves intensively studied [1], [2], [3]. The growing interest for this problem is due to the applications in fusion experiments, pulsar electrodynamics, propagation of electromagnetic waves in ionosphere and other applications In the present paper, by applying a previously given method [4], we will study the parametric action of a left-hand elliptically polarized electric field on a magnetized plasma. The parametric oscillations of magnetized plasma in a right hand elliptically polarized field was also studied [5]

On the other hand the linear and nonlinear stage of the parametric effects due to an extraordinary electromagnetic pump field is studied in [6], [7]; in the framework of nonlinear relativistic theory it is found that parametric instabilities due to interaction of four elliptically polarized electromagnetic transvers waves can occur

By using the propagation equation

$$\left(\text{grad div} - \nabla^2 + \frac{1}{c^2}\frac{\partial_2}{\partial t^2}\right) E_{\text{ext}} = -\frac{4\pi}{c^2}\frac{\partial \vec{j}}{\partial t} \tag{1.1}$$

and the motion equations

$$\frac{d\vec{v}}{dt} = -\frac{e}{m}\vec{E}_{\text{ext}} - \frac{e}{mc}[\vec{v}\ \vec{H}] \tag{1.2}$$

we have arrived for the pump field, which propagates in the same direction as the externally imposed magnetic field, to the expressions

$$\vec{E}_{\text{ext}} = Re\left\{(E_{oy}\vec{e}_2 - iE_{oz}\vec{e}_3)\exp[i(k_r x - \nu t)]\right\} \tag{1 3a}$$

$$\vec{H}_{\text{ext}} = \vec{e}_1\ H_0 \tag{1 3b}$$

* *University of Cluj-Napoca, Faculty of Mathematics and Physics, 3400 Cluj-Napoca, Romania*

at the following algebraic system for the electric field amplitudes:

$$E_{oy}\left[c^2k_0^2 - \nu^2 + \omega_0^2 \frac{\nu^2}{\nu^2 - \Omega^2} + E_{oz}\,\omega_0^2 \frac{\nu\Omega}{\nu^2 - \Omega^2}\right] = 0 \tag{1.4a}$$

$$E_{oy}\omega_0^2 \frac{\nu\Omega}{\nu^2 - \Omega^2} + E_{oz}\left[c^2k_0^2 - \nu^2 + \omega_0^2 \frac{\nu^2}{\nu^2 - \Omega^2}\right] = 0 \tag{1.4b}$$

where

$$\omega_0^2 = \frac{4\pi n_0 e^2}{m} \tag{1.5}$$

represents the square of the plasma frequency, n_0 is the electron density and e and m represents the electron charge and mass.

On the other hand the electron cyclotron frequency is

$$\Omega = e\,H_0/mc \tag{1.6}$$

c being the light velocity

Following the usual method, from (1 4) we can obtain the dispersion relation for the externally imposed field (1 3):

$$c^2k_0^2 - \nu^2 + \frac{\omega_0^2\nu}{\nu - \Omega} = 0 \tag{1.7}$$

which is identical with that obtained in an other paper [4] for circular polarized field

2. **The zero order state.** Here we will neglect the spatial variation of the pump field and consider only the time variation of this field:

$$\vec{E}_{\text{ext}} \cong \vec{e}_2 \cdot E_{oy}\cos\nu t - \vec{e}_3 \cdot E_{oz}\sin\nu t \tag{2.1}$$

If we liniarize the Boltzmann—Vlasov equation we will obtain

$$\frac{\partial f_0}{\partial t} + \left(-\frac{eE_{oy}}{m}\cos\nu t - \frac{eH_0}{mc}v_z\right)\frac{\partial f_0}{\partial v_y} + \left(\frac{eE_{oz}}{m}\sin\nu t + \frac{eH_0}{mc}v_y\right)\cdot\frac{\partial f_0}{\partial v_z} = 0 \tag{2.2}$$

The equation for the characteristics are, therefore, the following.

$$\frac{dt}{1} = \frac{dv_x}{0} = \frac{dv_y}{-\frac{eE_{oy}}{m}\cos\nu t - \Omega v_z} = \tag{2.3a}$$

$$= \frac{dv_z}{\frac{eE_{oz}}{m}\sin\nu t + \Omega v_y} \tag{2.3b}$$

From the equations (2 3) we obtain that

$$v_x = A_1\,; \quad \frac{dv_y}{dt} = -\frac{eE_{oy}}{m}\cos\nu t - \Omega\, v_z\,; \tag{2.4a}$$

$$\frac{dv_z}{dt} = \frac{eE_{oz}}{m}\sin\nu t + \Omega\, v_y \tag{2 4b}$$

$$(v_y(t) + i v_z(t))\exp(-i\,\Omega\, t) = -\frac{eE_{oy}}{2m}\left[\left(\frac{e^{i(\nu+\Omega)t}}{i(\nu-\Omega)} - \frac{1}{i(\nu-\Omega)}\right) + \right.$$

$$+\frac{e^{-i(\nu+\Omega)t}}{i(\nu+\Omega)} + \frac{1}{i(\nu+\Omega)}\Bigg] + \frac{eE_{oz}}{2m}\left[\frac{e^{i(\nu-\Omega)t}}{i(\nu-\Omega)} - \frac{1}{i(\nu-\Omega)} + \right.$$

$$\left. + \frac{e^{-i(\nu+\Omega)t}}{i(\nu+\Omega)} - \frac{1}{i(\nu+\Omega)}\right] + v_y(0) + i v_z(0) \tag{2.4c}$$

where $v_x(0)$, $v_y(0)$ and $v_z(0)$ are the velocity components at $t = 0$. The general solution of Eq (2 2) may be written as

$$f_0 = F(A_1,\ A_2,\ A_3) \tag{2.5}$$

where F denotes an arbitrary functional relation A_1, A_2 and A_3 are the constants of integration given by (2 4) and

$$A_2 = v_y(0) \tag{2 6a}$$

$$A_3 = v_z(0) - \frac{eE_{oy}}{2m}\left(\frac{1}{\nu-\Omega} - \frac{1}{\nu+\Omega}\right) + \frac{eE_{oz}}{2m}\left(\frac{1}{\nu-\Omega} + \frac{1}{\nu+\Omega}\right) \tag{2 6b}$$

One can see from (2.4) and (2 6) that A_1, A_2 and A_3 are related to $v_x(0)$, $v_y(0)$ for a particular orbit

On the other hand (2 4) gives the velocity of a particle on the unperturbed orbit

$$\vec{v}(t) = \vec{V}(t) + \vec{U}(t) \tag{2.7}$$

where

$$\vec{V}(t) = \vec{e}_1 v_x(0) + \vec{e}_2\{v_y(0)\cos\Omega\, t - v_z(0)\sin\Omega\, t\} +$$

$$+ \vec{e}_3\{v_z(0)\cdot\cos\Omega\, t + v_y(0)\cdot\sin(\Omega\, t)\}$$

$$\vec{U}(t) = -\vec{e}_2\,\frac{eE_{oy}}{2m}\sin\nu t\left(\frac{1}{\nu-\Omega} + \frac{1}{\nu+\Omega}\right) + \vec{e}_2\,\frac{eE_{oz}}{2m}\sin\nu t\,\cdot$$

$$\cdot\left(\frac{1}{\nu-\Omega}+\frac{1}{\nu+\Omega}\right)+\vec{e}_3\frac{eE_{oz}}{2m}\cos\nu t\left(-\frac{1}{\nu-\Omega}+\frac{1}{\nu+\Omega}+\right.$$

$$+\vec{e}_2\cdot\frac{eE_{oy}}{2m}\sin\Omega t\left(\frac{1}{\nu-\Omega}-\frac{1}{\nu+\Omega}\right)+\vec{e}_2\frac{eE_{oz}}{2m}\sin\Omega t\cdot$$

$$\cdot\left(-\frac{1}{\nu-\Omega}-\frac{1}{\nu+\Omega}\right)-\vec{e}_3\frac{eE_{oy}}{2m}\cos\Omega t\left(\frac{1}{\nu-\Omega}+\frac{1}{\nu+\Omega}\right)+$$

$$+\vec{e}_3\frac{eE_{oz}}{2m}\cos\Omega t\cdot\left(\frac{1}{\nu-\Omega}+\frac{1}{\nu+\Omega}\right)=\vec{v}^{(0)\nu}+\vec{V}^{(0)\Omega} \qquad (2.7')$$

For the distribution function we choose f_0 to be Maxwellien in velocity space

$$f_0(\vec{v},t)=\frac{n_0}{(2\pi\theta)^{3/2}}\exp\sqrt{\left\{\frac{A_1^2+A_2^2+\left[A_3+\frac{eE_{oy}}{2m}\left(\frac{1}{\nu-\Omega}-\frac{1}{\nu+\Omega}\right)+\right.}{2\theta}\right.}$$

$$\left.\frac{\frac{eE_{oz}}{2m}\left(-\frac{1}{\nu-\Omega}-\frac{1}{\nu+\Omega}\right)^2}{2\theta}\right\}=\frac{n_0}{(2\pi\theta)^{3/2}}\exp\left(-\frac{(\vec{v}-\vec{U}(t))^2}{2\theta}\right) \qquad (2.8)$$

θ beeing the kinetic temperature of the plasma As it was mentioned in [4] we need the zero order external current in view of the full description of the time dependent zero order state. We arrive at the following result

$$-4\pi\,\vec{j}_{ext}=\nu(-E_{oy}\vec{e}_2\sin\nu t-\vec{e}_3E_{oz}\cos\nu t)-\omega_0^2\left\{-\frac{1}{2}\vec{e}_2E_{oy}\sin\nu t\right.$$

$$\cdot\left(\frac{1}{\nu-\Omega}+\frac{1}{\nu+\Omega}\right)+\vec{e}_2\frac{E_{oz}}{2}\sin\nu t\cdot\left(\frac{1}{\nu-\Omega}-\frac{1}{\nu+\Omega}\right)-\vec{e}_3\cdot\frac{E_{oy}}{2}\cos\nu t\cdot$$

$$\cdot\left(-\frac{1}{\nu-\Omega}+\frac{1}{\nu+\Omega}\right)+\vec{e}_3\cos\nu t\frac{E_{oz}}{2}\cdot\left(-\frac{1}{\nu-\Omega}-\frac{1}{\nu+\Omega}\right)+$$

$$+\vec{e}_2\sin\Omega t\frac{E_{oy}}{2}\left(\frac{1}{\nu-\Omega}-\frac{1}{\nu+\Omega}\right)+\vec{e}_2\sin\Omega t\cdot\frac{E_{oz}}{2}\left(-\frac{1}{\nu-\Omega}-\right.$$

$$\left.-\frac{1}{\nu+\Omega}\right)-\vec{e}_3\cos\Omega t\frac{E_{oz}}{2}\left(-\frac{1}{\nu-\Omega}-\frac{1}{\nu+\Omega}\right)-\vec{e}_3\cos\Omega t\cdot\frac{E_{oy}}{2}\cdot$$

$$\cdot\left(\frac{1}{\nu-\Omega}-\frac{1}{\nu+\Omega}\right)=-4\pi\,j_{ext}^{(0)\nu}-4\pi\,j_{ext}^{(0)\Omega} \qquad (2.9)$$

3. **The first-order state.** The first order distribution function f_1 and the electric and magnetic fields $\vec{E}_1$ and $\vec{H}_1$ determine the first order state. The Boltzmann—Vlasov equation with collision relaxation term is

$$\left(\frac{\partial f}{\partial t}\right)_s = -\nu_s \cdot f_1 \tag{3.1}$$

together with Maxwell equations give for f_1 the result

$$f_1(v, x, t) = \frac{ek_0 t}{m\theta(2\pi\theta)^{3/2}} \exp\left(-\frac{v^2(0)}{2\theta}\right) \cdot \left\{E^x_{mn} \cdot \frac{v_x(0)\exp(-i(m, n)t)}{kv_x(0) - (m, n, \nu_s)} + \right.$$

$$+ E^{(+)}_{mn}\left[\frac{v^{(-)}(0) \cdot \exp(-i(m+1, n)t)}{kv_x(0) - (m+1, n, \nu_s)} + \frac{i\nu v_x(0)}{(m, n)}\left[(\varepsilon^+_y + \varepsilon^+_x) \cdot \right.\right.$$

$$\cdot \frac{\exp(-i(m, n-1)t)}{kv_x(0) - (m, n-1, \nu_s)} - (\varepsilon^-_y + \varepsilon^+_y - \varepsilon^-_x + \varepsilon^+_x)\frac{\exp(-i(m+1, n)t)}{kv_x(0) - (m+1, n, \nu_s)} -$$

$$\left.\left.\left. - (-\varepsilon^-_y - \varepsilon^-_x) \cdot \frac{\exp(-i(m, n+1)t)}{kv_x(0) - (m, n+1, \nu_s)}\right]\right]\right\} + E^{(-)}_{mn}\left[\frac{v^{(+)}(0)\exp(-i(m-1, n)t)}{kv_x(0) - (m-1, n, \nu_s)} - \right.$$

$$- \frac{i\nu v_x(0)}{(m, n)}\left[(\varepsilon^+_y + \varepsilon^+_x)\frac{\exp(-i(m, n+1, t))}{kv_x(0) - (m, n+1, \nu_s)} + (-\varepsilon^-_y - \varepsilon^+_y + \varepsilon^-_x - \varepsilon^+_x) \cdot \right.$$

$$\left.\left. \cdot \frac{\exp(-i(m-1, n)t))}{kv_x(0) - (m-1, n, \nu_s)} + (\varepsilon^-_y - \varepsilon^+_x) \cdot \frac{\exp(-i(m, n-1)t)}{kv_x(0) - (m, n-1, \nu_s)}\right]\right]$$

where the assumption

$$\vec{E}_1(x, t) = \exp[i(kx - \omega t)] \sum_m \sum_n E_{mn}(x)\{\exp - i(m\Omega + n\nu)t\} \tag{3 3}$$

was made.

The following notations were introduced in eq. (3 3)

$$E^y_{mn} \pm iE^z_{mn} = E^{(+),(-)}_{mn}; \quad v_y(0) \pm iv_z(0) = 2v^{(+),(-)}(0) \tag{3 4a}$$

$$(m, n) = \omega + m\Omega + n\nu; \quad (m, n, \nu_s) = (m, n) + i\nu_s; \tag{3 4b}$$

$$E^{\pm}_{y,z} = \frac{ekE_{0y,z}}{4m\nu(\Omega \pm \nu)} \tag{3 4c}$$

Using the propagation equation for E^x_{mn}, $E^{(+)}_{mn}$, and $E^{(-)}_{mn}$, and taking into account the first order current density, we obtain an infinite algebraic system in which the transverse and longitudinal components of the electric field are coupled.

4 **The dispersion equation and discussion.** If we follow the method of [4] we can obtain the dispersion relations for $E^{\pm}_{mn}$ up to ϵ_s^2

$$c^2k^2 - p^2 + \frac{\omega_0^2 p}{p \pm \Omega} - i\,\omega_0^2 \frac{p}{p \pm \Omega}\left(\frac{\nu_c}{p \pm \Omega} + f(p \pm \Omega)\right) +$$

$$+ 2\nu^2\omega_0^2(\varepsilon_y^- + \varepsilon_y^+ - \varepsilon_z^- + \varepsilon_z^+)^2 \cdot \left[(p \pm \Omega)^2 - \omega_0^2 + i\omega_0^2 \cdot \left(\frac{\nu_c}{p \pm \Omega} + \frac{(p \pm \Omega)^2}{k^2\theta} +\right.\right.$$

$$\left.\left. + (p \pm \Omega)\right)\right] + 2(\varepsilon_y^+ + \varepsilon_z^+)^2\nu^2\omega_0^2 \cdot \left[\frac{(p \mp \nu)^2}{k^2} - \omega_0^2 + i\omega_0^2\left(\frac{\nu_c}{p \mp \nu} + \frac{(p \mp \nu)^2}{2\theta} \cdot\right.\right.$$

$$\left.\left. \cdot f(p \pm \nu)\right)\right]^{-1} + 2(\varepsilon_y^- - \varepsilon_z^-)^2\nu^2\omega_0^2\left[\frac{(p \pm \nu)^2}{2k^2} - \omega_0^2 + i\,\omega_0^2\left(\frac{\nu_c}{p \pm \nu} +\right.\right.$$

$$\left.\left. + \frac{(p \pm \nu)^2}{2\theta} f(p \pm \nu)\right)\right]^{-1} = 0 \tag{4.1}$$

with $p = (m, n)$ and

$$f(p) = \frac{\pi^{1/2} p}{k(2\theta)^{1/2}} \exp\left(-\frac{p^2}{2k^2\theta}\right) \tag{4.2}$$

The instability can occur for left hand polarized wave with frequency $\Omega - \omega_0$, and with the growth rate of the following form

$$\gamma_i = \frac{1}{2}\left\{\left[\frac{4(\varepsilon_y^- + \varepsilon_y^+ - \varepsilon_z^- + \varepsilon_z^+)^2\nu^2\omega_0}{a} + \left(d - \frac{b}{a}\right)^2\right]^{1/2} - (d + b/a)\right\} \tag{4.3}$$

The following notations were used:

$$a = 3\Omega - 2\omega_0 \tag{4.4a}$$

$$b = \omega_0(\Omega - \omega_0)\left(\frac{\nu_c}{\omega_0} + f(\omega_0)\right) \tag{4.4b}$$

$$d = \frac{\omega_0}{2}\left(\frac{\nu_c}{\omega_0} + \frac{\omega_0^2}{k^2\theta} f(\omega_0)\right) \tag{4.4c}$$

On the other hand the threshold condition is

$$(\varepsilon_y^- + \varepsilon_y^+ - \varepsilon_z^- + \varepsilon_z^+)^2\nu^2\omega_0 > bd \tag{4.5}$$

If the following inequalities are fulfilled

$$\frac{\sqrt{bd}\,|\,\Omega^2 - \nu^2\,|\,2m}{ek\sqrt{\omega_0}\,\cdot} < E_{oy} < \frac{\sqrt{bd}\,|\,\Omega^2 - \nu^2\,|\,2m}{ek\sqrt{\omega_0}\,\cdot} + \frac{\nu}{\Omega} E_{ox_1} \tag{4.6}$$

$$0 < E_{ox} < E_{ox_2} \tag{4.7}$$

where

$$E_{os_2} = 2\,\frac{\sqrt{bd}\cdot m}{ek\sqrt{\omega_0}}\,\frac{(\Omega+\nu)}{\Omega}\,\frac{\Omega^2}{\Omega^2+\nu^2}\left[-\frac{\nu}{\Omega}\,|\nu-\Omega|+\Omega+\nu\right] \tag{4.8}$$

with

$$\nu > \Omega > \left(\sqrt{2}-1\right) \text{ or } \Omega > \nu \tag{4.8'}$$

the power of the threshold field of the elliptic polarized pump field is less than the power of the circular polarized pump field. The conditions for dipol approximation are, respectivelly, for left-hand response field with frequency $\Omega - \omega_0$ and $\nu - \omega_0$, the following:

$$1 - \frac{y^2}{1-x} \ll [(x-y)^2 + y(x-y)] \tag{4.9}$$

$$1 - \frac{y^2}{1-x} \ll \left[(1-y)^2 - \frac{y^2(1-y)}{1-x-y}\right] \tag{4.10}$$

and for the right hand response field

$$1 - \frac{y^2}{1-x} \ll \left[(x-y)^2 - \frac{y^2(x-y)}{2x-y}\right] \tag{4.11}$$

and

$$1 - \frac{y^2}{1-x} \ll \left[(1-y)^2 - \frac{y^2(1-y)}{1-x+y}\right] \tag{4.12}$$

$$\text{with } x = \Omega/\nu \text{ and } y = \omega_c/\nu \tag{4.13}$$

In our discussion we have generalized the grafical conditions from [4], for the case $y = 0.8$, giving more general analitical cerditions (4.9), (4.10), (12) and (4.13)

We can conclude the following The analysis from [4], for parametric oscillations of a magnetized plasma is generalized in this paper, taking into account a left-hand eliptically polarized pump electric field. The dispersion relation for response fields contains four small parameters which depend on amplitudes of pump fields instead of a single parameter used in the case of circular polarized field It is found that there are cases in which the power of the elliptically polarized pump field which assumes the onset of the instability is less than the power for circularly polarized pump field. We have obtained the analitical conditions for spatial cmcgcneity of the pump field [8]

REFERENCES

1. C. S. Liu, V. K. Tripathi, *Physics Reports*, **130**, 143 (1986).
2. M. Porkolab, *Nuclear Fusion*, **18**, 367 (1978)
3. V. P. Silin, *Parametriceskoe vozdeistvie izlucenija bolshoi moschinosti na plazmu*, Izdatelstvo Nauka, Moskva, 1973; Y. A. Aliev, V. P. Silin, *Zh. Exp. Teor. Fiz.*, **48**, 901 (1965).
4. R. Prasad, *Phys. Fluids*, **13** nr. 11, 1310 (1970); *Phys. Fluids*, **11**, 1768 (1968).
5. C. Băleanu, în "Probleme actuale de fizică", Coord. I. Ardelean, Univ. Cluj-Napoca, vol VI, p. 117 (1986).
6. B. Chakriborty, *Phys. Rev. A*, **16**, 1297 (1977).
7. V. F. Kovalev, A. B. Romanov, *Zh Exsp. Teor. Fiz.*, **77**, 918 (1979).
8. C. Băleanu, S. Coldea, J Karacsony Contract M.t.I 13/1986.

STUDIA UNIV. BABEŞ–BOLYAI, PHYSICA, XXXIV, 2, 1989

COMPUTER MONITORED SYSTEM FOR AUTOMATIC TEMPERATURE CONTROL

D. S. IANCU, G. D. POPESCU*

Received. July 5, 1989

ABSTRACT. — This paper presents a practical achievement for programming and adjusting the temperature of electric furnaces with heating currents up to 63 A. The installation proves to be very useful for obtaining some substances whose preparation and thermal treatment need a more complex thermal diagram; among these materials are the new high T_c superconductors.

When we were concerned to prepare different samples of 1—2—3 superconductors, a serious inconvenience arose from the necessity to survey and adjust the temperature of the furnace during a long period of time — tens of hours or even days. Thus, it appeared the necessity to design a system able to automatically run the thermal diagram of the furnace. A short description of the resulted apparatus is presented below

The block-diagram of the system is given in Fig. 1 A thermocouple (TC) is used as temperature sensor in the furnace ⑧, its voltage is amplified by stage ① and compared in the stage ② with a reference voltage, U_{REF}, corresponding to the needed temperature The reference may be constant (given by stage ③) or may change in time according to a program for thermal cycling carried out by processor ⑤ and transmitted to the comparator through the digital-analogic converter ⑥. The switch SW1 makes possible to select the references (U_{REF} "Automat" or "Manual") and the other switch, SW2, enables the alternate reading of the voltages to be compared (U_{REF} and U_{TC}) by a digital voltmeter ④. The comparator output drives the power unit ⑦ which connects the heater of the furnace to the power network A On Fig 1 also appears the voltage supply unit ⑨. To prevent the erasure of the computer memory in the case of a voltage drop, an independent-power supply of the processor is provided (B)

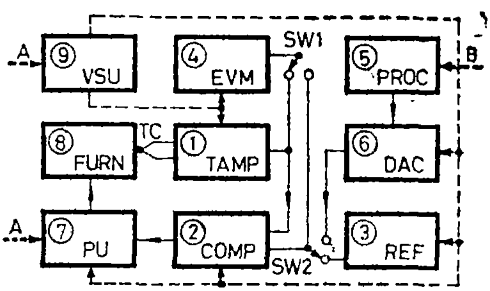

Fig 1

Fig. 2 shows three of the mentionned units. The thermocouple amplifier ① uses integrated circuits of βA 726 X-type with temperature stabilized transistors, ensuring thus a small drift of the amplification Care was taken about thermal compensation also in the ② and ③ stages by using opposite diodes The helical

* *University of Cluj-Napoca, Faculty of Mathematics and Physics, 3400, Cluj-Napoca Romania*

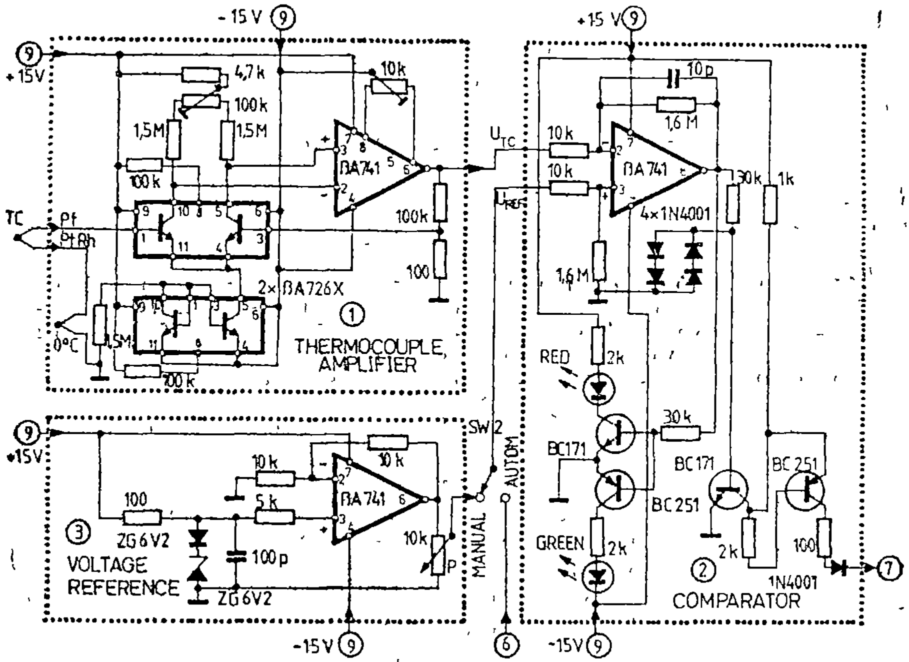

Fig. 2

potentiometer P (10 turns) serves for manual choice of the reference voltage and lies together with the two comparator LEDs on the front panel of the apparatus. The red lamp lights up when the reference voltage exceeds the one provided by the thermocouple amplifier and signals the furnace heating; when U_{TC} equals the reference value the red LED goes out indicating the interruption of the heating. During this period, when the furnace cools out ($U_{TC} > U_{REF}$), the green lamp is lighting The comparator output drives an unijunction transistor oscillator (Fig. 3) and the period of generated pulses determines the phase for opening the thyristor. The thyristor current is the heating current of the furnace and its intensity belongs to the voltage amplitude at the comparator output

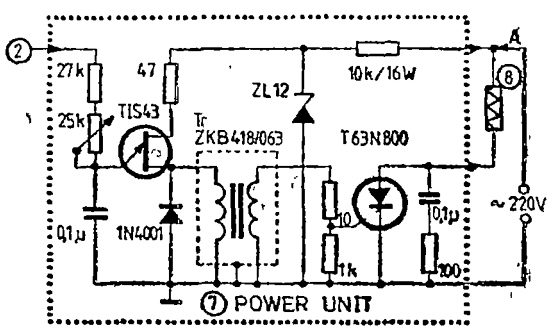

Fig. 3

In Fig. 4 is shown the circuit of the voltmeter used at the inputs of the comparator. It contains three ICs and displays millivolts on three digits, enough for the temperature range of the furnace

The digital-analogic converter (Fig. 5) is the interface between the parallel output bus of the processor (8 bits in the case of our TIM—S-type computer)

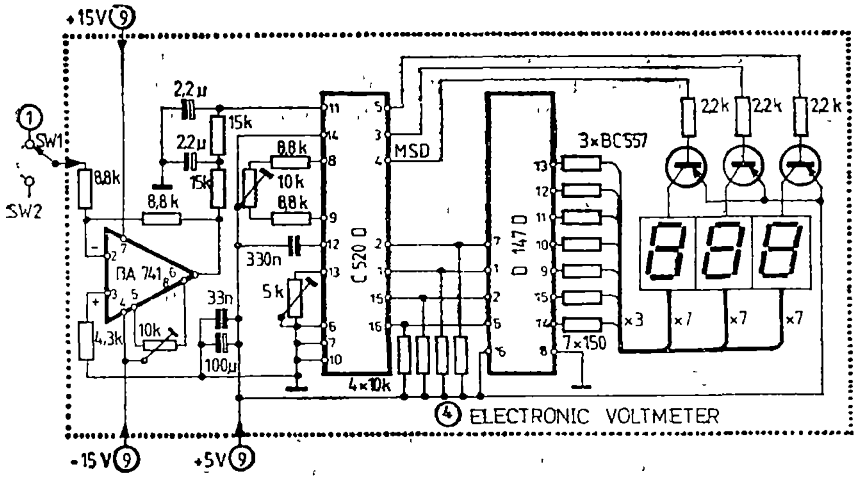

Fig. 4

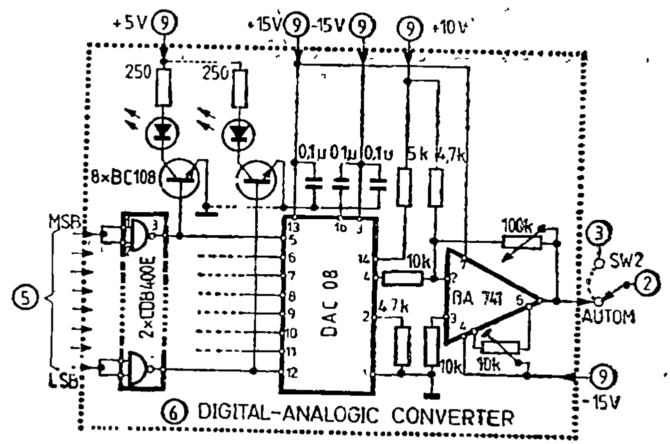

Fig. 5

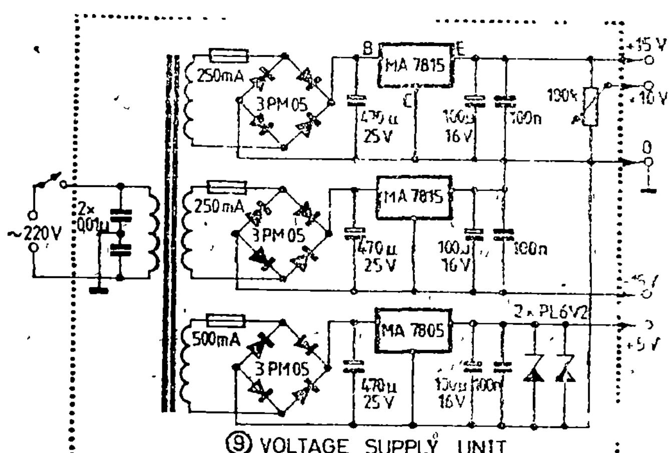

Fig 6

and one of the comparator inputs. Eight LEDs enable us to observe on the front panel the state of the data bus. Switching SW2 in the "Automat" position makes the furnace temperature to follow the thermal diagram imposed by computer programming.

Fig. 6 presents the voltage supply unit for almost all of the system blocks. As mentionned above, in order to preserve the processor memory its voltage supply (+12 V, ±5 V) is made from a 12 V battery via the circuits shown in Fig. 7.

The calibration curves of the apparatus are plotted in Fig 8.

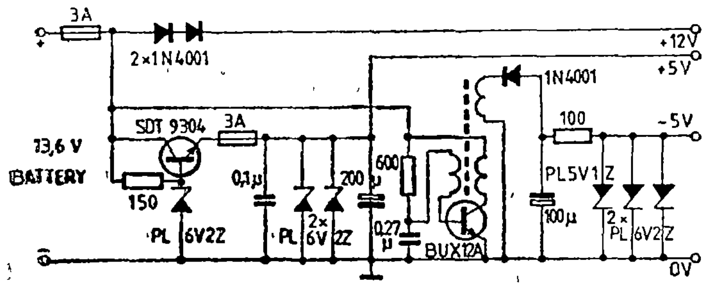

Fig 7

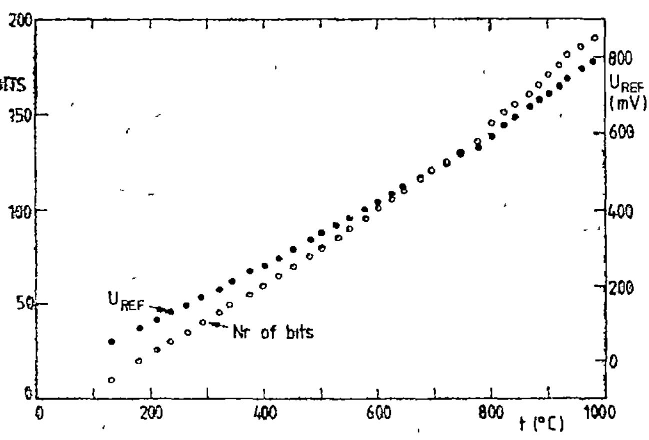

Fig. 8

The empty circles stand for the number of bits, decimally written, corresponding to the binar significance of the LED display at the parallel output of the processor, and the solid circles are the reference voltage measured by the voltmeter. In both cases there is a satisfactory linearity; the temperature on the abscissa was measured at the middle of the furnace by a Pt-PtRh thermocouple.

In the Appendix we propose a BASIC program for a thermal treatment having three plateaus. The heating and, respectively, cooling rates, together with the temperature and time intervals for the three plateaus are given by INPUT to the computer, according to the calibration curve from Fig. 8. In principle, in the limits of a given situation, the above described method allows thermal cycling of any duration and any form.

Appendix

Program for three steps thermal treatment

```
2 OPEN #3, "a": LLIST
3 BORDER 7: PAPER Ø  INK 7
5 PRINT AT Ø,Ø; "Acest program furnizează un exemplu de diagramă termică cu trei paliere şi pante variabile de încălzire respectiv răcire. Alegînd în mod corespunzător variabilele se pot obţine o infinitate de posibilităţi de tratament termic. Cunoscînd puţina programare, acest program poate fi adaptat pentru orice tip de diagramă termică."
6 PAUSE Ø  CLS
8 PRINT AT 19,Ø, "Timp: minute" ,AT 2Ø,Ø, "Temp.n ¤ (= const. aparat)"
1Ø PLOT Ø,8Ø
2Ø FOR n=Ø TO 48 STEP 8· DRAW 8,Ø· PLOT n,8Ø+n· NEXT n
3Ø PLOT 8,8Ø: FOR n=Ø TO 48 STEP 8: DRAW Ø,8: PLOT n+8,8Ø+n. NEXT n
4Ø FOR n=1 TO 4· PRINT AT 5-n, 6+n; ".". NEXT n
5Ø PLOT 88,162: DRAW 32,Ø
6Ø PLOT 12Ø,162: FOR n=Ø TO 32 STEP 8: DRAW 8,Ø: PLOT 12Ø+n,162-n: NEXT n
7Ø PLOT 128,162: FOR n=Ø TO 32 STEP 8: DRAW Ø,-8: PLOT 128+n,162-n: NEXT n
8Ø DRAW -8,Ø. DRAW 24,Ø
9Ø PLOT 178,122: FOR n=Ø TO 32 STEP 8: DRAW 8,Ø: PLOT 178+n,122-n: NEXT n
1ØØ PLOT 178,122: FOR n=Ø TO 32 STEP 8: DRAW Ø,8: PLOT 178+n,122-n: NEXT n
11Ø PLOT 21Ø,98· DRAW 8,Ø
12Ø PLOT 218,98: FOR n=Ø TO 24 STEP 8: DRAW 8,Ø  PLOT 218+n,98-n: NEXT n
13Ø PLOT 226,98: FOR n=Ø TO 24 STEP 8: DRAW Ø,-8  PLOT 226+n,98 -n: NEXT n
14Ø PLOT INVERSE 1,25Ø,74: PLOT INVERSE 1,21Ø,9Ø
15Ø PRINT AT 13,Ø;"k",AT 11,2,"-->1",AT Ø,12;"t1",AT 3,19;"-->m ",AT 2,18; "p"
16Ø PRINT AT 4,19,"t2",AT 6,24, "-->0",AT 7,25,"q"
17Ø PRINT AT 8,26,"t3",AT 13,27 ,"-->r",AT 1Ø,3Ø;"f"
18Ø INPUT "k(pas timp)=",k  INPUT "1 (pas temp)=",1. INPUT "t1(timp palier 1)=", t1
19Ø INPUT "p(pas timp răcire)=",p· INPUT "m(pas temp racire)=",m· INPUT "t2(timp palier 2)=",t2
2ØØ INPUT "q(pas timp racire)=",q· INPUT "o(pas temp racire)=",o  INPUT "t3(timp palier3)=",t3
21Ø INPUT "r(pas timp racire)=",r. INPUT "f(pas temp racire)=",f
213 INPUT "teØ(temp de start )=",teØ
215 INPUT "te1(temp. palier1)=",te1
216 INPUT "te2(temp palier2)=",te2
217 INPUT "te3(temp palier3)=",te3
219 PRINT AT 19,Ø, ",AT 2Ø,Ø,"
22Ø OPEN #3,"a"
23Ø FOR n=1 TO 255· POKE 6ØØØØ+n,n: NEXT n
24Ø FOR n=teØ TO te1 STEP 1: OUT 226,PEEK 6ØØØØ+n: PRINT AT 1Ø,12;PEEK 6ØØØØ+n· LPRINT PEEK 6ØØØØ+n: PRINT AT 14,14;"INCĂLZIRE"  FLASH 1: PAUSE 3ØØØ*k  PRINT AT 1Ø,12,"  "  NEXT n
```

```
250 FOR n=1 TO t1  PRINT AT 10,12,n, "min"· PRINT AT 14,14,"PALIER 1 ":
PAUSE 3000. PRINT AT 10,12;"  " NEXT n
260 FOR n=te1 TO te2 STEP -m OUT 226,PEEK 60000+n PRINT AT 10,12;
PEEK 60000+n. LPRINT PEEK 60000+n  PRINT AT 14,14, "RACIRE 1"  PAUSE
3000 *p PRINT AT 10,12,"  ": NEXT n
270 FOR n=1 TO t2. PRINT AT 10,12,n, "min": PRINT AT 14,14,"PALIER 2". PAUSE
3000 PRINT AT 10,12,"  ": NEXT n
280 FOR n=te2 TO te3 STEP -o OUT 226,PEEK 60000+n PRINT AT 10,12;
PEEK 60000+n· LPRINT PEEK 60000+n: PRINT AT 14,14,"RACIRE 2" PAUSE 3000
*q. PRINT AT 10,12,"  ": NEXT n
285 FOR n=1 TO t3  PRINT AT 10,12;n, "min.": PRINT AT 14,14,"PALIER 3":
PAUSE 3000: PRINT AT 10,12;"  "· NEXT n
290 FOR n=te3 TO 0 STEP -f: OUT 226,PEEK 60000+n: PRINT AT 10,12,PEEK
60000+n· LPRINT PEEK 60000+n: PRINT AT 14,14;"RACIRE 3 ": PAUSE 3000*r:
PRINT AT 10,12,"  ": NEXT n
295 FLASH 0
296 PRINT AT 14,14,"SFIRSIT !"
300 STOP
```

REFERENCES

1. "Circuite integrate liniare Manual de utilizare" (M. Bodea, A. Vătăşescu coordonatori), vol 4, p 252, Ed Tehnică, Bucureşti, 1985,
2. "TIM—S, Manual de funcţionare şi utilizare".
3. N. Sprînceană, R Dobrescu, T. Borangiu, "Automatizări discrete în industrie", Ed. Tehnică, Bucureşti, 1978.

STUDIA UNIV BABEŞ–BOLYAI, PHYSICA, XXXIV, 2, 1989

THE VALENCE STATES OF IRON ION IN CADMIUM-BORATE OXIDE GLASSES

I. ARDELEAN*, GH. ILONCA*, O. COZAR* and GEORGETA MUREŞAN*

Received · July 12, 1989

ABSTRACT. — We report the results of magnetic measurements performed on $x\mathrm{Fe_2O_3}(1-x)[2\mathrm{B_2O_3}\ \mathrm{CdO}]$ glasses having $x \leqslant 50$ mol % In the glasses with $x \leqslant 3$ mol % the iron ions manifest themselves as isolated species, but at higher concentrations they participate in negative superexchange interactions. From experimental Curie constant and atomic magnetic moment values we have assumed that in the glasses with $x > 1$ mol % the iron ions are present as Fe^{3+} and Fe^{2+} valence states, whose molar fraction was calculated.

Introduction. Several experimental results relating to the magnetic behaviour of some oxide glasses with transition metal ions suggest that the valence states and distribution mode of these ions in the network of the oxide glasses depend on the glass matrix structure [1], the preparation conditions [2], and the nature of the transition — metal ions [3] These conclusions have been reached from $\mathrm{Fe_2O_3 \cdot B_2O_3 \cdot PbO}$ glasses investigations, too [4]

In order to obtain information on the part played by the glass matrix composition on the iron valence states, we studied the magnetic behaviour of $\mathrm{xFe_2O_3}$ $(1-\mathrm{x})[2\mathrm{B_2O_3} \cdot \mathrm{CdO}]$ glasses with $0 < \mathrm{x} \leqslant 50$ mol %.

Experimental. We have studied the $x\mathrm{Fe_2O_3}(1-x)[2\mathrm{B_2O_3} \cdot \mathrm{CdO}]$ glasses with $0 < x \leqslant 50$ mol % maintaining the $\mathrm{B_2O_3/CdO}$ ratio constant In this way initially the glass matrix $2\mathrm{B_2O_3} \cdot \mathrm{CdO}$ was prepared by mixing $\mathrm{H_3BO_3}$ and $\mathrm{CdCO_3}$, and melting this admixture in a sintered corundum crucible We used the technique previously reported [5] After cooling, the host glass was crushed and the resulting powder was mixed with appropriate amounts of $\mathrm{Fe_2O_3}$, before final melting at $T = 1150$°C for 1 h The molten glass was poured onto a stainles steel plate The structure of these glasses has been studied by X-ray diffraction analysis and did not reveal any crystalline phase up to 50 mol % $\mathrm{Fe_2O_3}$

The magnetic susceptibility data were performed using a Faraday type balance in the temperature range 80 to 300 K.

Results and discussion. The temperature dependence of the reciprocal magnetic susceptibility of these glasses is presented in Figs 1 and 2 For the glasses with $x \leqslant 3$ mol % a Curie law is observed This suggest that in this concentration range are predominant the isolated iron ions and no magnetic order is present For $x > 3$ mol %, the reciprocal magnetic susceptibility obeys a Curie—Weiss behaviour with a negative paramagnetic Curie temperature — θ_p. For these compositions, the high temperature susceptibility data indicate that the iron ions in the glasses experience negative exchange interactions and are coupled antiferromagnetically In this case, the antiferromagnetic order takes place only at short-range and the magnetic behaviour of the glasses can be descri-

* *University of Cluj-Napoca, Faculty of Mathematics and Physics, 3400 Cluj-Napoca, Romania*

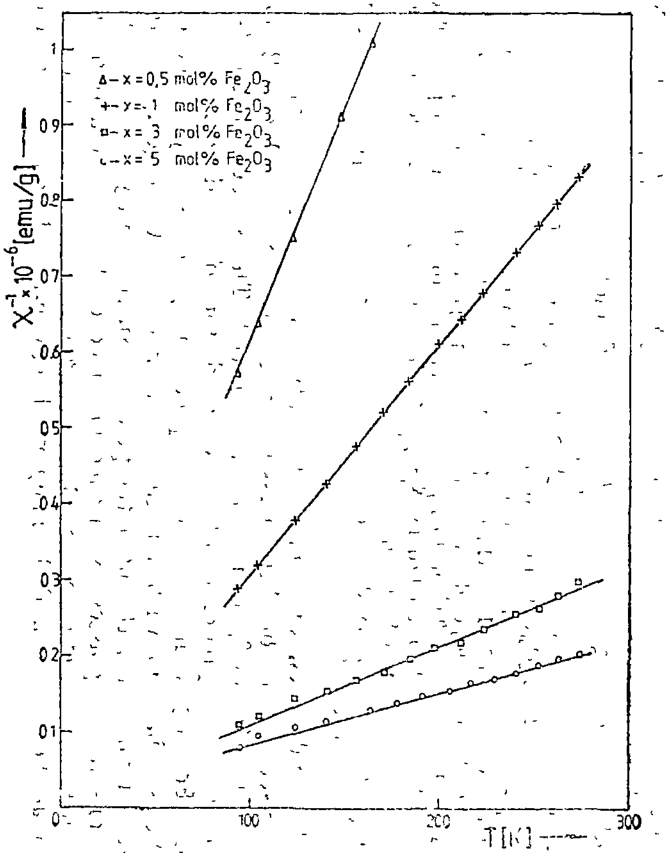

Fig. 1. The temperature dependence of the reciprocal magnetic susceptibility for the glasses with $x \leqslant 5$ mol %.

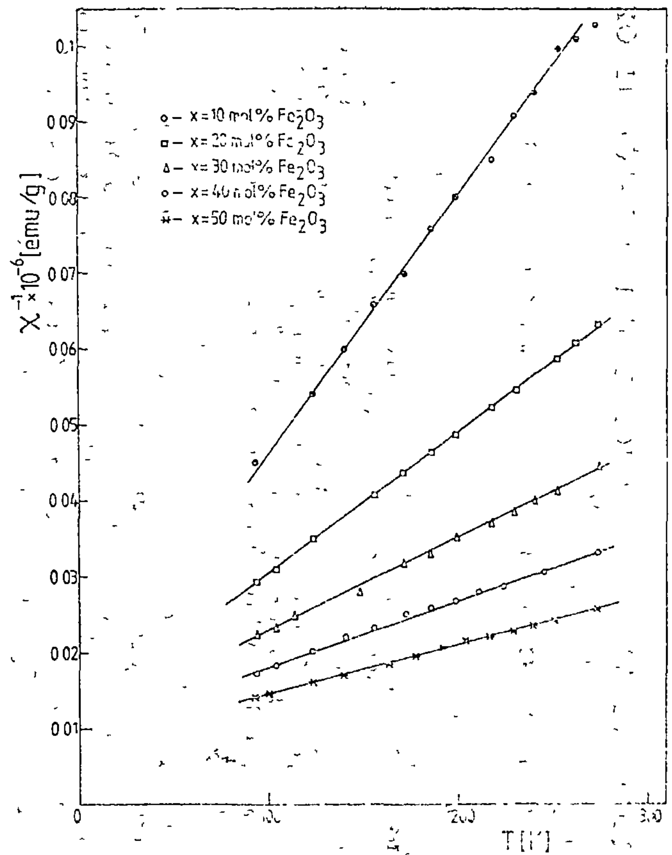

Fig. 2. The temperature dependence of the reciprocal magnetic susceptibility for the glasses with $10 \leqslant x \leqslant 50$ mol %

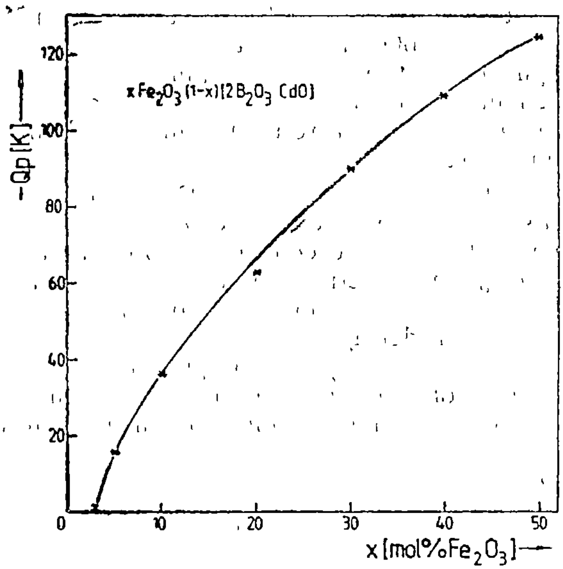

Fig. 3. The composition dependence of the paramagnetic Curie temperature.

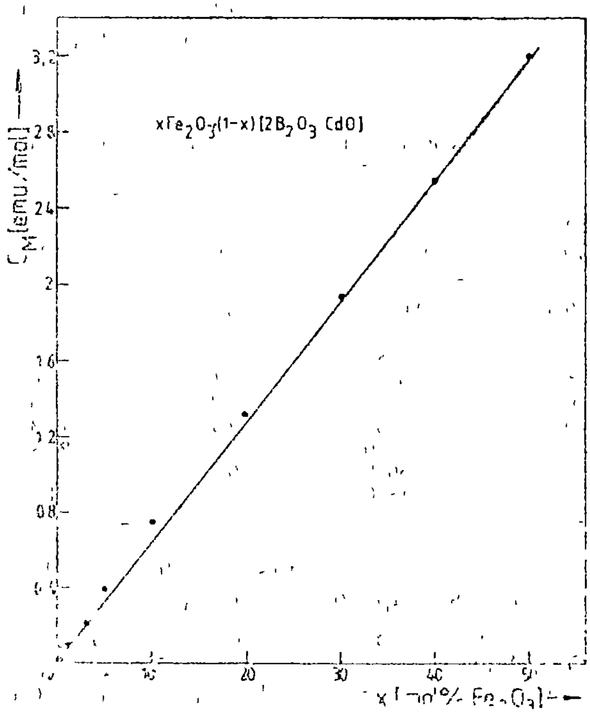

Fig. 4 The composition dependence of the Curie constant.

bed by the so-called mictomagnetic [6] type order A similar conclusion was obtained for $Fe_2O_3 \cdot B_2O_3 \cdot PbO$ glasses [4].

The absolute magnitude of the values of θ_p increases for $x > 3$ mol % (Fig. 3). In general the exchange integral increases as the concentration of the iron ions is increased in the glass [7] As a result the magnitude of the paramagnetic Curie temperature increases.

To determine accurately the values of the Curie constants, C_M, corrections due to the diamagnetism of the matrix and Fe_2O_3 were taken into account. The composition dependence of the Curie constant is presented in Fig 4 For the glasses with $x > 1$ mol %, the experimental values obtained for Curie constant and consequently for atomic magnetic moments are lower than those which correspond to Fe_2O_3 content, considering that all iron ions are in Fe^{3+} valence state. In this way, we consider that in these glasses are present both, Fe^{2+}, and Fe^{3+} ions The presence of the Fe^{3+} ions was evidenced by EPR measurements [8] In this case, having in view the atomic magnetic moment values $\mu_{Fe3+} = 5.92\ \mu_B$ and $\mu_{Fe2+} = 4.90\ \mu_B$ [9], we have estimated the molar fraction of these ions in the glasses using relations

$$x\mu^2_{exp} = 2.83^2 \cdot C_M = x_1\mu^2_{Fe3+} + x_2\mu^2_{Fe2+} \tag{1}$$

and

$$x = x_1 + x_2,$$

where $\mu_{exp} = 2.83\sqrt{C_M/x}$ the experimental atomic magnetic moment, x_1 and x_2 the molar fractions of iron in Fe^{3+} and Fe^{2+} valence states The results are presented in Table 1. From these data it results that the molar fraction of the Fe^{2+} ions in these glasses increases up to 50 mol %

Table 1

Curie constants and the molar fraction of iron ions in Fe^{3+} and Fe^{2+} valence states.

x [mol % Fe_2O_3]	C_M [emu/mol]	x_1 [mol % $Fe_2^{3+}O_3$]	x_2 [mol % $Fe_2^{2+}O_3$]
0.5	0.0437	0 5	—
1	0 0874	1	—
3	0 2482	2.5	0 5
5	0 3828	3 0	2 0
10	0.7498	5,4	4.6
20	1 3301	4 7	15 3
30	1 9440	5.2	24.8
40	2.5649	6.2	34 8
50	3.1886	6 8	44 2

Conclusions. By means of the magnetic susceptibility investigations of $xFe_2O_3(1-x)[2B_2O_3 \cdot CdO]$ glasses with $0 < x \leq 50$ mol % we have obtained information concerning the iron ions distribution in the cadmium-borate glass matrix which explains their magnetic behaviour.

The magnetic properties of $xFe_2O_3(1-x)[2B_2O_3 \cdot CdO]$ glasses are a function of Fe_2O_3 content. For the glasses with $x > 3$ mol % Fe_2O_3, antiferromagnetic behaviour is evidenced.

From Curie constant and atomic magnetic moment values, it results that in these glasses the iron ions are present as Fe^{3+} and Fe^{2+} valence states, whose molar fraction was calculated

REFERENCES

1. E. Burzo, I. Ardelean and I. Ursu, *J. Mater. Sci.*, **15**, 581 (1980).
2. E. Burzo, I. Ursu, D. Ungur and I. Ardelean, *Mater. Res. Bull.*, **15** 1273 (1980)
3. I. Ardelean, Gh. Ilonca, D. Bărbos and H. Adams, *Solid State Commun.*, **40**, 769 (1981).
4. I. Ardelean and E. Burzo, "Physical Properties of $B_2O_3-PbO-Fe_2O_3$ and $B_2O_3-PbO-GeO_2-Fe_2O_3$ Glasses", Ed. by University of Cluj-Napoca, 1980
5. E. Burzo and I. Ardelean, *Phys. Chem. Glasses*, **20**, 15 (1979)
6. D. A. Beck, *Met. Trans.*, **2**, 2015 (1971)
7. E. J. Friebele, L. K. Wilson, A. W. Dozier and D. L. Kinser, *Phys. Status Solidi (b)*, **45**, 323 (1971)
8. O. Cozar, I. Ardelean and Gh. Ilonca, to be published
9. E. Burzo, *Fizica fenomenelor magnetice*, vol. 1, Acad. RSR, Bucureşti, 1979, p. 241.

STUDIA UNIV BABEŞ–BOLYAI, PHYSICA, XXXIV, 2, 1989

THE ABSORPTION OF THE ULTRASOUND BY THE CARBON TETRACHLORIDE-HEXANOL SYSTEM

I. LENART*, D. AUSLÄNDER* and A. CIUPE*

Received July 20, 1989

ABSTRACT. — The paper reports experimental work leading to information on the nature and the intensity of the intermolecular interactions in CCl_4 and $C_6H_{13}-OH$ mixtures of different concentrations, at 20°C. The values of the ultrasonic velocity, density, attenuation constant and dynamic viscosity enabled the evaluation of the relaxation absorption, the volumic viscosity and some relaxation parameters as well as the excess quantities The results demonstrate the existence of interactions between the component molecules of the system

Introduction. The process of ultrasound energy disipation in the propagation medium is a result of several effects, based on different mechanisms.

According to the hydrodynamic theory of attenuation by absorption, the energy disipation is due to the effects of viscosity, thermal conductibility and thermal radiation Since for most liquids we can neglect the last two terms, the absorption is given by

$$\frac{\alpha_v}{f^2} = \frac{8\pi^2}{3\rho v^3}\,\eta \tag{1}$$

In order to obtain agreement with the experimental data, we had to take into account an extra absorption term, resulting from the molecular mechanisms of relaxation, hence

$$\frac{\alpha_{exp}}{f^2} = \frac{\alpha_v}{f^2} + \frac{\alpha_{rel}}{f^2} = \frac{2\pi^2}{\rho v^3}\left(\frac{4}{3}\,\eta + \eta_v\right) \tag{2}$$

where α_{exp} is the experimental attenuation constant, f — the ultrasonic frequency, α_v the viscosity attenaution constant, α_{rel} — the relaxation attenuation constant, ρ — the density of the propagation medium, η — the dynamic viscosity, η_v — the volumic viscosity.

Material and Method. The experimental determinations were made on carbon tetrachloride-hexanol mixtures, with one polar and one apolar component in a full range of concentrations (including the system components) at the temperature of 20°C

The ultrasonic velocity was measured by an optical diffraction method, the attenuation constant by a pulse method on the basis of repeated echoes at a fixed distance, at 8 MHz frequency, the density and the dynamic viscosity coefficient were determined using the picnometer and the Hoppler viscosimeter, respectively

* University of Cluj-Napoca, Faculty of Mathematics and Physics, 3400, Cluj-Napoca Romania

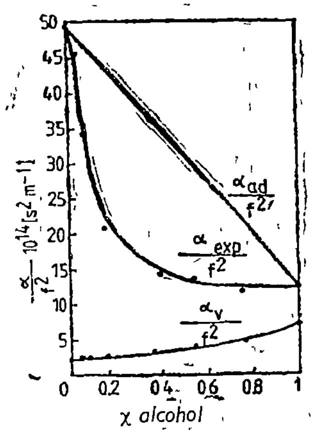

Fig. 1. The variation of absorption with the alcohol concentration.

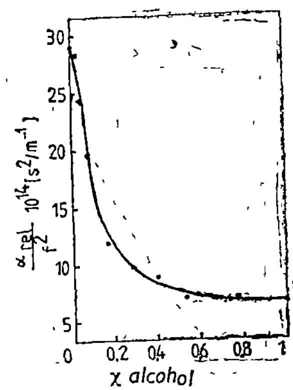

Fig. 2. The variation of the relaxation absorption with the alcohol concentration.

The data obtained permitted to evaluate the viscosity absorption from equation (1), the relaxation absorption and the volumic viscosity from equation (2).

By means of relationship:

$$\tau = \frac{2\eta + \eta_v}{\rho v^2} \tag{3}$$

the viscosity relaxation time of the components and of the mixtures at different concentrations was computed

Results and Discussions. The variation of the Stokes—Kirchhoff absorption and of the experimental absorption with the alcohol concentration is given in fig. 1. The term α_v/f^2 increases linearly with the concentration. The experimental attenuation is much higher than the viscosity one, especially for CCl_4. We note its marked decrease at small concentrations, till approximately $\chi = 0.2$ alcohol, tending to level close to the polar component.

The difference between the experimental attenuation constant and the viscosity one is attributed to the relaxation absorption, its variation with the concentration is given in fig. 2.
As we expected, the curves from fig. 1 show the considerable difference of this quantity for the two components, the strong descent in the range of small alcohol concentrations and a slower one for high concentrations.

The experimental absorption has a pronounced deviation from additivity as shown in fig. 3. The deviation is negative in the whole range of concentrations with a pronounced minimum at $\chi = 0.2$ alcohol.

The viscosity coefficients vary in opposite directions with the alcohol concentration of the mixture, as results from the curves in fig. 4. The lower curve, of the dynamic viscosity measured directly, increases with the concentration, more strongly for high alcohol concentrations. The volumic viscosity computed from

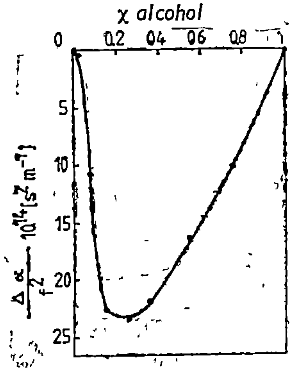

Fig. 3. The ghaph of the deviation of the absorption from additivity, as function of the alcohol concentration.

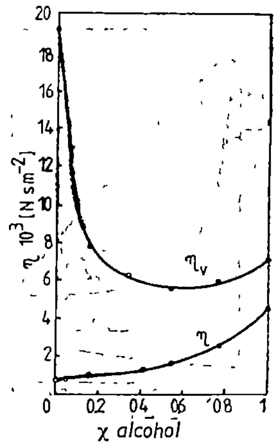

Fig 4. The variation of the dynamic and volumic viscosity coefficients with the alcohol concentration.

the absorption terms, is higher than the dynamic one and varies similarly with the experimental attenuation constant

By means relatioship 3, the viscosity relaxation time was computed, which varies with the concentration according to the graph of fig. 5.

Being higher in CCl_4, it decreases exponentially with the increase of the alcohol concentration in the mixture, to a minimum value lyeing between 0.5 and 0.6 molar fractions of alcohol; it then linearly increases to the value corresponding to hexanol

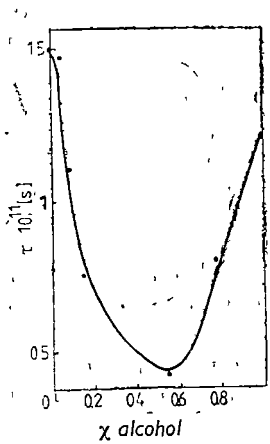

Fig. 5. The variation of the viscosity relaxation time with the alcohol concentration.

The relaxation processes being strictly dependent on the interactions, the values of the relaxation absorption give information about the intensity of these interactions Thus, the two components of the studied mixture are characterized by weak intermolecular interactions in CCl_4 and much stronger in $C_6H_{13}-OH$ because of the presence of the Hydrogen bonds which limit the possibilities of relaxation. This difference gives the higher absorption and relaxation time in carbon tetrachloride compared with hexanol.

The negative deviations from the additivity of the experimental attenuation constant indicate the presence of interactions between the molecules of the two componets of the system The pronounced deviation in the range of small concentrations of alcohol shows the presence of stronger interactions between the molecules of the components than the corresponding ones between the molecules of carbon tetrachloride. The increase of the alcohol concentration leads to the further decrease of the deviation from additivity, because of the increasing number of interacting molecules; the deviation attains a minimum followed by the predomination of the Hydrogen bonding characteristic to hexanol

Concluding, the variation of the quantities characterizing the relaxation processes with the alcohol concentration in the studied mixture reveals the shift of the equilibrium determined by the ensemble of the following intermolecular interactions polar-polar, polar — apolar, apolar — apolar.

REFERENCES

1 Murata, Yoshitada, Nishikawa, Keiko, *Chem Abst.*, vol. 93, 23, 1980, p 587.

2 Ram Lakhan Mishra, *Some acoustical and thermodynamic parameters*, Allahabad India, 1977

3 Schaafs W, *Molekularakustike*, Springer Verlag, Berlin, 1963.

4 Kumar A, Prakash S, *Chem Abst*, vol. 93, nr. 4, 1980, p 353.

5 Kononenko V S, *Akusti Jurnal*, Tom XXII, nr. 1, 1987, p. 688.

STUDIA UNIV BABEŞ—BOLYAI, PHYSICA, XXXIV, 2, 1989

TRANSITION TEMPERATURE MEASUREMENTS ON SOME SUPERCONDUCTING OXIDE MATERIALS BY INDUCTIVE METHOD

I. BARBUR*, V. IONCU*, S. SIMON*, I. ARDELEAN*, GH. ILONCA*, E. BURZO** and V. POP**

Received: July 22, 1989

ABSTRACT. — An inductive technique is described and used to characterize the normal to superconducting transition in small volume samples. As the sample temperature, T, is lowered through the transition, magnetic flux eclusion from the superconductor sample modifies L in an inductor coil of an LC circuit A plot of f versus T characterizes the transition The method is used for characterizing the superconducting transition in $Y_{0,6}Dy_{0,4}Ba_2Cu_3O_{7-\delta}$, $Y_1Ba_2Cu_3O_{7-\delta}$ and $Y_{0,5}Ba_{2,5}Cu_3O_{7-\delta}$ samples

Introduction. The transition temperature of superconducting materials is usually determined by measuring the temperature at wich the resistence of the material falls to zero (four — terminal resistence method) In nonhomogeneous materials different parts of the sample may have different transition temperature. In this case the four-terminal resistence measurements are not quite adequate.

To characterize the superconducting transition for some sample geometries such as powders, small sample crystals, and small fragments of thin films or sintered pellets an inductive method is used [1]

In this paper an inductive technique is described and used to characterize the normal to superconducting transition for small volume samples as $Y_{0.6}Dy_{0.4}Ba_2Cu_3O_{7-\delta}$, $Y_1Ba_2Cu_3O_{7-\delta}$ and $Y_{0.5}Ba_{2.5}Cu_3O_{7-\delta}$

Experimental. The sample is mounted on a copper support which is placed in the inductor coil of an LC circuit that oscillates at a resonant frequency $f = 1/2\pi \sqrt{LC}$ (Fig 1) As temperature T is lowered and the sample becomes superconducting, its diamagnetism decreases L and hance increases f A plot of f versus T characterizes the superconducting transition

The copper support is attached to a cold finger within the sample chamber of the cryostat. The sample temperature is measured using a calibrated diode thermometer attached to the copper support and controled with a temperature innstrument controller [2] The sample is cooled by immersion of the finger in either liquid nitrogen or liquid air

The inductor coil is a part of the modified integrated oscillator circuit TAA—66 [3]

The sample $Y_{0.6}Dy_{0.4}Ba_2Cu_3O_{7-\delta}$ was prepared by the following method appropriate amounts of Dy_2O_3, Y_2O_3, CuO and $BaCO_3$ powders were thoroughly mixed and heated in a flowing oxygen atmosphere at (930—950)°C for 24 hours The resulting mixture was reground, pelletized and heated at (940—960)°C for 24 hours in oxygen atmosphere The samples were then slowly cooled together with furnace X-rays measurements show the presence of single phase material having orthorombic crystal structure [4]

* University of Cluj-Napoca, Faculty of Mathematics and Physics, 3400 Cluj-Napoca, Romania
** Central Institute of Physics, Bucharest, Romania

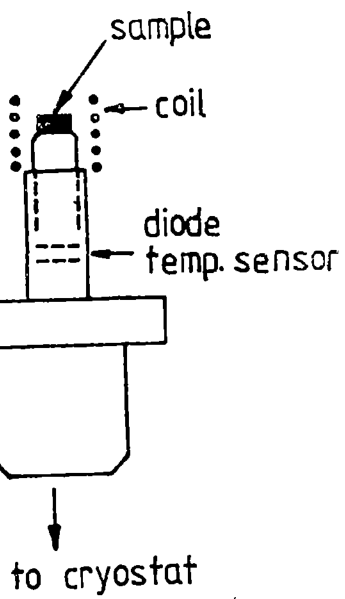

Fig. 1. Sample holder.

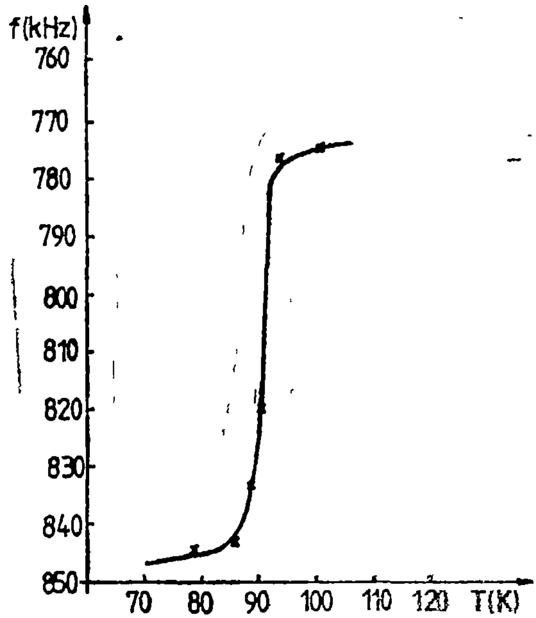

Fig. 2. An f versus T curve for $Y_{0.6}Dy_{0.4}Ba_2Cu_3O_{7-\delta}$

The samples $Y_1Ba_2Cu_3O_{7-\delta}$ and $Y_{0.5}Ba_{1.5}Cu_3O_{7-\delta}$ were obtained by calcination of the corresponding amount of Y_2O_3, $BaCO_3$ and CuO mixtures to 850°C for 8 hours, in air. After calcinations the samples were crushed again and recalcinated at the same temperature for 8 hours in order to obtain a higher homogeneity. Finally, the samples were pressed into pellets and sinterized for 16 hours, in oxygen flow at 930°C and then cooled down to 300°C with a cooling rate of 3°C/minute and with a temperature shoulder of 1 hour at 500°C.

Results and discussion. In Figure 2, an f versus T curve is shown for a sample of $Y_{0.6}Dy_{0.4}Ba_2Cu_3O_{7-\delta}$ of 3 mm diameter cilyndrical form. As can be seen, from Figure 2, the superconducting transition is narrow (middle point at 93 K) indicating a simple orthorombic phase in good agreement with the X-rays measurements [4].

In contrast to $Y_{0.6}Dy_{0.4}Ba_2Cu_3O_{7-\delta}$, for $Y_1Ba_2Cu_3O_{7-\delta}$ and $Y_{0.5}Ba_{1.5}Cu_3O_{7-\delta}$ samples, a broad superconducting transition is observed (Fig. 3 and 4, respectively) indicating a multiphase system in this materials also identified by ESR method [5]. The ESR signal of these samples is due to the Cu^{2+} ions from superconducting phases of Y_2BaCuO_5 and $CaCuO_2$ type [6].

In case of single phase material $Y_{0.6}Dy_{0.4}Ba_2Cu_3O_{7-\delta}$ the sintering temperature is higher than in case of multiphase systems $Y_1Ba_2Cu_3O_{7-\delta}$ and $Y_{0.5}Ba_{1.5}C_3O_{7-\delta}$.

The magnitude of the effect in increasing or decreasing of the f versus temperature is due to the difference in the magnetic properties of the samples (with

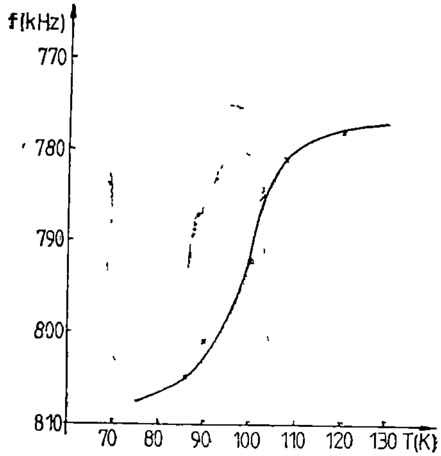

Fig. 3 An f versus T curve for $Y_1Ba_2Cu_3O_{7-\delta}$.

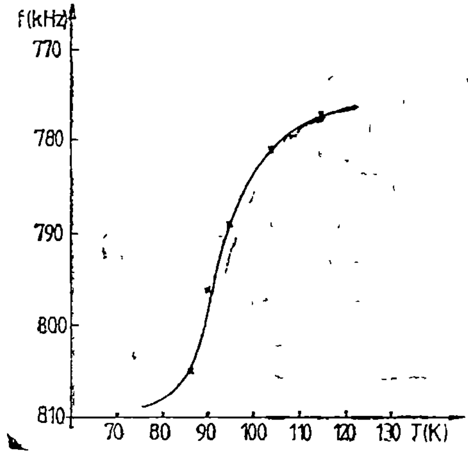

Fig 4 An f versus T curve for $Y_{0.5}Ba_{2.5}Cu_3O_{7-\delta}$.

and without Dy) and also to the size of the samples which influences the coil filling factor (space factor)

It may be concluded that the inductive method described is useful to characterize the superconducting transition (T_c, transition width) for small and different shapes of samples.

REFERENCES

1 Ciszek T. F., Tarsa E., *Preprint*, 1988.
2. Ioncu V., *Thesis, Univ of Cluj-Napoca*, 1988.
3. Ioncu V., Stănilă D., Cozar O., Fiat T., *Studia Univ. Babeş—Bolyai, Physica*, **26**, 23 (1981).
4 Burzo E., Pop V., Walace W. E., *Seminars on High-T Superconductors*, Preprint HTS—1, 15, 1989, Cluj-Napoca.
5. To be published.
6 S Simon, I. Barbur, I Ardelean, R Redac, *Seminars on High-T Superconductors*, Preprint HTS—1, 3, 1989, Cluj-Napoca.

STUDIA UNIV BABEŞ–BOLYAI, PHYSICA, XXXIV, 2, 1989

EPR ON VITROCERAMICS WITH GADOLINIUM OXIDE

S. SIMON*, GH. ILONCA*, I. BARBUR* and I. ARDELEAN*

Received July 23, 1989

ABSTRACT. — Changes of the structural and magnetical properties of glasses from $Bi_{2-x}Gd_xSr_2Ca_2Cu_3O_z$ system, in function of x and of heat treatment parameters, were investigated by electron paramagnetic resonance and magnetic susceptibility measurements Increase of the Gd_2O_3 content and of the heat treatment time at 840 °C determines significant modifications in the shape and parameters of the EPR spectra, which denotes a pronounced change of the microenvironments around the paramagnetic ions Cu^{2+} and Gd^{3+}.

Introduction. The discovery of the superconducting Bi—Sr—Ca—Cu—O system, initialy at relatively low temperature [1] and later also above nitrogen temperature [2, 3], impulsed the research on this class of ceramic materials. Interest arises both from the identification of superconductive phases with critical temperature $T_c > 100$ K and from the lower cost of this system Samples were obtained by the classical method of calcination and sintering of oxides mixture corresponding to desired composition The vitroceramic technique was also applied early to obtain samples by partial crystallization of glasses In the case of bismuth system glasses were prepared by the melt quenching method [4—6]

The advantages of the new technique are (1) due to melting of the mixtures, homogeneity of the samples is higher than that of the samples obtained by sintering, (2) calcination processes are completely or partially eliminated; (3) samples obtained by this technique are much denser than ceramic samples of the same composition, (4) the microstructure of the crystallized materials is highly controllable, (5) it is possible to obtain samples with various shape and size, inclusively fibers of radius and length adequate for applications in electrotechnics

As addition of rare earths to these ceramic materials determines an increase of critical temperature from 80 K to 100 K [7—9], we studied the $Bi_{2-x}Gd_xSr_2Ca_2Cu_3O_z$ system The structural modifications induced by heat treatment in glasses belonging to this system were investigated by electron paramagnetic resonance (EPR) and magnetic susceptibility measurements The addition of Gd_2O_3 may rise critical temperature and facilitate obtainment of complete vitreous samples, because it favours to obtain vitreous materials even in the absence of the classical glass formers [10, 11]

Experimental. Samples were prepared from Bi_2O_3, Gd_2O_3, $SrCO_3$, $CaCO_3$ and CuO mixtures corresponding to the compositions $Bi_{2-x}Gd_xSr_2Ca_2Cu_3O_z$, where x = 0, 0 01, 0 02, 0 03, 0 05, 0 07, 0 1, 0 15, 0 2, 0 25 and 0 3. Melts were maintained at 1200 °C for 15—20 minutes and were quickly

* *University of Cluj-Napoca, Faculty of Mathematics and Physics, 3400 Cluj-Napoca, Romania*

cooled by casting into large stainless crucibles, and pressed in order to obtain flat samples with a thickness between 1 and 2 mm. In the sensitivity limits of the X-ray diffraction these samples do not present any crystalline phase.

The partial crystallization of the samples was realized by heat treatments carried out at 840°C for times up to 20 hours. The presence or absence of the superconductive phases with $T_c >$ > 80 K was tested by means of an inductive method [12] which follows the temperature dependence of the inductance of a coil containing the investigated sample as core.

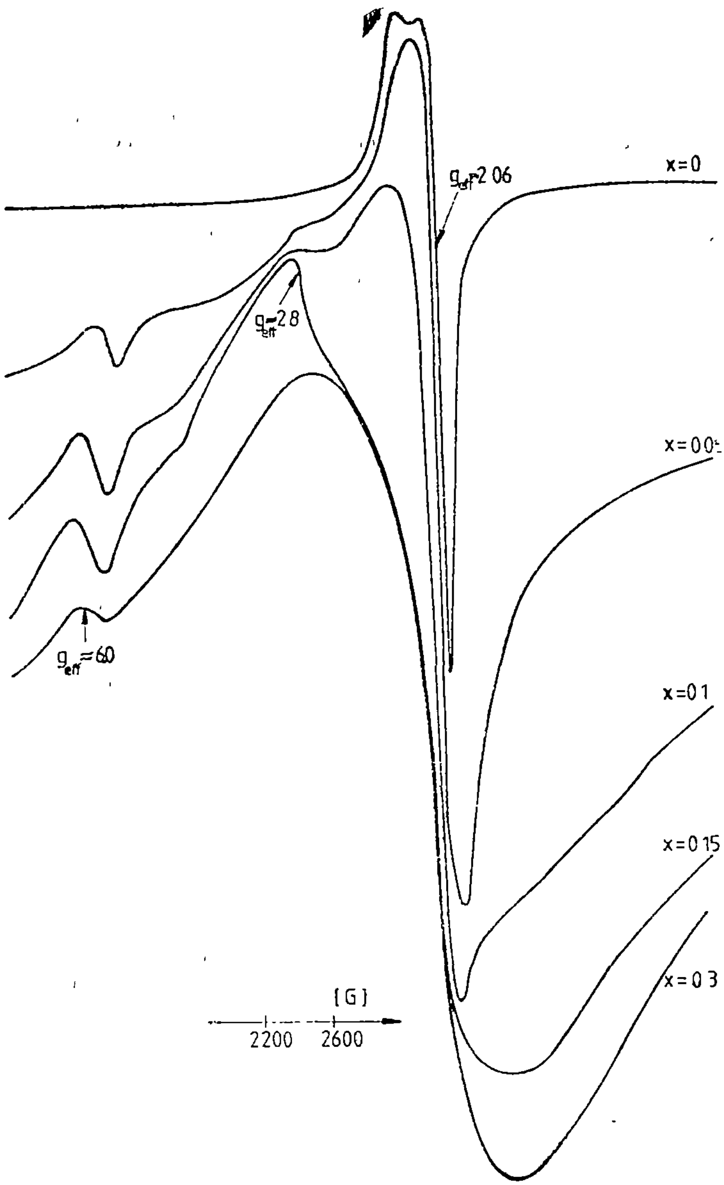

Fig 1. EPR spectra of $Bi_{2-x}Gd_xSr_2Ca_2Cu_3O_z$ glasses

The EPR spectra were recorded with a standard JEOL spectrometer, in X band, at the room temperature, on powder samples. The magnetic susceptibility measurements were carried out by means of a standard Faraday balance and an applied field of 7,5 kGs.

Results. The glass sample without Gd_2O_3 exhibits a relatively weak EPR signal with unresolved hyperfine structure (Fig. 1), typical of the Cu^{2+} ions disposed in sites of axial symmetry [13—15], with a large distribution of the spin Hamiltonian parameters. The addition of Gd_2O_3 leads to the appearance of an EPR signal specific to the Gd^{3+} ions in vitreous matrices [16—20]. The lines with $g_{eff} > 2.0$ are less visible and with increasing Gd_2O_3 content the line with $g_{eff} = 2.0$ predominates (Fig. 1).

The magnetic susceptibility measurements indicate a paramagnetic behaviour of the samples (Fig. 2) and allow to estimate the ratio between the Cu^{2+} ions and the total copper ions number (Table 1). The contribution of the Cu^{2+} ions to the EPR spectra may be observed in Fig. 1.

Table 1

The Cu^{2+} fraction (f) from the total copper ions number in $Bi_{2-x}Gd_xSr_2Ca_2Cu_3O_z$ glasses

x	$f(\%)$
0.01	30.06
0.05	28.96
0.075	8.33
0.10	9.17
0.15	9.57
0.20	22.97
0.25	30.97
0.30	36.67

The inductive measurements do not evidence any superconductive phase with $T_c > 80$ K in the glass samples.

The partial crystallization of the samples determines important changes in the shape and parameters of the EPR spectra, which denotes a pronounced change of the microenvironments around the paramagnetic ions Cu^{2+} and Gd^{3+}. The EPR signal intensity for the sample without Gd_2O_3 gradually decreases with heat treatment time (Fig. 3) and practically disappears after heat treatments longer than 10 hours.

The shape of the EPR spectra from the samples containing Gd_2O_3 modifies with the increase of the crystallization degree of the samples. One remarks a share diminution for the signals with $g_{eff} \simeq 6.0$, and a broading of the line with $g_{eff} \simeq 2.0$ respectively. This fact is illustrated in figure 4 by the ratio between the intensity of the line with $g_{eff} \simeq 6.0$ and that of the line with $g_{eff} \simeq 2.0$ and by the line width in function of the heat treatment time, for the sample with $x = 0.1$. The share of the superconducting phase with $T_c = 80$ K identified in the vitroceramic samples resulted after a heat treatment applied at 840 °C for 10 hours proved to be maximum for the sample with $0.1 \leqslant x \leqslant 0.2$.

Discussion and conclusions. The unresolved hyperfine structure of the Cu^{2+} EPR spectra is a consequence both of the strong dipole interactions and of the high disorder degree existing in the samples obtained from quickly undercooled melts. The high disorder degree and the homogeneous distribution of the paramagnetic ions in the vitreous matrix are proved both by Gd^{3+} EPR spectra typical of the amorphous systems and by the magnetic susceptibility measurements. The pronounced decrease of the signal intensity with heat treatment time is an evidence for the diminution of the localized Cu^{2+} ions number and, on the other hand it reflects the achievement of the structural and magnetical ordering specific to these superconductive materials. In this meaning, it is known the fact that the Cu^{2+} EPR signal recorded from ceramic samples of Y—Ba—

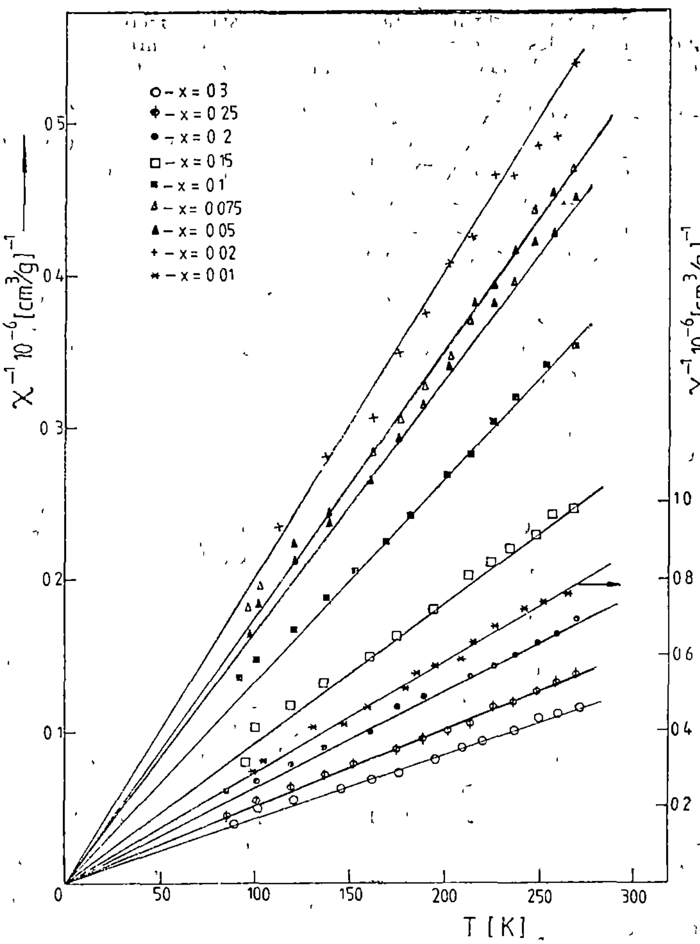

Fig 2 Temperature dependence of reciprocal susceptibility for $Bi_{2-x}Gd_xSr_2Ca_2Cu_3O_z$ glasses

Cu—O and Bi—Sr—Ca—Cu—O systems is assigned to the Cu^{2+} ions from the nonsuperconductive phases [21—25] and the resonance signal diminution denotes the decrease of the share of these phases

Having in view the assignment of the resonance lines with $g_{eff} > 2.0$ from the EPR spectra of the Gd^{3+} ions in glasses [19, 20], one may assert that in the samples belonging to the investigated system only a small part of the Gd^{3+} ions are disposed in sites of low symmetry and that the most ones are disposed in sites of cubic symmetry with minor axial components By the partial crystallization of glasses it takes place a relaxation of the sites of low symmetry. This relaxation is illustrated by the share diminution of the lines with $g_{eff} < 2.0$. At the same time, the microenvironment of the Gd^{3+} ions disposed in sites of cubic symmetry is easily distored, what involves a broadening of the distribution

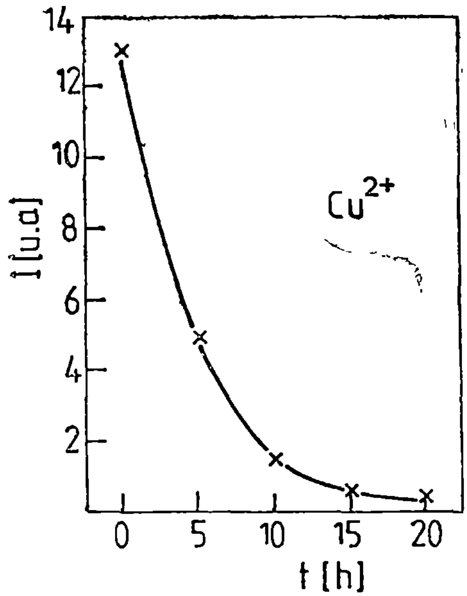

Fig 3 Heat treatment time dependence of Cu^{2+} EPR signal intensity for $Bi_2Sr_2Ca_2Cu_3O_x$ sample

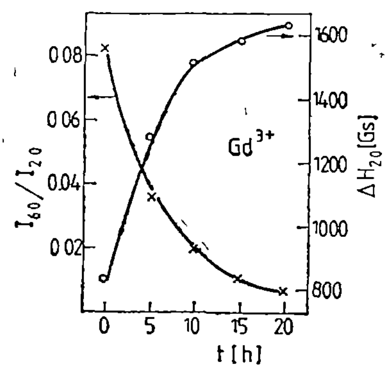

Fig 4 Heat treatment time dependence of EPR parameters for $Bi_{1.9}Gd_{0.1}Sr_2Ca_2Cu_3O_x$ sample

range of the values corresponding to the axial symmetry cristalline field parameters This leads to the broadening of the line with $g_{eff} \simeq 2.0$ The increasing magnetic interaction between the Gd^{3+} ions from the partially crystallized matrix also contributes to the broadening of the line with $g_{eff} \simeq 2.0$

Unlike other vitroceramics [26] in this case does not take place a sufficient uniformization of the Gd^{3+} microenvironment, at least in the range of the 20 hours of heat treatment applied at 840 °C, so that it does not obtain EPR spectra specific to the Gd^{3+} ion from polycrystalline materials [27]

The correlation between the effect of the heat treatment time and temperature on the shape and parameters of the Gd^{3+} EPR spectra from $Bi_{2-x}Gd_xSr_2Ca_2Cu_3O_z$ vitroceramics allows to establish new relations between the local order degree and the superconducting characteristics of these vitroceramics materials

REFERENCES

1 *Michel* C, Herrieu M., Borel M M, Grandiu A, Deslandes D, *Provest, J Reveau B, Z Phys*, **B 68**, 421 (1987)
2 Maeda H, Tanaka Y, Fukutomi M, Asano T, *Jpn J Appl Phit Lett*, **27**, L 209 (1988)
3 Hazeu R M, Prewitt C T, Angel R J, Ross N L, Finer L W, Hadidiacos C C, Veblin D R, Heang P J, Hor P H, Meng R.L, Sun Y.Y, Wang

Y Q, Xue Y.Y, Huang Z J, Gao L, Bechtold J, Chu C W, *Phys Rev Lett*, **60**, 1174 (1988)

4 Komatsu T, Imai K, Sato R, Matusita K, Yamashita T, *Jpn J Appl Phys* **27**, L 533 (1988).

5 Hinks D G, Soderholm L, Capone D.W, II Dabrowski B, Mitchel A W, Shi D, *Appl. Phys Lett*, **53**, 423 (1988).

6. Ihoue A, Kimura H, Matsuzaki K, Isai A, Masumoto T, *Jpn J Appl Phys*, **27**, L 941 (1988).

7. Tamegai T, Watanabe A, Koga K, Oguro I, Iye Y, *Jpn J Appl Phys* **27**, L 1074 (1988)

8 Yoshizaki R, Saito Y, Abe Y, Ikeda H, *Physica C*, **152**, 408 (1988)

9 Tallou J L, Buckly R G, Stainles M P, Piesland M R, Gilbert P W *Appl. Phys Lett* (1988)

10. Simon S, Nicula Al, *Rev Roum. Phys*, **28** (1), 59 (1983)

11. Simon S, Giurgiu A., Petrişor T, Nicula Al, *Proc Int Conf on Magn Rare Earth and Actinides*, Bucharest 1983, p. 217

12 Barbur I, Ioncu V, Simon S, Ardelean I, *Studia Phys*, (2) (1989).

13 Imagawa H, *Phys Status Solidi*, **30**, 469 (1968).

14 Bogomolova L D, Jachkin V A, Lazukin V.N, Shapovalova N F *Dokl Akad Nauk SSSR*, **198**, 805 (1971)

15 Simon S, Nicula Al, *Solid St Commun*, **39**, 1251 (1981)

16 Chepeleva T V, Lazukin V N, Dembovskii A S, *Sov. Phys Dokl*, **11**, 864 (1967)

17 Nicklin R C, Johnstons Y K, Barnes R C, Wilder R, *J Chem Phys* **59**, 1652 (1973).

18 Simon S, Tolea F, Duca I, Nicula Al, *Studia, Physica*, **24** (1), 37 (1979)

19 Cugunov L, Kliava K, *J Phys Sol St Phys*, **17**, 5795 (1984)

20 Brodbeck C M, Iton L E, *J Chem Phys*, **83** (9), 4285 (1985)

21 Mehram F, Barnes S E, McGuire T R, Gallagner W J, Saudstrom R L, Dinger T R, Change D A, *Phys Rev B*, **36** (1), 740 (1987)

22. Simon S, Barbur I, Ardelean I, *Studia, Physica*, **32** (2), 96 (1987).

23 Tyagi S, Basoum M, Rao K V, *Phys Lett A*, **12**, 82225 (1988), Luc J T, *Phys Rev*, **36** (7), 4592 (1988)

24 Dance J M, Tressand A, Chevalier B, Darriet J, Etourneau J, *Solid State Ionics* (1988)

25 Simon S, Barbur I, Ardelean I, Redac R, vol HTS-1, Cluj-Napoca, 1989, p 3

26. Simon S, Nicula Al, *Phys Status Solidi (a)* **81**, K1 (1984)

27 Heilbron M A, Nieuwenhuijse, Vrijheeven R P J, Gellings P J, *Mat Res Bull*, **11**, 1131 (1976).

STUDIA UNIV. BABEŞ-BOLYAI, PHYSICA, XXXIV, 2, 1989

SOME ELECTRICAL PROPERTIES OF THE SILVER-CONTAINING $84B_2O_3-15Li_2O-1SiO_2$ GLASS SYSTEM

V. CRISTEA*, LAVINIA COCIU*, MIRELA KRATOCHWILL* and AL. NICULA*

Received July 31, 1989

ABSTRACT. — The electrical property measurements have been performed on a silver containing glass system Two experimental methods have been used. The temperature dependence of both electrical resistance (R) and dielectric constant, as well as the modification of R with the applied electrical field have been discussed.

1 **Introduction.** The interest in the study of silver — containing glasses results from the possibility of their utilization in dosimetry In a previous work [1], the paramagnetic silver centers in gamma-irradiated glass systems have been reported In the present paper we concentrate on the temperature dependence of the both electrical resistance and dielectric constant of $84B_2O_3-15Li_2O-1SiO_2$ doped with 10% (wt) Ag_2O

2 **Experimental procedure.** The glass was prepared by fusing reagent grade substances $B(OH)_3$ Li_2CO_3, SiO_2, Ag_2O in corrundum crucibles The melt of oxides was maintained for an hour at 1 000 °C, then supercooled at room temperature in cylindrical form In order to obtain a tablet sample, the glass was heated in a flame and flattened until a flat elipsoid has arisen During first electrical measurements indium amalgam contacts have been used, but they proved to be inadequate because their electrical resistance has been rising with time With a soldering gun, an indium stratum was laid on every side of the samples and good contacts have been obtained An ORION type teraohmmeter with 50 V, 100 V, 200 V, 500 V, and 1 000 V output voltages, was used to measure the electrical resistance

Then the sample was polished on the two sides obtaining a parallel plate of 1.19 mm thickness By means of vacuum evaporation on the same two sides of the sample have been performed circular silver electrodes with diameters lower than that of the sample. We measured the electrical resistance (R) using a capacitor discharge method

$$R = \frac{t_2 - t_1}{C \ln \dfrac{U(t_1)}{U(t_2)}},$$

with the usual significance of the notations The same $U(t_1) = 94{,}5$ V and $U(t_2) = 77\,5$ V voltages were measured with a Dolezalek electrometer in idiostatic connection The measurements were carried out using a capacitor with negligible losses and such a capacitance (C), that the length of discharge time, $t_2 - t_1$, was 10 seconds, at least.

The sample holder and heater was described in the paper [2], in such a device, the sample with circular silver electrodes has been fixed between two platinum sheets The temperature was measured with a Pt—PtRh thermocouple using the compensation method. The heating conditions have been chosen so that during measurement, the temperature modification was impreceptable. A double switch allowed the sample connection either to the charged capacitor terminals (in order to find R), or to an RLC bridge output (in order to measure the capacitance of the sample electrodes capacitor — C_g)

* *University of Cluj-Napoca, Faculty of Mathematics and Physics, 3400 Cluj-Napoca, Romania*

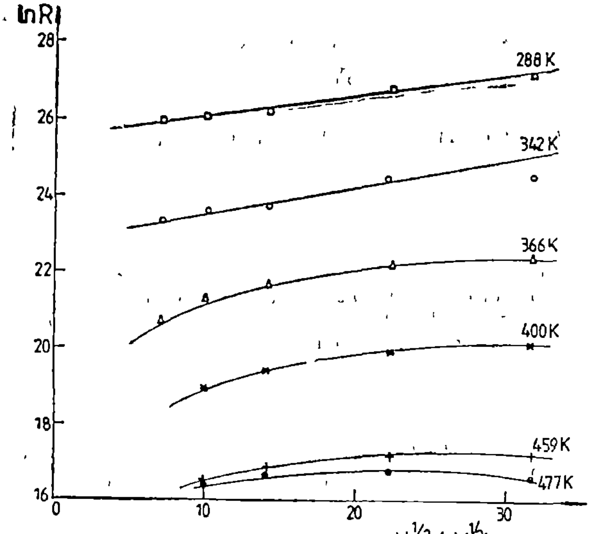

Fig 1 Change of the electrical resistance with the applied voltage.

3 **Experimental results.** Figure 1 shows the dependence of the electrical resistance on applied voltages, in a $\ln R - \sqrt{U}$ scale, at various temperatures; at lower temperatures this dependence is described by the experimental relationship

$$R = R_0 \, e^{A+BU^{1/2}}, \qquad (1)$$

where A and B coefficient values depend on the temperature (T) at 288 K, $A = 25.52$ and $B = 5.62 \cdot 10^{-2}$ $V^{-1/2}$, at 342 K, $A = 22.75$ and $B = 7.52 \times 10^{-2}$ $V^{-1/2}$ The same (1) dependence is right for the electric field $E = U/d$, where $d = 1.5$ mm is the sample tickness For $T = 288$ K, all the experimental points lie on the straight line; at 342 K, the point with $U = 1\,000$ V is below line and at higher temperatures, the relationship (1) is no more available

The temperature dependence of electrical resistance, corresponding to the two experimental methods, are shown in Fig 2. In every case, a straight line might be drawn in a ln R vs $\frac{10^3}{T}$ plot and the electrical resistance,

$$R = R_0 e^{\frac{W}{kT}}, \qquad (2)$$

shows an exponential decay when the temperature is rising

The dielectric constant was calculated with formula $\varepsilon = C_g/C_c$, where C_g is the capacitance of the sample electrodes capacitor minus the capacitance of the conductors, and C_c is the computed capacitance of the capacitor consisting of silver electrodes with vacuum instead of glass Fig 3 shows the dielectric constant variation with the temperature. It is observed in the 358 K — 405 K temperature range, ε does not depend on the temperature At higher temperatures ($T > 410$K) the temperature dependence $\varepsilon(T)$ may be described by the experimental relationship:

$$\varepsilon = \varepsilon_0 + bT \qquad (3)$$

where $\varepsilon_0 = -13.16$ and $b = 0.12$ K^{-1}.

4 **Discussions.** The dependence of electrical resistance on the applied voltage is due to Poole effect [3] in dielectrics the generation of new free carriers leads to the modification of electrical conductivity (σ) with the electric field

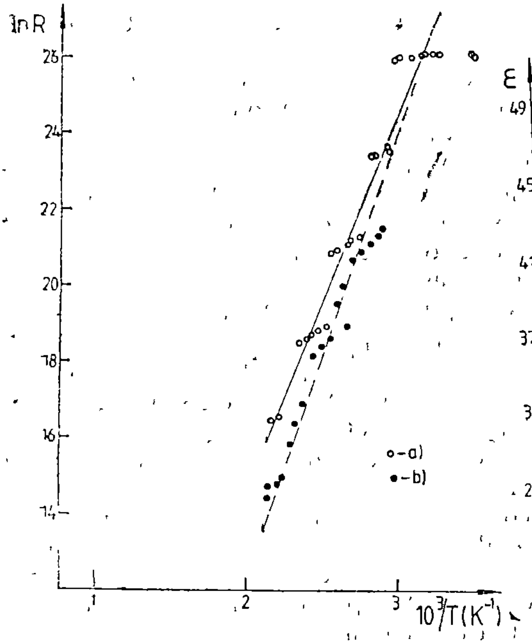

Fig 2 Temperature dependence of the electrical resistance of the samples a) with indium contact and teraohmmeter measurements, b) with silver electrodes and electrometer measurements

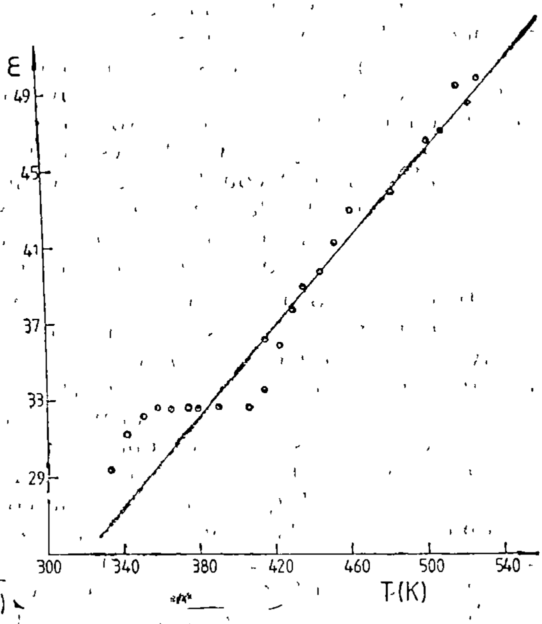

Fig 3. Temperature dependence of the dielectric constant.

magnitude (E) according to empirical formula $\sigma = A\ e^{\alpha E}$ In the paper [4] it is shown that such a law is true for $BaO - B_2O_3$ glass system In turn, the $BaO - B_2O_3$ — 5% (wt) In_2O_3 glass shows a Frenkel dependence of electrical resistivity (ρ) vs electric field intensity [5], $\rho = \rho_0 e^{-\beta\sqrt{E}}$, which in a $\ln\rho - \sqrt{E}$ plot, represents a negative slope straight line ($\beta > 0$) At the lower temapertures, the experimental data in Fig 1, follow such a law, but with a positive slope ($\beta < 0$) In contrast with Poole and Frenkel effects, we found an electrical resistance of the studied glass system which rises with applied electric field increase. Such a behaviour can be explained taking into account the glass polarization. The electric field between the teraohmmeter terminals causes the appearance of a polarization charge which is the greater so as the output voltage rises. Hence, inside the glass the electric field felt by current carriers diminishes and, in consequence, the sample apparent resistivity rises At higher temperatures, as it is seen in figure 1, the above explanation does not hold true because as the temperature rises, the polarization charge is diminishing. The similar polarization phenomena have been observed in materials with electronic conduction [6] such as TiO_2 whose conductivity lowers when the electric field is switch on.

Our experimental data in figure 2a were obtained with a teraohmmeter at 1 000 V output voltage, different series of experimental points arranged in the short lines with more and more slight slopes, correspond to the various measurement ranges of the instrument. In order to test these results, we used the second method and silver contacts on the sample To our surprise, the experimental points also appear as a series of short lines (Fig 2b) Besides, appropriate R values have been found with the two experimental methods. Computing the activation energies according to the expression (2), we have obtained $W_a = 0.88$ eV and $W_b = 1.04$ eV, respectively As far as the conduction kind concerns, taking into account the glass components, we suppose that the electrical conduction in this glass may be ionic. Nevertheless, owing to the sample preparation, we must mention that the conduction mechanism is sometimes changing [7] during flame processing of the glass

In the case of the dielectrics, usually, the literature [8] indicates a lowering electrical permitivity when the temperature is rising But, sometimes the permitivity of the dielectrics increases at higher temperatures It was reported [9] a strong increasing permitivity of the $Na_2O-BaO-Nb_2O_5-O2SiO_2$ glass system, especially at the temperatures higher than 200 °C The greater values of the dielectric constant are conditioned by a more pronounced polarization of the glass. When the temperature is increasing, the polarization diminishes but as it seen in the Fig 3, the dielectric constant (ε) of the silver containing glass becomes greater We could give a possible explanation to the experimental results (fig. 3), taking into account the dielectric losses It is known [10] that the imaginary part (ε'') of the dielectric constant is proportional to the electrical conductivity (σ), $\varepsilon'' = \sigma/\varepsilon_0\omega$, where ε_0 is the vacuum electrical permitivity and ω is the frequency of the operation voltage. Since the electrical conductivity increases with temperature, the greater values of ε'' are expected at higher temperatures and constant frequencies, but, ε dependence on the temperature is not an exponential one, so that our explanation has just a qualitative aspect

REFERENCES

1. Lavinia Cociu, I Ciogolaş, Al. Nicula, *Studia Univ Babes—Bolyai, Physica* XXVI(1), 57 (1981).
2. I. Ursu, F Puskás, V. Cristea, *Studia Univ. Babes—Bolyai, series Mat—Phys*, 1 127 (1962).
3. H. Poole, *Phyl. Mag*, 32, 112 (1916)
4. A. A. Deshkovskaya, N. M. Bobkova, *Stekloobraznoe sostoyanie*, Izd. Akad. Nauk Erevan, 1974, p. 103.
5. Ya. N. Frenkel, J.E.T.F., 8, 1292 (1938).
6. F. Cardon, *Phys. Status Solidi*, 3, 415 (1963).
7. A. M. Pisarevskiy, A. A. Belyustin, S. E. Volkov. O. S. Ershov, *Stekloobraznoe sostoyanie*, Izd. Akad. Nauk ASSR, Erevan, 1974, p. 186.
8. I. Bunget, M. Popescu, *Fizica dielectricilor solizi*, Ed. şt. encicl., Bucureşti, 1978, p 172.
9. S S. Maksimova, L. V. Korzunova, *Fizika i himiya stekloobrazuyvshchikh system* vyp. 2, Izd. LGU. Riga, 1974, p 163.
10. Yu M. Poplavko, *Fizika dielektrikov*, Izd. Vishcha shkola, Kiev, 1980, p. 226.

STUDIA UNIV BABEŞ–BOLYAI, PHYSICA, XXXIV, 2, 1989

CIRCULAR MOTIONS AROUND A PULSATING STAR

IOACHIM GIURGIU*

Received August 28, 1989

ABSTRACT. — The case of a body moving in an initially circular orbit around a pulsating star, under the only influence of gravitation and radiation pressure, is studied Some relations between the pulsation period and the orbital one are considered. The deformations undergone by the orbit in some peculiar cases are estimated.

1. **Disturbing Acceleration.** Let us consider a spherical body of mass m and radius r', with uniform albedo, orbiting a central body of mass $M \gg m$ Let this orbit be circular of radius a Let also the attracting body be a star whose luminosity changes in time, $L = L(t)$, and let this change be periodic. We consider that the only forces acting on the body m are the gravitation and the radiation pressure The radiation force per unit mass which acts on the orbiting body has the expression

$$F_r = A\, L(t)/(4\pi\, mcr^2), \tag{1}$$

where r is the radius vector of the body m, A is the effective cross-sectional area of the same body and c is the speed of light.

We shall write the luminosity $L(t)$ of the central source in the following form :

$$L(t) = L_0(1 + f(t)), \tag{2}$$

where L_0 is the mean luminosity.

Let us consider that the central source is a pulsating star In this case, the varying part of the luminosity is periodic (as we already assumed), let us write this part in the form

$$f(t) = a_p \sin(n_p t), \tag{3}$$

where $a_p < 1$ is the relative amplitude of the pulsation, while n_p is the pulsation frequency. We have assumed that $f(0) = 0$ and this fact eliminates the $\cos(n_p t)$ term.

With these considerations, the disturbing acceleration acquires the expression :

$$F_r = K(1 + a_p \sin(n_p t))/r^2, \tag{4}$$

* Industrial Sseconadary School, 3379 Baia de Arieş, Romania

where we have introduced the notation:

$$K = A\ L_c/(4\pi mc) \tag{5}$$

Let S, T, W be respectively the radial, transversal and binormal components of the disturbing acceleration Since the disturbing force is a central one we can write [3]·

$$S = K(1 + a_p \sin(n_p t))/r^2,\ T = 0,\ W = 0 \tag{6}$$

2 **Variation of the Eccentricity.** We supposed that the orbit of the body m is circular. So, the notion of periastron losses its meaning and that of true anomaly v, too; however, the notions of node and argument of latitude u remain valid if we consider a reference plane differing from the plane in which the orbit lies We may therefore assimilate v with u, without restricting the generality In this case we may write

$$u = n\ t, \tag{7}$$

where n is the mean motion, given by:

$$n = 2\pi/T = \mu^{1/2}a^{-3/2}, \tag{8}$$

in which μ is the gravitational parameter of the attracting body and T will henceforward denote the orbital period of the body m (according to our considerations T is a nodal period). It is also clear from (7) that we considered the moment at which the body m passes through the ascending node as the origin of time ($t = 0$)

We shall study what deformations undergoes the initially circular orbit under the disturbing influence of the radiation pressure, after a revolution of the body m (or after a period T) For this purpose, consider the Newton—Euler equations for the osculating orbital elements. The equation corresponding to the eccentricity e has the form:

$$de/du = Z\ \mu^{-1}\ a^2 S \sin u, \tag{9}$$

where we took into account the above considerations. For integration purposes one usually considers $Z \cong 1$ (see, *e.g.*, [1]).

The variation of the eccentricity over a period is given by:

$$\Delta e = \int_0^{2\pi} (de/du)du, \tag{10}$$

or:

$$\Delta e = \int_0^T (de/dt)dt. \tag{11}$$

We shall use this last equation Taking into account the formulae (6)—(9), the integrand of the equation (11) has the form.

$$de/dt = K\, \mu^{-1/2} a^{-3/2} (1 + a_p \sin(n_p t)) \sin(nt) \tag{12}$$

Now, we take into account the fact that $\int_0^T \sin(nt)dt = 0$, with this and with (12), the variation of the eccentricity over a period will acquire the expression

$$\Delta e = K a_p \mu^{-1/2} a_0^{-3/2} \int_0^T \sin(nt) \sin(n_p t) dt, \tag{13}$$

where the index „0'' signifies the value of the respective quantity at the initial moment of the considered period.

Performing the above integral, we obtain

$$\Delta e = (K/\mu) a_p \sin(2\pi n\ /n_c) / ((n_p/n_c)^2 - 1), \tag{14}$$

or, in terms of periods

$$\Delta e = (K/\mu) a_p \sin(2\pi T_c/T_p) / ((T_0/T_p)^2 - 1), \tag{15}$$

where T_p denotes the pulsation period

3. **Deformations of the Orbit.** Taking into account the fact that the initial orbit is circular, we must consider only the case $\Delta e \geqslant 0$ For this purpose, we analysed the sign of the expression (15) for Δe One sees that $\Delta e \geqslant 0$ when:

$$T_c/T_p \in [1/2,\ 3/2] \cup I_1, \tag{16}$$

where we denoted

$$I_1 = \bigcup_{k \in \mathbf{N}^*} [k + 1,\ k + 3/2]. \tag{17}$$

The equality $\Delta e = 0$ (i e the eccentricity does not change) occurs for all extremities of the above intervals

Observe that $T_0 = T_p$ ($n_0 = n$) leads to an indeterminacy in the equation (15) or (14). In this case we way apply l'Hospital's rule or integrate directly the equation (13) for $n = n_p$, obtaining

$$\Delta e = \pi (K/\mu) a_p. \tag{18}$$

Now we consider the case $\Delta e < 0$ (which cannot be taken into account). This situation occurs when

$$T_0/T_p \in (0,\ 1/2) \cup I_2, \tag{19}$$

where we denoted

$$I_2 = \bigcup_{k \in \mathbb{N}^*} (k + 1/2,\ k + 1) \tag{20}$$

If we plot Δe (in $(K/\mu)a_p$ units) versus the ratio T_0/T_p, we obtain that a significant variation Δe ("normalized") takes place only for small values of the T_0/T_p ratio As to the real values of this variation, they will be estimated in the next section.

4 **Numerical Estimates.** Considering the equation (15), we can easily deduce that the maximum variation of the eccentricity, after one period, will be.

$$(\Delta e)_{\max} = 3\,172 \quad (K/\mu)a_p, \tag{21}$$

which occurs for $T_0/T_p = 0\,961$ We take also into account the fact that [10]

$$K/\mu \cong 6 \cdot 10^{-5} \rho r' (L_0/L_\odot)/(M/M_\odot), \tag{22}$$

or .

$$K/\mu \cong 2\,5 \cdot 10^{-4} (r'^2/m)(L_0/L_\odot)/(M/M_\odot), \tag{23}$$

formulae in which ρ (the density of the orbiting body) is expressed in g/cm^3, r' is expressed in cm and m in grammes So, the formula (21) becomes:

$$(\Delta e)_{\max} \cong 8 \cdot 10^{-4} (r'^2/m) a_p (L_0/L_\odot)/(M/M_\odot), \tag{24}$$

obviously, with the condition $T_0/T_p = 0\,961$.

We shall firstly consider an RR Lyrae pulsating star; such stars are adequate since their masses and luminosities are generally known [6] Before applying the formula (24), we shall see whether such a case may occur. For this purpose, we estimate the radius of the initial orbit·

$$a_0 \cong (0.9\ \mu (T_p/(2\pi))^2)^{1/3}. \tag{25}$$

Taking roughly into account the following parameters for such a star [2, 9, 11] $T_p = 0\,6$ days, $M = 1{,}5 \cdot 10^{33}$g, one obtains $a_0 = 2 \cdot 10^{11}$ cm. But the radius of the star reaches more than $3 \cdot 10^{11}$ cm; therefore the formula (24) cannot be applied in the case of an RR Lyrae star.

Remaining to such stars, let us consider a particle orbiting around an RR Lyrae variable with a period such that T_0/T_p is of the order 10^2. Taking into account the fact that (see [9])·

$$(L_0/L_\odot)/(M/M_\odot) \cong 0.5 \cdot 10^2, \tag{26}$$

and considering the r'^2/m ratio of the order of unity, we obtain from the formula (15) that $\Delta e < 10^{-6}$, namely, after one revolution, the particle practically returns to its circular orbit.

Let us consider now a long-periodic pulsating star, in order to may apply the formula (24). Suppose that the orbiting body is a fictitious artificial satellite with the physical and geometrical features of PAGEOS 1 [5] For such a balloon satellite, we obtain that $r'^2/m \cong 42$. Let us also consider that this satellite orbits at such a distance that $T_0/T_p = 0.961$. In this case, (24) yields:

$$\Delta e \cong (1/30)a_p(L_0/L_\odot)/(M/M_\odot). \tag{27}$$

This means that, if the considered long-periodic pulsating star is such that $a_p(L_0/L_\odot)/(M/M_\odot) \geqslant 30$, the initially circular orbit of the body m is unstable; it becomes unbound after merely one revolution.

5. **Comments.** We see that, in order to obtain significant changes of the eccentricity after one revolution, the star must have a long enough pulsation period; also, the orbiting body must have a great area-to-mass ratio. Generally, the perturbations turn out to be very small, but cases in which the eccentricity can undergo a sensible increase are also possible. Moreover, there are also cases when the eccentricity growth can make the orbit unbound.

However, a question remains: what happens with orbiting bodies having revolution periods which fulfil the condition (19)? Although decreases of the initial eccentricity after one revolution cannot be admitted (namely negative values for the eccentricity), such orbits are nevertheless equally probable as those for which the condition (16) is fulfilled. This question will be treated elsewhere

A last remark the problem of the behaviour of the initially circular orbits around pulsating stars can also be treated by using the changing gravitational parameter theory (see [4, 7, 8]). Nevertheless, the methods and results exposed in the quoted works are valid for the orbit evolution along very large time intervals, while the present results concern a time interval of one revolution only.

REFERENCES

1. G. A. Chebotarev, "Analytical and Numerical Methods of Celestical Mechanics", Nauka, Moscow (1965) (Russ.).
2. R. F. Christy, *Astrophys. J.*, **144**, 108 (1966).
3. G. N. Duboshin, "Celestial Mechanics. Basic Problems and Methods", Gos Izd. Fiz.—Mat. Lit., Moscow (1963) (Russ.).
4. I. Giurgiu, Thesis, University of Cluj-Napoca (1988)
5. D. G. King—Hele, H. Hiller, J. A. Pilkington, "Revised Table of Earth Satellites", Vol. 1, Farnborough (1978).
6. N Lungu, „Pulsații stelare. Teorie matematică". Ed. științifică și enciclopedică, București (1982).
7. V. Mioc, Á Pál, I. Giurgiu, *Babeș—Bolyai Univ., Fac. Math. Phys. Res. Sem.*, Preprint **1**, 79 (1988).
8. V. Mioc, Á. Pál, I. Giurgiu, *Studia Univ. Babeș—Bolyai, Physica*, **33**, No. 2, 85 (1988).
9. V. Pop, *Babeș—Bolyai Univ., Fac. Math Res. Sem.*, Preprint 2, 64 (1985)
10. W C. Saslaw, *Astrophys J.*, **226**, 240 (1978).
11. R. F Stellingwerf, *Astrophys. J.*, **195**, 441 (1975).

STUDIA UNIV. BABEŞ–BOLYAI, PHYSICA, XXXIV, 2, 1899

ON THE TWO-BODY PROBLEM WITH CYCLICALLY CHANGING GRAVITATIONAL PARAMETER

VASILE MIOC*

Received: September 4, 1989

ABSTRACT. — The orbital motion in the frame of the two-body problem with changing gravitational parameter is studied Estimates for some osculating orbital elements in the case of a monotonic variation of the gravitational parameter are presented These estimates are used to the study of the orbital motion under the influence of a cyclic variation (constant amplitude, but changing frequency) of gravitational parameter, considering an initially elliptic orbit. Conditions for the stability of the motion (neither fall, nor escape) during an arbitrary number of cycles of the gravitational paramater are given

1 **Introduction.** The two-body problem with variable mass was studied by many authors (*e g* [4, 5, 7, 17]), from different points of view and by various methods The physical frame of this problem is the following one, a point mass m orbits at a distance r another point mass M, under the influence of the gravitational attraction of this last one Of course, the motion is plane and featured by the equation (*e g.* [16])

$$d^2r/dt^2 - C^2/r^3 = -G(M+m)/r^2, \tag{1}$$

where C is the constant angular momentum, while G is the gravitational constant If the masses are constant, we are in the frame of the standard two-body problem, which is well known and studied The two-body problem with variable mass assumes that the sum of the masses changes in time (usually due to the time-dependence of M). In this case the motion remains plane and is described by the same equation (1), but the numerator of the right-hand member is function of time

This problem is a peculiar case of a more general one the two-body problem with variable gravitational parameter The features of this problem, formulated in [9], are given below

2. **Variable Gravitational Parameter.** Consider the same dynamic system as in the classical two-body problem, but this time the point mass m is also subjected to a perturbing force (of unspecified nature) which is central (its support containing the attractive centre M), acts continuously and obeys an inverse square law. The relative motion of m will still de plane, the equation which describes this motion will be:

$$d^2r/dt^2 - C^2/r^3 = -G(M+m)/r^2 + K/r^2, \tag{2}$$

where K/r^2 is the perturbing acceleration undergone by m as an effect of the above mentioned perturbing force.

* *Centre for Astronomy and Space Sciences, 3400 Cluj-Napoca, Romania*

With the general hypothesis that the quantities M, m, K and even G are time-dependent

$$M = M(t), \quad m = m(t), \quad K = K(t), \quad G = G(t), \tag{3}$$

the equation of motion acquires the form:

$$d^2r/dt^2 - C^2/r^3 = -\mu/r^2, \tag{4}$$

where we denoted

$$\mu = \mu(t) = G(M + m) - K \tag{5}$$

The equation (4) has the same form as the equation of motion in the classical two-body problem (if μ were constant, the respective equation describes the standard Kepler problem) For this reason, although the nature of the perturbing force is not specified, we called μ of the form (5) variable gravitational parameter

The variation of μ in this general meaning can be due to different factors or combinations of factors We give here some examples: the variation of M is the most used condition (see above): the variation of both masses was considered in [1], the variation of G is assumed in [6, 20], the problem with time-dependent M and/or G is studied in [19], lastly, the variation of K (due in the quoted papers to the luminosity change of the central body) was considered in [10, 14, 18]

Different aspects of the orbital motion with changing gravitational parameter were studied in [2, 3, 8—15], either for a specified law of variation, or for the case when only the type of variation (monotonic, periodic, stochastic, mixed) is precised Every peculiar or more general case can be applied to the study of a concrete astronomical problem or situation (for details see [2]).

3 **Monotonic Variation of the Gravitational Parameter.** In the next two sections we shall assume that the gravitational parameter changes monotonically in time (increases or decreases continuously) The study of the motion in these conditions can be performed by using various methods. For instance, one can use the general method described in [9], based on the stroboscopic averaging method The theory of the adiabatic invariants can also be applied, as in [19]. We also mention the method used in [5], or those used in [3] and [4] for the study of the evolution of the osculating orbit.

The essential condition which must be fulfilled along the time interval $[t_1, t_2]$ on which the motion is studied is .

$$d\mu/dt \geqslant 0, \quad \forall t \in [t_1, t_2] \subset \mathbf{R}, \tag{6}$$

for monotonically increasing gravitational parameter, or:

$$d\mu/dt \leqslant 0, \quad \forall t \in [t_1, t_2] \subset \mathbf{R}, \tag{7}$$

for monotonically decreasing gravitational parameter.

4. **Basic Equations.** The starting equation for this study is the equation (4) of the trajectory, in which $\mu = \mu(t)$ is in our case a continuous, monotonic

function of time. Since the point mass m moves under the influence of a central resulting force, its motion observes the theorem of angular momentum:

$$r^2\, du/dt = C, \tag{8}$$

where u is the argument of latitude, taken here as polar argument in the system of polar coordinates $(r,\ u)$

Another basic equation we use is the integral of energy written in the same polar coordinates $(r,\ u)$:

$$(dr/dt)^2 + r^2(du/dt)^2 = 2\mu/r + h \tag{9}$$

In the standard two-body problem, μ (the purely gravitational parameter) is constant, and h as well (h denotes the constant of energy) In the present case both μ and h are time-dependent The quantity $h = h(t)$ was called in [4] the quasi-integral of energy

If we remove du/dt between (8) and (9), the integral of energy can be written as a prime integral of the trajectoty equation (4) under the form

$$(dr/dt)^2 + C^2/r^2 - 2\mu/r = h \tag{10}$$

Differentiating this equation with respect to time and taking into account the equation of motion (4), we obtain the law describing the time-variation of h:

$$dh/dt = -(2/r)d\mu/dt, \tag{11}$$

or, immediately, the dependence of h on the gravitational parameter

$$dh/d\mu = -2/r. \tag{12}$$

Starting from these formulae, we determined in [3] the osculating orbit of the point mass m at an arbitrary instant For the present study, we shall use only few orbital elements, namely the eccentricity

$$e = (1 + C^2h/\mu^2)^{1/2}, \tag{13}$$

and the distance of the pericentre

$$q = r_{\min} = (C^2/\mu)/(1 + e) \tag{14}$$

If the osculating orbit is elliptic, the apocentre does exist, too, and its distance is given by the formula

$$Q = r_{\max} = (C^2/\mu)/(1 - e). \tag{15}$$

In this case, we obviously have

$$q \leqslant r \leqslant Q. \tag{16}$$

A fact must be emphasized: since the real orbit is a perturbed one, the elements e, q and Q refer to the osculating orbit corresponding to a given instant t.

5. Basic Inequalities for the Initially Elliptic Motion. In [4] there were given double-sided estimates for some osculating orbital elements in the case of the monotonically changing gravitational parameter (whose time-dependence is due to the time-dependence of M) For this purpose, the following double inequality was used

$$-2\mu(1+e)/C^2 \leqslant dh/d\mu \leqslant -2\mu(1-e)/C^2, \tag{17}$$

which can easily be deduced from (12), (14), (15) and (16). Of course, the first inequality is valid for every type of orbit, while the second one is deduced with the assumption that the osculating orbit is elliptic.

Let us mark by the index "0" the values corresponding to the initial instant. Let also suppose that the initial motion is performed on an elliptic-type orbit ($e_0 < 1$ or $h_0 < 0$). The estimates given in [4] are obtained in two main situations:

(A) $\mu \geqslant \mu_0$, with the subcases:

$$\begin{aligned}&(\mathrm{A1}): \mu \leqslant \mu_0(1+e_0),\\ &(\mathrm{A2}): \mu \geqslant \mu_0(1+e_0);\end{aligned} \tag{18}$$

(B) $\mu \leqslant \mu_0$, with the subcases:

$$\begin{aligned}&(\mathrm{B1}): \mu \geqslant \mu_0(1-e_0),\\ &(\mathrm{B2}): \mu \geqslant \mu_0(1-e_0);\end{aligned} \tag{19}$$

$$\begin{aligned}&(\mathrm{B'1}): \mu \leqslant \mu_0(1-e_0)/2,\\ &(\mathrm{B'2}): \mu \leqslant \mu_0(1-e_0)/2.\end{aligned} \tag{20}$$

Obviously, the cases (A) correspond to the motion with increasing gravitational parameter, while the cases (B) feature the motion with decreasing gravitational parameter.

The above mentioned double-sided estimates, determined by starting from (17), are the following ones:

$$1-(\mu_0/\mu)(1-e_0) \geqslant e \geqslant \begin{cases}(\mu_0/\mu)(1+e_0)-1, & (\mathrm{A1}),\\ 0, & (\mathrm{A2});\end{cases} \tag{21}$$

$$C^2/(2\mu-\mu_0(1-e_0)) \leqslant q \leqslant \begin{cases}q_0 = C^2/(\mu_0(1+e_0)), & (\mathrm{A1}),\\ C^2/\mu, & (\mathrm{A2}),\end{cases} \tag{22}$$

$$Q_0 = C^2/(\mu_0(1-e_0)) \geqslant Q \geqslant \begin{cases}C^2/(2\mu-\mu_0(1+e_0)), & (\mathrm{A1}),\\ C^2/\mu, & (\mathrm{A2});\end{cases} \tag{23}$$

$$h_0 - 2(\mu-\mu_0)/Q_0 \geqslant h \geqslant \begin{cases}h_0 - 2(\mu-\mu_0)/q_0, & (\mathrm{A1}),\\ -\mu^2/C^2, & (\mathrm{A2});\end{cases} \tag{24}$$

$$(\mu_0/\mu)(1+e_0)-1 \geqslant e \geqslant \begin{cases}1-(\mu_0/\mu)(1-e_0), & (\mathrm{B1}),\\ 0, & (\mathrm{B2});\end{cases} \tag{25}$$

$$q_0 = C^2/(\mu_0 (1 + e_0)) \leqslant q \leqslant \begin{cases} C^2/(2\mu - \mu_0(1 - e_0)), & \text{(B1)}, \\ C^2/\mu, & \text{(B2)}, \end{cases} \tag{26}$$

$$Q_0 = C^2/(\mu_0(1 - e_0)) \leqslant Q \leqslant \begin{cases} C^2/(2\mu - \mu_0(1 + e_0)), & \text{(B'1)}, \\ \infty, & \text{(B'2)}, \end{cases} \tag{27}$$

$$h_0 - 2(\mu - \mu_0)/q_0 \geqslant h \geqslant \begin{cases} h_0 - 2(\mu - \mu_0)/Q_0, & \text{(B1)}, \\ -\mu^2/C^2, & \text{(B2)} \end{cases} \tag{28}$$

Remark 1 If, for instance, we consider $e_0 \to 1$ (near parabolic initial orbit) in the left-hand sides of the estimates (22) and (23), we obtain

$$C^2/(2\mu) < q \leqslant C^2/\mu \leqslant Q < \infty. \tag{29}$$

These limits were found by us in [3, 13]. Other such results obtained by us in the quoted papers (concerning, for instance, the orbital energy) can also be found again on the basis of the series of estimates (21)—(28)

6. **Cyclic Variation of the Gravitational Parameter.** Let us now consider a special type of variation of the gravitational parameter Suppose that μ reaches successive maxima and minima, and, in addition, all maxima are equal to a fixed value $\mu_{\max}$, while all minima are equal to another fixed value $\mu_{\min}$ In other words, plotting μ versus time, one obtains a curve whose maxima are all lying on a parallel to the time axis (which is the axis $\mu = 0$) at a distance $\mu_{\max}$ from this one, and whose minima are all situated on another parallel to the time-axis at a distance $\mu_{\min}$ from this one On this curve, the variation of μ between two neighbouring extremal points is monotonic.

We shall call *cyclic variation* this kind of variation of the gravitational parameter. Let us justify this denomination, for this purpose, consider a parallel to the time-axis, situated at a distance $\mu_0 \in [\mu_{\min}, \mu_{\max}]$ from this one Denote by μ_0^i, μ_0^{i+1}, μ_0^{i+2}, . the intersections of this parallel with the i—th, $(i + 1)$-th, $(i + 2)$-th, ... branches of the same type (ascendent or descendent) of the curve, respectively. Also denote by t_i^0, t_{i+1}^0, t_{i+2}^0, the moments of time corresponding respectively to the mentioned intersections. In other words

$$\mu(t_i^0) = \mu_0^i = \mu(t_{i+1}^0) = \mu_0^{i+1} = \mu(t_{i+2}^0) = \mu_0^{i+2} = \ldots = \mu_0, \tag{30}$$

namely t_i^0, t_{i+1}^0, t_{i+2}^0, represent the moments when μ reaches the value μ_0 on branches of the same type of the curve During every interval $[t_i^0, t_{i+1}^0)$, $[t_{i+1}^0, t_{i+2}^0)$, etc, μ reaches in a certain order all possible values between $\mu_{\min}$ and $\mu_{\max}$, each such a value is reached twice (obviously, except the values $\mu_{\max}$ and $\mu_{\min}$, which are each reached once) That is why we called cyclic the variation of μ An interval $[t_i^0, t_{i+1}^0)$ will be called by us μ_0-cycle (associated to the value μ_0) However, in the following we shall consider that the end of a cycle coincides with the beginning of the next cycle (*i.e* we shall consider the cycles as closed intervals).

An essential fact must be emphasized. For a given $\mu = \mu_0$, the μ_0-cycles are not of the same length; also, for a given $\mu = \mu_1$, the μ_1-cycles are different each other. Moreover, if $\mu_0 \neq \mu_1$, we have, generally, with our notations:

$$t^0_{i+1} - t^0_i \neq t^1_{i+1} - t^1_i, \tag{31}$$

namely the cycle defined by two successive ascending (or descending) branches (the i-th and the (i + 1)-th ones) has a variable length, according to the value of μ chosen for the beginning of the cycle.

With these considerations, we see that the cyclic variation of the gravitational parameter is more general than a periodic variation (with only primary maxima and minima). Indeed, a cyclic variation (in the above defined meaning) for which all cycles have the same length is a periodic variation. This peculiar case of cyclic variation of μ (periodic variation) was studied in [2, 15, 18].

7. Evolution of the Initially Elliptic Orbit over One Cycle. It is clear now that the orbital motion in the case of a cyclic variation of the gravitational parameter can be studied cycle by cycle. Consider such a cycle of length $T_1 = t_1 - t_0$ and a partition of this cycle

$$t_0 \leqslant t_a < t_b \leqslant t_1, \tag{32}$$

such that:

$$\mu(t_0) = \mu_0, \ \mu(t_a) = \mu_{\max}, \ \mu(t_b) = \mu_{\min}, \ \mu(t_1) = \mu_0. \tag{33}$$

The manner in which this cycle, determined by (32) and (33), is chosen shows that the initial instant corresponds to an ascending branch of the curve $\mu(t)$. In other words, during this cycle, μ increases, reaches its maximum (at t_a), then decreases, reaches its minimum (at t_b), then increases again upto its initial value (at the moment t_1). If the cycle is chosen such that:

$$\mu(t_0) = \mu_0, \ \mu(t_a) = \mu_{\min}, \ \mu(t_b) = \mu_{\max}, \ \mu(t_1) = \mu_0, \tag{34}$$

namely μ evolves conversely (decrease — increase — decrease), only the intermediate results (at t_a and t_b) will differ from the previous case. The results at the end of the cycle are the same, as we shall see.

Coming back to the cycle defined by (32) and (33), we shall study the motion applying successively the estimates (21) — (28) to each of the three intervals: $[0, t_a]$, $[t_a, t_b]$ and $[t_b, t_1]$. We may proceed in this way since during each such an interval the variation of the gravitational parameter is monotonic. As to the notations, each considered parameter will be marked by the same index as the corresponding instant (e.g. $e(t_0) = e_0$ and so on).

Let the initial orbit be elliptic ($e_0 < 1$). For the eccentricity, the estimates (21) can be written in the form:

$$(\mu_0/\mu_{\max})(1 + e_0) - 1 \leqslant e_a \leqslant 1 - (\mu_0/\mu_{\max})(1 - e_0). \tag{35}$$

Applying (25) to (35), we find after calculations:

$$(\mu_0/\mu_{\min})(1 + e_0) - 2(\mu_{\max}/\mu_{\min}) + 1 \leqslant e_b \leqslant$$
$$\leqslant 2(\mu_{\max}/\mu_{\min}) - (\mu_0/\mu_{\min})(1 - e_0) - 1 \tag{36}$$

Finally, by (21) and (36), we obtain the estimates for the osculating eccentricity at the end of the cycle

$$e_0 - 2A \leqslant e_1 \leqslant e_0 + 2A, \tag{37}$$

where, for simplicity, we denoted by A the ratio

$$A = (\mu_{\max} - \mu_{\min})/\mu_0, \tag{38}$$

namely a relative amplitude of the cyclic variation of the gravitational parameter.

For the distance of the pericentre, the estimates (22) acquire in this case the form:

$$C^2/(2\mu_{\max} - \mu_0(1 - e_0)) \leqslant q_a \leqslant q_0 = C^2/(\mu_0(1 + e_0)) \tag{39}$$

The estimates (26) applied to (39) give after calculations

$$C^2/(2\mu_{\max} - \mu_0(1 - e_0)) \leqslant q_a \leqslant q_b \leqslant C^2/(\mu_0(1 + e_0 - 2A)). \tag{40}$$

The distance of the pericentre at the end of the cycle can be estimated from (40) to which one applies (22)

$$C^2/(\mu_0(1 + e_0 + 2A)) \leqslant q_1 \leqslant q_b \leqslant C^2/(\mu_0(1 + e_0 - 2A)) \tag{41}$$

Finally, we estimate the distance of the apocentre By (23) we have in our case

$$C^2/(2\mu_{\max} - \mu_0(1 + e_0)) \leqslant Q_a \leqslant Q_0 = C^2/(\mu_0(1 - e_0)) \tag{42}$$

From (27) and (42) we find

$$C^2/(2\mu_{\max} - \mu_0(1 + e_0)) \leqslant Q_a \leqslant Q_b \leqslant C^2/(\mu_0(1 - e_0 - 2A)), \tag{43}$$

while applying (23) to (43) one obtains the estimates for the apocentric distance at the end of the cycle

$$C^2/(\mu_0(1 - e_0 + 2A)) \leqslant Q_1 \leqslant Q_b \leqslant C^2/(\mu_0(1 - e_0 - 2A)) \tag{44}$$

Remark 2. The above results constitute estimates for the osculating elements e, q and Q at the significant instants of the considered cycle of length T_1. If such a cycle (of length T_1) is performed conversely by the gravitational parameter, namely observing (34), only the intermediate estimates are different.

For instance, using the same procedure, the estimates for the eccentricity at t_a and t_b are respectively:

$$1 - (\mu_0/\mu_{\min})(1 - e_0) \leqslant e_a \leqslant (\mu_0/\mu_{\min})(1 + e_0) - 1, \tag{45}$$

$$2(\mu_{\min}/\mu_{\max}) - (\mu_0/\mu_{\max})(1 - e_0) - 1 \leqslant e_b \leqslant$$

$$\leqslant (\mu_0/\mu_{\max})(1 + e_0) - 2(\mu_{\min}/\mu_{\max}) + 1. \tag{46}$$

As to the eccentricity at the end of the cycle defined by (32) and (34), from (25) and (46) one obtains the same estimate (37) as in the case of the cycle defined by (32) and (33).

Remark 3 Consider a cycle defined by

$$t_0 < t_a < t_1, \tag{47}$$

such that:

$$\mu(t_0) = \mu_{\min} = \mu_0, \ \mu(t_a) = \mu_{\max}, \ \mu(t_1) = \mu_0, \tag{48}$$

namely a peculiar case of the cycle (32) — (33) In this case, the estimates (37) or the eccentricity at the end of the cycle become

$$e_0 - 2(\mu_{\max}/\mu_0 - 1) \leqslant e_1 \leqslant e_0 + 2(\mu_{\max}/\mu_0) - 1 \tag{49}$$

This result was obtaine d in [4], where a cycle defined by the relationships (47) — (48) was considered

Remark 4 Consider the cycle defined by (32) — (33) and the estimates (37) for the final eccentricity. The left-hand side inequality of the estimate (37) passes into the triv al inequality $e_1 \geqslant 0$ for

$$A \geqslant e_0/2 \tag{50}$$

If the condition:

$$A < e_0/2 \tag{51}$$

is fulfilled, the final eccentricity cannot become zero (the osculating orbit corresponding to the instant t_1 cannot be circular) In order to have $e_1 < 1$, the following condition

$$A < (1 - e_0)/2 \tag{52}$$

must be fulfilled It is interesting that the conditions (51) and (52) coincide for $e_0 = 0.5$, in other words, an orbit with this initial eccentricity remains purely elliptic at the end of the cycle (it cannot become neither circular, nor parabolic or hyperbolic) In the peculiar case of the cycle defined by (47) — (48), the amplitude A is replaced in (50) — (52) by $\mu_{\max}/\mu_0 - 1$, the formulae obtained in this way coincide with the similar conditions given in [4]

8 **Evolution of the Initially Elliptic Orbit During Long Time Intervals.** The estimates for the orbital parameters e, q and Q corresponding to the osculating orbit at the end of one cycle are given by (37), (41) and (44), respectively. Let us now see what happens after a time interval including n cycles (obviously, of different lengths). For this purpose, we shall denote by y_j, $j = 1, n$, the value of the element $y \in \{e, q, Q\}$ at the end of the j-th cycle. Since at the beginning of each cycle the gravitational parameter has the same value μ_0, we obtain the estimates for y_2 applying (37), (41) and (44) to y_1. One easily obtains, for instance, the estimates for the eccentricity e_2.

$$e_0 - 4A \leqslant e_2 \leqslant e_0 + 4A \tag{53}$$

The estimates for q_2 and Q_2 are obtained analogously

Generalizing, we repeat the procedure $n - 1$ times in order to obtain estimates for the elements y_n. So, the estimates for the eccentricity after n cycles are:

$$e_0 - 2nA \leqslant e_n \leqslant e_0 + 2nA \tag{54}$$

From (41) one obtains the estimates for the distance of the pericentre after n cycles:

$$C^2/(\mu_0(1 + e_0 + 2nA)) \leqslant q_n \leqslant C^2/(\mu_0(1 + e_0 - 2nA)) \tag{55}$$

Finally, the estimates for the distance of the apocentre at the end of the n-th cycle are determined from (44) in the form

$$C^2/(\mu_0(1 - e_0 + 2nA)) \leqslant Q_n \leqslant C^2/(\mu_0(1 - e_0 - 2nA)) \tag{56}$$

Remark 5. As in the case of Remark 4, one notices that for $A \geqslant e_0/(2n)$ the left-hand side inequality (54) passes into the trivial inequality $e_n \geqslant 0$. The eccentricity e cannot reach the value zero (circular orbit) as long as the condition:

$$A < e_0/(2n) \tag{57}$$

is fulfilled, and cannot reach or exceed the unit (unbound orbit) if the inequality:

$$A < (1 - e_0)/(2n) \tag{58}$$

holds. The conditions (57) and (58) coincide for $e_0 = 0.5$, as in the case of the conditions (51) and (52).

9 **Stability Conditions.** There are two limit situations for an initially elliptic orbit which is continuously perturbed: the radius vector becomes zero (the point mass m falls on the attractive body M) or the orbit becomes unbound (parabolic or hyperbolic, $e \geqslant 1$). As long as no such a limit situation occurs, we say that the orbit is stable. We shall examine the stability conditions for an initially elliptic orbit in the case when the gravitational parameter changes cyclically (in the meaning of the two previous sections).

Consider, firstly, the fall situation. One easily notices from (16), (55) and (56) that the radius vector cannot become zero (in other words, m cannot fall on M). Of course, this situation changes if we consider M as being a body of nonzero and finite dimensions.

Denote by R the radius of the central body. The nonfall condition after n cycles is:

$$q_n > R. \tag{59}$$

Using the estimates (55), the condition (59) becomes

$$n \leqslant (C^2/(\mu_0 R) - (1 + e_0))/(2A), \tag{60}$$

where the necessary condition $C^2/(\mu_0 R) > 1 + e_0$ is fulfilled for an initial real orbit if we use (14) and the trivial inequality $q_0 > R$.

The inequality (60) shows that, at least as long as the number n of cycles fulfils this condition, the orbit remains stable from the point of view of the fall (m does not fall on M).

Let us consider now the other limit situation, namely the escape. Taking into account the inequality (58), the condition for nonescape after n cycles is:

$$n \leqslant (1 - e_0)/(2A). \tag{61}$$

In other words, at least as long as the number n of cycles fulfils the condition (61), the orbit remains stable from the point of view of the escape (its osculating eccentricity does not reach the unit).

Examining the stability conditions (60) and (61), we notice that two situations can occur. If the condition

$$C^2/\mu_0 \leqslant 2R \tag{62}$$

is fulfilled, then (61) is a consequence of (60). Conversely, if the opposite condition:

$$C^2/\mu_0 \geqslant 2R \tag{63}$$

is fulfilled, then (60) is a consequence of (61). In the case in which $C^2/\mu_0 = 2R$, the conditions (60) and (61) are equivalent.

Remark 6. It is clear that the probability for escape is maximum when μ reaches its minimum value. Let us find the nonescape condition for the instant $\mu = \mu_{min}$ inside the n-th cycle. Using (36), this condition acquires the form:

$$2(\mu_{max}/\mu_{min}) - (\mu_0/\mu_{min})(1 - e_{n-1}) - 1 < 1, \tag{64}$$

from which, taking into account (54), one obtains the already established condition (61).

Remark 7. The nonescape condition at the end of the n-th cycle can also be formulated in another way, namely imposing the condition $r_n < \infty$, where

r_n denotes the radius vector of m on the osculating orbit corresponding to this instant Using (16) and (56), this condition is equivalent to (61)

Remark 8 Since when $\mu = \mu_{min}$ the escape probability reaches its maximum, let us determine, as we made in the case of Remark 6, the nonescape condition for the respective moment inside the n-th cycle, but using this time the condition $r < \infty$ Using (16) and (43), this condition becomes

$$C^2/(\mu_0(1 - e_{n-1} - 2A)) < \infty, \tag{65}$$

from which, taking into account (54), we obtain once again the condition (61)

Remark 9 We notice from (60) that the greater C^2/μ_0 and the smaller e_0 are (namely the higher q_0 is), the greater the number of cycles to elapse until a possible fall on the attractive body will be The same formula shows that the smaller A is, the greater n will be Also notice from (61) that the smaller e_0 and A are, the greater the number of cycles to elapse until a possible escape will be.

Resuming, we may assert that, for a dynamic system (M, m) whose gravitational parameter undergoes a cyclic variation (in our meaning constant amplitude, but variable frequency), the initially elliptic relative orbit of the attracted point mass remains stable (neither fall, nor escape) at least as long as the number of elapsed cycles fulfil the conditions (60) and (62) or (61) and (63) On the basis of this result, physical conditions which ensure the stability of the orbit during a long time interval are slow variation of the gravitational parameter (long cycles), small amplitude of this variation, initial orbit of small eccentricity and great pericentric distance

REFERENCES

1. G N. Duboshin, "Celestial Mechanics. Basic Problems and Methods", Gos Izd Fiz.—Mat. Lit, Moscow (1963) (Russ).
2. I Giurgiu, *Thesis,* University of Cluj-Napoca (1988)
3. I Giurgiu, V Mioc, *Studia Univ. Babeş—Bolyai, Physica,* **33,** No 2 94 (1988).
4. L G Glikman, *Astron. Zh*, **53,** 185 (1976).
5. L. G. Glikman, *Astron. Zh*, **55**, 873 (1978).
6. R. A Lyttleton, J P Finch, *Astrophys J.*, **221,** 412 (1978)
7. I V Meshchersky, "Works in the Mechanics of Bodies of Variable Mass", Gostehizdat, Moscow, Leningrad (1949) (Russ)
8. V. Mioc, *Babeş—Bolyai Univ, Fac. Mat Phys Res Sem,* Preprint **10,** 63 (1988)
9. V. Mioc, Á Pál, I Giurgiu, *Babeş—Bolyai Univ, Fac. Math. Phys. Res. Sem*, Preprint **1,** 79 (1988)
10. V Mioc, Á Pál, I Giurgiu, *Babeş—Bolyai Univ., Fac Math. Phys. Res. Sem.*, Preprint **4,** 41 (1988)
11. V. Mioc, Á Pál, I Giurgiu, *Babeş—Bolyai Univ., Fac. Math. Phys. Res. Sem*, Preprint **10,** 3 (1988)
12. V. Mioc, Á. Pál, I Giurgiu, *Babeş—Bolyai Univ, Fac. Math. Phys. Res. Sem*, Preprint **10,** 21 (1988).

13. V Mioc, Á. Pál, I. Giurgiu, *Babeş—Bolyai Univ, Fac Math Phys Res Sem*, Preprint **10**, 91 (1988).
14 V Mioc, Á Pál, I. Giurgiu, *Studia Univ Babeş—Bolyai, Physica*, **33**, No 2, 85 (1988)
15. V Mioc, Á Pál, I Giurgiu, *Studia Univ. Babeş—Bolyai*, Mathematica, **33**, No 4, 67 (1988)
16 F. R Moulton, "An Introduction to Celestial Mechanics", 13-th ed, Macmillan, New York (1959)
17. V V Radzievsky, B E Gelfgat, *Astron. Zh*, **34**, 581 (1957)
18 W. C Saslaw, *Astrophys. J.*, **226**, 240 (1978).
19 M P Savedoff, S Vila, *Astron J*, **69**, 242 (1964)
20. C M Will, *Astrophys. J*, **169**, 141 (1971).

STUDIA UNIV BABEŞ–BOLYAI, PHYSICA, XXXIV, 2, 1989

EXTENSION OF A RESULT CONCERNING THE DYNAMICS OF EXPANDING SHELLS

VASILE MIOC*

Received October 10, 1989

ABSTRACT. – The motion of an expanding shell influenced by the matter accretion on its surface and the attraction of the central body is studied with the assumption that the mass of inner matter is not negligible as against the initial mass of the shell. The stop of the expansion and the subsequent contraction of the shell are pointed out. Formulae which feature both the expansion and the contraction, generalizing the results given in [5], are established.

1 **Introduction.** There are many astronomical phenomena which can entail the formation of expanding shells of matter Such shells appear, for instance, as a consequence of nova and supernova explosions. The matter flowing out of certain stars, as the Wolf–Rayet ones, can also form expanding shells around the respective star. The activity of galactic nuclei and quasars constitutes a possible source of expanding shells, too.

A concise survey of the researches performed on the dynamics of expanding shells was given by Minin [5] So, Oort [9] gave an exact solution of the problem, considering only the shell expansion drag due to the environment (resisting medium), and used the results to the case of late stages of novae. Mustel [7, 8] considered that the shell mass growth is due to two factors the matter captured by the shell (on its exterior surface) from the environment and the matter ejected from the central body which reaches the interior surface of the shell. On the basis of this hypothesis, he studied numerically the shell expansion drag. Exact analytical solutions of the same problem were given by Minin [4] and Gorbatsky and Minin [3] The only influence of the matter ejected from stars on the expansion of their surrounding shells was studied by Gorbatsky and applied to the case of early stages of novae [1, 2]

Recently, Minin [5] studied analytically the shell expansion drag due to two factors the shell mass increase due to the matter captured from the environment, and the gravitational attraction of the central body In this paper we shall give an extension to Minin's results

2. **Hypotheses.** Consider a spherically symmetrical thin shell (its thickness being negligible as against its radius r), of mass m, expanding with the velocity v into a homogeneous medium of density ρ At the initial instant $t = t_0$ the shell and its motion are featured by the following values

$$r(t_0) = r_0, \qquad m(t_0) = m_0, \qquad v(t_0) = v_0. \tag{1}$$

---

* *Centre for Astronomy and Space Sciences, 3400 Cluj-Napoca, Romania*

We define two space positions with respect to the shell. Let d be the distance between an object in space and the attractive centre around which the shell is expanding. We shall hereafter use for the respective object the adjectives *inner* if $d < r$ and *outer* if $d > r$. The medium is divided with respect to the shell into inner medium and outer medium. The matter of which this medium consists is accordingly divided into inner matter and outer matter. Of course, the central body is not considered as belonging to the inner matter.

In order to study the motion of the shell, Minin [5] took into account the following hypotheses.

(i) The gasodynamic effects are neglected.

(ii) The gravitational attraction of the central body is considered.

(iii) The mass of the shell increases during the expansion as a consequence of the capture of outer matter on the exterior surface of the shell.

(iv) The inner matter is not captured by the shell during the expansion (it cannot reach the interior surface of the shell).

(v) The mass of inner matter is negligible as against the initial mass of the shell.

Let us denote by m' the mass of inner matter. The condition (v) is written by Minin [5] under the form

$$m' = (4\pi/3)\rho r_0^3 \ll m_0. \tag{2}$$

These conditions need some specifications. Taking into account the hypotheses (iv) and (v), we see that only at the instant t_0 the inner medium and the outer medium have the same density ρ, as the condition (2) shows. For $t > t_0$, as long as the shell expansion lasts (r increases), only the density of the outer medium keeps its constant value ρ. The density of the inner medium ρ' diminishes as r increases, according to the law

$$\rho' = (r_0/r)^3\rho \tag{3}$$

Consider $t = 0$ as being the instant when the shell is ejected from the central body. Between this instant and the instant t_0, some matter continued to flow out of the central body, but with a speed much lower than the expansion speed of the shell. Also consider that at an instant $t' \in (0, t_0)$ the matter flow ends, the matter flowed out of the central body during the time interval $(0, t']$ has the mass m' and we assume that $m' = (4\pi/3)\rho r_0^3$. In this way, we give an explanation to both the condition (iv) and the existence of a constant mass of inner matter.

As to the condition (i), Minin [5] shows that, even neglecting the gasodynamic effects, the results approximate the reality with a sufficient accuracy.

For our study we shall take into account only the hypotheses (i) — (iv). Rejecting the condition (v), we shall consider that m' has the expression given by (2), but this mass is no longer negligible as against m_0. We obtain in this way an extension of Minin's results exposed in [5].

3. **Expansion Speed.** The equation of motion of the shell can be written by using the well-known theorem of impulse

$$d(mv)/dt = -GMm/r^2, \tag{4}$$

where G is the gravitational constant, M is the mass of the central body, while the other notations were already precised. Since the shell motion is radial, we have:

$$v = dr/dt. \tag{5}$$

Now we can introduce in the equation of motion the independent variable r instead of t. Taking into account (5), equation (4) acquires the form:

$$(m/2)d(v^2)/dr + v^2 dm/dr = -GMm/r^2 \tag{6}$$

The law describing the variation of the shell mass with the shell radius has the form

$$m = m_0 + (4\pi/3)\rho r^3 - (4\pi/3)\rho r_0^3, \tag{7}$$

where we took into account the hypotheses (iii) and (iv)

Introducing, analogously to [5], the notations

$$a(r) = (4\pi/3)\rho r^3/m_0, \tag{8}$$

$$a_0 = a(r_0) = (4\pi/3)\rho r_0^3/m_0, \tag{9}$$

the dependence of the shell mass on its radius will be expressed by the formula:

$$m = m(r) = m_0(1 - a_0 + a(r)) \tag{10}$$

With this, the equation of motion (6) becomes

$$d(v^2)/dr + 6(a(r)/(r(1 - a_0 + a(r))))v^2 = -2GM/r^2, \tag{11}$$

with the initial condition

$$v^2(r_0) = v_0^2 \tag{12}$$

Integrating the equation (11) with the initial condition (12), we obtain

$$v = F(r)/(1 - a_0 + a(r)), \tag{13}$$

where we denoted

$$F^2(r) = v_0^2 - (2GM/r)(-(1 - a_0)^2 + (1 - 3a_0 + 9a_0^2/5)r/r_0 +$$
$$+ (1 - a_0)a(r) + a^2(r)/5) \tag{14}$$

The formula (13) features the variation of the shell expansion speed as function of the shell radius If we consider the hypothesis (v), hence the restriction (2) holds, we have $a_0 \ll 1$ In this situation, considering $a_0 \cong 0$, the equation of motion (13) acquires the form

$$v = F(r)/(1 + a(r)), \tag{15}$$

while the formula (14) reduces to

$$F^2(r) = v_0^2 - (2GM/r)(r/r_0 - 1 + a(r) + a^2(r)/5) \tag{16}$$

The solution (15) — (16) was found by Minin [5]

Coming back to our more general formulae (13) and (14), we observe that the expansion speed decreases montonically as the shell radius increases. Subsequently, there exists a critical value r of the shell radius for which the following equality

$$v_0^2 = (2GM/r_c)(-(1 - a_0)^2 + (1 - 3a_0 + 9a_0^2/5)r_c/r_0 + (1 - a_0)a(r_c) + + a^2(r_c)/5) \tag{17}$$

holds In other words, when the shell radius reaches the value r fulfilling the condition (17), the expansion of the shell ends

In order to estimate the critical radius r, we shall consider (as in [5]) that the following condition is fulfiled

$$v_0^2 \gg 2GM/r_0, \tag{18}$$

which means that the shell has an initial velocity much higher than the corresponding parabolic velocity With the restriction (18) and taking into account (8), the relationship (17) yields

$$r_c^5 = 45\, m_0^2 v_0^2/(32\pi^2 GM\rho^2) \tag{19}$$

The same estimate for r_c was found in [5]

4. **Contraction Speed.** We saw that at an instant t, when the radius of the shell reaches the value r_c, the shell expansion motion is stopped Let us see what happens later, for $t > t_c$ The particles of the shell will begin to move in the opposite direction, towards the central body, hence a contraction of the shell starts

In order to feature analytically the shell contraction, we shall use the same equation of motion (4) As to the mass variation, we shall use the law

$$m = m(r) = m_c + m' - (4\pi/3)\rho' r^3, \tag{20}$$

where we denoted

$$m_c = m(r_c) = m_0(1 - a_0 + a_c) \tag{21}$$

and

$$a_c = a(r_c) = (4\pi/3)\rho r_c^3/m_0 \tag{22}$$

With (21), and taking into account the expressions of m' (given by the first part of (2)) and ρ' (given by (3)), we obtain that the mass of the contracting shell depends on the shell radius according to the law

$$m = m(r) = m_0(1 + a_c - (a_0/r_c^3)r^3) \tag{23}$$

Observe that m continues to increase, since the radius r of the shell is now decreasing

Taking into account the fact that the contraction motion of the shell is also radial (condition expressed by equation (5)), we can use the equation of motion (6). Considering the mass variation as obeying the law (23), the equation of motion acquires the form:

$$d(v^2)/dr - 6((a_0/r_c^3)r^2/(1 + a_c - (a_0/r_c^3)r^3))v^2 = -2GM/r^2, \tag{24}$$

with the initial condition:

$$v^2(r_c) = 0. \tag{25}$$

Integrating the equation (24) with the initial condition (25), we obtain:

$$v = -F_1(r)/(1 + a_c - (a_0/a_c)a(r)), \tag{26}$$

where the minus sign emphasizes the fact that the motion is directed towards the central body, while $F_1(r)$ is given by

$$F_1^2(r) = (2GM/r)((1 + a_c)^2(1 - r/r_c) - a_0(1 + a_c)(r/r_c - a(r)/a_c) + a_0^2(r/r_c - a^2(r)/a_c^2)/5). \tag{27}$$

The formula (26) features the variation of the shell contraction speed as function of the shell radius Examining the formulae (26) and (27), we see that the denominator in the right-hand member of (26) increases as r decreases, tending to the value $1 + a_c$ when r tends to zero, while $F_1(r)$ tends to infinity when r tends to zero It follows that the velocity will tend to infinity for $r \to 0$ and this result is in agreement with the collision theory. In other words, the contraction motion is accelerated and the sheel ends by falling on the central body.

5. Expansion and Contraction Time Scales. The estimate of the time scales for expansion and contraction of the shell is of a great interest Let us denote these two interval by

$$T_e = t_c - t_0$$

for the expansion time scale, and

$$T_c = t_f - t_c \tag{29}$$

for the contraction time scale (where t_f represents the instant when the contracting shell falls on the central body)

Taking into account the fact that both motions are radial, we can obtain T_e and T_c by integrating the equation (5) So, the expansion time scale is given by

$$T_e = \int_{r_0}^{r_c} ((1 - a_0 + a(r))/F(r))\,dr \tag{30}$$

Using the condition (18), and the expressions (15) for the expansion velocity and (16) for the function $F(r)$, Mioc [5] estimated the order of magnitude of T_e, obtaining

$$T_e = 4\pi\rho r_c^4 I/(15 m_0 v_0^2), \tag{31}$$

where I denotes the integral

$$I = \int_{0} (1 - x)^{-1/2} x^{-1/5} dx = 2.30. \tag{32}$$

Analogously, the time scale for the shell contraction is obtained by performing the integral

$$T_c = - \int ((1 + a_c - (a_0/a_c)a(r))/F_1(r))dr. \tag{33}$$

6. Concluding Remarks. Recapitulating the above results, we can formulate some conclusions

The motion of a shell surrounding a central body, under the only influence of two factors : the attraction of the central body and the accretion of matter from the environment on the surfaces of the shell, goes on according to the following scenario

At the instant $t = 0$ the shell is ejected from the central body and begins its expansion. Its motion under the influence of the two above mentioned factors is studied starting from an arbitrary moment t_0 of the expansion. During the interval $[0, t']$, with $t' < t_0$, the central body continues to eject matter, but this ejection is much slower than the shell ejection, such that this inner matter cannot reach the interior surface of the shell during the expansion. Due to both the gravitational attraction of the central body and the accretion of the environmental matter on the exterior surface of the shell, the expansion motion is decelerated, such that at an instant t_c the shell expansion is stopped After this instant, the shell begins to contract ; the motion of contraction is accelerated due to both the attraction of the central body and the accretion of inner matter on the interior surface of the shell. This motion lasts till the instant T when the shell falls on the central body

Using the hypotheses (i) — (v), Minin [5] studied in his paper only the expansion of the shell It is obvious that, taking into account the hypothesis (v), concretized into the restriction (2), the contraction motion can be satisfactorily modelled by a free fall and its study becomes uninteresting Indeed, for such a case, the velocity is given by the formula

$$v = - ((2GM/r)(1 - r/r_c))^{1/2}, \tag{34}$$

the minus sign indicating the direction of the motion, while the fall time can be obtained from the integral

$$T_c = \int_{r_c}^{0} - (2GM/r)^{-1/2} \, (1 - r/r_c)^{-1/2} dr. \tag{35}$$

One easily observes that our results constitute an extension of the results obtained in [5] Indeed, as we showed, if we put $a_0 \cong 0$, our formulae (13) and

(14) corresponding to the expansion reduce respectively to Minin's formulae (15) and (16), while the time scale for expansion (30) acquires the expression:

$$T_e = \int_{r_0}^{r_c} ((1 + a(r))/F(r))dr, \tag{36}$$

used by Minin [5] (with $F(r)$ provided by (16)) Also, if we put $a_0 \cong 0$ in our formulae corresponding to the contraction, (26) reduces to (34), while (33) reduces to (35).

As to the expansion end and contraction start, a necessary condition emphasized by Minin must be fulfilled The shell mass growth at great distances from the central body must be so fast that the diminution of the attractive force exerted by this body with the distance is comparatively slower

A last specification must be made here Neither Minin's study, nor our study did take into consideration the repulsive force due to the radiation of the central body If we take into account the effects of the radiation pressure on the particles constituting the shell (effects depending on the characteristics of both the central body and the particles), the results could be qualitatively (or at least quantitatively) modified In certain conditions (see [6]), the expansion can indefinitely continue, or the process of expansion/contraction can go on according to very different scenarios The study of the shell motion in such cases could have a particular importance for the analysis of various cosmogonical problems

REFERENCES

1 V G Gorbatsky, *Vestnik LGU*, ser *Math Mech Astron*, No 1, 142 (1960)
2 V G. Gorbatsky, *Vestnik LGU*, ser *Math Mech Astron*, No 13, 131 (1960)
3. V. G. Gorbatsky, I N Minin, "Nonstationary Stars", Fizmatgiz, Moscow (1963) (Russ).
4. I N Minin, *Astron Zh*, **37**, 939 (1960)
5. I N Minin, *Astrofizika*, **29**, 208 (1988)
6. V. Mioc, A V. Pop, I Giurgiu, *Studia Univ Babeş—Bolyai, Physica*, **33**, No 2, 36 (1988).
7. E. P Mustel, *Izv Krym Astrophys Obs*, **19**, 153 (1958)
8 E P Mustel, *Izv. Krym Astrophys Obs*, **21**, 24 (1959)
9. J. Oort, *Mon Not Roy. Astron. Soc*, **106**, 159 (1946).

STUDIA UNIV BABEŞ–BOLYAI, PHYSICA, XXXIV, 2 1989

PERIODIC ORBIT SURVIVAL PROBABILITY AFTER A SUPERNOVA EXPLOSION INTO A BINARY SYSTEM

VASILE MIOC* and GHEORGHE DORIN CHIŞ*

Received November 2, 1989

ABSTRACT. — The survival probability of a binary star following a rapid mass loss (due to a supernova explosion) is studied and a survival criterion is stated Previous results in this problem are corrected and completed. The evolution of the orbit after a possible supernova-like mass loss is investigated for four concrete long-periodic binary systems

1. **Hypotheses.** A supernova-type explosion undergone by one of the components of a binary system entails a rapid and consistent mass loss from the system Subsequently, the initial orbit of this one is altered. Moreover, under certain conditions, the relative orbit can become unbound and the two stars do no longer form a binary system

The problem of the survival of a double star orbit after a rapid mass loss was discussed in [7], which constitutes the basic paper for our research. The following restrictive conditions were supposed to be fulfilled:

(i) The mass ejection is spherically symmetrical

(ii) The initial speed of the ejected matter is high as against the orbital velocities of the components

(iii) The mass loss duration is short as against a tenth of the orbital period.

If the hypothesis (i) is fulfilled, we are in the case of the Kepler problem with secularly time-dependent gravitational parameter (*e g* [2, 6]) The very high value of the ejection speed comparatively to the orbital velocities (condition considered in [3—5]), involved by the hypothesis (ii), makes negligible the gravitational interaction between the components of the system and the ejected matter The last hypothesis ensures a negligible change of the position and velocity during the rapid mass loss (see *e g* [8])

2 **Basic Formulae.** Consider the relative motion in the frame of a binary system The well-known prime integral of energy is written under the form:

$$V^2 = GM(2/r - 1/a), \tag{1}$$

where V = velocity, G = gravitational constant, $M = M_1 + M_2$ = total mass of the system (M_1, M_2 being the masses of the components), r = radius vector, a = semimajor axis The initial orbit is assumed to be elliptic.

* *Centre for Astronomy and Space Sciences 3400 Cluj-Napoca, Romania*

Let one of the component stars be affected by a rapid mass loss due to a supernova explosion. Taking into account our hypotheses, the integral of energy for the new relative orbit will be

$$V^2 = GM'(2/r - 1/a'), \tag{2}$$

where M' is the new (diminished) total mass of the system and a' is the new semi-major axis.

Consider now another well-known formula used to the two-body problem:

$$r = a(1 - e \cos E), \tag{3}$$

where e = eccentricity and E = eccentric anomaly. From (1), (2) and (3) one deduces:

$$a' = ma(1 - e \cos E)/(2m - 1 - e \cos E), \tag{4}$$

in which we used the notation [7] $m = M'/M$.

Let h, h' the values of the constant of energy before and after explosion, respectively. We have:

$$h = -GM/a, \quad h' = -GM'/a', \tag{5}$$

and, by (4):

$$h' = h(2m - 1 - e \cos E)/(1 - e \cos E). \tag{6}$$

As to the eccentricity of the relative orbit before and after explosion, we can write:

$$e = (1 + hC^2/(GM)^2)^{1/2}, \quad e' = (1 + h'C^2/(GM')^2)^{1/2}, \tag{7}$$

where C is the constant angular momentum. By (6) and (7) we have:

$$e'^2 = 1 - (1 - e^2)(2m - 1 - e \cos E)/(m^2(1 - e \cos E)). \tag{8}$$

3. Survival Criterion. Let us introduce the following abbreviating notations:

$$K_a = ma(1 - e \cos E), \tag{9}$$

$$K_h = h/(1 - e \cos E), \tag{10}$$

$$K_e = (1 - e^2)/(m^2(1 - e \cos E)), \tag{11}$$

$$f(m, e) = 2m - 1 - e \cos E, \tag{12}$$

with which (4), (6) and (8) acquire respectively the forms:

$$a' = K_a/f(m, e), \tag{13}$$

$$h' = K_h f(m, e), \tag{14}$$

$$e'^2 = 1 - K_e f(m, e) \tag{15}$$

Since the initial orbit was assumed to be elliptic (namely one of the equivalent conditions $a > 0$, $h < 0$, $e < 1$ is fulfilled), we observe easily that $K_a > 0$, $K_h < 0$, $K_e > 0$.

If the relative orbit after explosion remains elliptic, the binary system survives Taking into account (13) — (15), the survival criterion is

$$f(m, e) > 0 \tag{16}$$

For $f = 0$ the new orbit becomes parabolic, and hyperbolic for $f < 0$

4. Survival Probability. Denote by $P(m, e)$ the survival probability and examine the formula (12). If $(2m - 1)/e \geq 1$, we always have $f > 0$ ($P = 1$), hence the orbit remains always bound. On the other hand, if $(2m - 1)/e < -1$, we always have $f < 0$ ($P = 0$), hence the orbit becomes always unbound. Let us now consider the case in which $(2m - 1)/e \in [-1, 1]$

Observe from (12) that there exist two critical values of the eccentric anomaly:

$$E_{e,j} = \cos^{-1}((2m - 1)/e), \quad j = 1, 2, \tag{17}$$

for which $f = 0$ These two values divide the orbit into an arc centered on the periastron (where $f < 0$) and an arc centered on the apastron (where $f > 0$). The survival probability is therefore the ratio

$$P(m, e) = T_a/T, \tag{18}$$

where T_a is the time interval into which the star lies on the apastron arc, while T is the orbital period.

Denote by t_e the instant corresponding to $E_{e,1}$ and by t_p the instant of periastron. It is obvious that

$$T_a = T - 2(t_e - t_p). \tag{19}$$

Now, taking into account Kepler's equation for this case:

$$n(t_e - t_p) = E_{e,1} - e \sin E_{e,1} \tag{20}$$

where n is the mean motion, and the fact that $T = 2\pi/n$, we obtain from (17) — (19)

$$P(m, e) = (\pi - \cos^{-1}((2m - 1)/e) + e^{1/2}(1 - ((2m - 1)/e^2))/\pi \tag{21}$$

We must mention here that (21) differs slightly from the corresponding formula given in [7], which is erroneous.

Resuming these results, the survival probability as function of m and e is synthesized in Table 1. As it is shown in [7], the case $m = 0.5$, $e = 0$ is singular, since $f = 0$ and E becomes undefined

Table 1

m	e	$P(m, e)$
>0.5	$\leqslant 2m - 1$	1
>0.5	$> 2m - 1$	(21)
0.5	>0	$1/2 + e/\pi$
<0.5	$\geqslant 1 - 2m$	(21)
$\leqslant 0.5$	$\leqslant 1 - 2m$	0

Table 2

e \ m	0.9	0.8	0.7	0.6	0.5	0.4	0.3	0.2	0.1	0.05
0.05	1	1	1	1	0.516	0	0	0	0	0
0.10	1	1	1	1	532	0	0	0	0	0
0.15	1	1	1	1	548	0	0	0	0	0
0.20	1	1	1	1	564	0	0	0	0	0
0.25	1	1	1	843	580	253	0	0		0
0.30	1	1	1	803	595	.339	0	0	0	0
0.35	1	1	1	785	611	398	0	0	0	0
0.40	1	1	1	777	.627	444	0	0	0	0
0.45	1	1	914	775	643	.482	.217	0	0	0
0.50	1	1	.891	.777	659	515	300	0	0	0
0.55	1	1	879	782	675	.545	361	0	0	0
0.60	1	1	875	788	691	572	410	0	0	0
0.65	1	954	874	.796	707	597	452	205	0	0
0.70	1	943	876	806	723	621	489	.287	0	0
0.75	1	938	881	816	.739	644	523	348	0	0
0.80	1	938	887	827	755	666	554	398	0	0
0.85	982	941	895	839	771	687	583	.442	201	0
0.90	980	946	903	851	786	708	610	481	.283	0
0.95	982	952	.913	863	802	728	636	516	344	.201
.099	.985	.958	.921	.873	815	744	656	543	386	.268

Using Table 1 and the formula (21), we calculated the survival probabilities for $(m, e) \in I^2$, where $I = (0, 1)$. The results are listed in Table 2.

Some remarks about Table 2 must be made. This table uses smaller steps than the corresponding table given in [7]. Another difference consists of some values of the probability $P(m, e)$. So, in [7] one gives $P(0.6, 0.4) = 0.766$, $P(0.6, 0.6) = 0.777$, $P(0.05, 0.95) = 0.200$. Our Table 2 gives the correct values: 0.777, 0.788 and 0.201, respectively. Also we did not consider the line $e = 1$ (since we supposed that the initial orbit is elliptic) and the column $m = 1$ (it is clear that $P(1, e) = 1$, whatever $e < 1$, is). If we consider a line $e = 0$ (initially circular orbit), we shall obtain $P(m, 0) = 1$ for $m > 0.5$ and $P(m, 0) = 0$ for $m < 0.5$. A last remark: if we consider a column $m = 0.01$ (namely a very drastic mass loss), we shall have $P(0.01, e) = 0$ for every $e < 0.98$. Only for more eccentric (near parabolic) orbits the survival probability becomes nonzero (but very small, e.g. $P(0.01, 0.99) = 0.090$).

5. **Survival Probability and Orbit Behaviour for some Concrete Binaries.** In order to apply the above exposed results to concrete cases, we dwelt upon four long-periodic spectroscopic binary systems, chosen in the catalogue [1]. The orbital characteristics of these binaries are given in Table 3.

Suppose that each of the four systems undergoes a hypothetical supernova-like mass loss, such that $M' \geqslant 0.8\ M$. The survival probabilities for such events are given in Table 4.

Let us now see what happens with each orbit after such an eventual explosion. Using the formulae (4) and (8), we calculated the deformations undergone by the four orbits. The results for $m = 0.9$ are listed in Table 5, while Table 6

Table 3

No	Star	e	$a(10^9$ km)	T (years)
1	58 e Per	0 65	1 414	28 7
2	Gamma Gem	0 90	0 268	12 6
3	Beta LMi	0 66	0 481	39 9
4	51 Ksi Sco	0 75	1 129	44 7

Table 4

No m	0 98	0 96	0 94	0 92	0 90	0 88	0 86	0 84	0 82	0 80
1	1	1	1	1	1	1	1	1	0 980	0 954
2	1	1	0 993	0 986	0 980	0 974	0 967	0 960	0 953	0 946
3	1	1	1	1	1	1	1	1	0 973	0 951
4	1	1	1	1	1	1	0 977	0 962	0 950	0 938

corresponds to $m = 0$ 8 These tables give for each system the values $E_{c,1}$, $E_{c,2}$ (if they exist), the values $a'_{\min}$, $e'_{\min}$ corresponding to $E = 180°$ (apastron), and the values $E_{e,1}$, $E_{e,2}$ for which $e' = e$ Table 5 also includes, only for $P = 1$, the values $a'_{\max}$, $e'_{\max}$ corresponding to $E = 0°$ (periastron) The values of E_c and E_e are expressed in degrees, while those of a' in 10^9 km

Table 5

Star	$E_{c,1}$	$E_{c,2}$	$a'_{\max}$	$e'_{\max}$	$a'_{\min}$	$e'_{\min}$	$E_{e,1}$	$E_{e,2}$
1	—	—	2 969	0 833	1 448	0 611	94 64	265 36
2	27 27	332 73	—	—	0 270	0 889	93 35	266 65
3	—	—	1 051	0 844	0.492	0 622	94 57	265.43
4	—	—	5 080	0 944	1 147	0 722	94 02	265 98

Table 6

Star	$E_{c,1}$	$E_{c,2}$	$a'_{\min}$	$e'_{\min}$	$E_{e,1}$	$E_{e,2}$
1	22 62	337 38	1 493	0 563	99 84	260 16
2	48,19	311 81	0 272	0 875	97 09	262 91
3	24 62	335 38	0 507	0 575	99 69	260 31
4	36 87	323 13	1 171	0 688	98 52	261 48

Table 7

Star	$P(0.2, e)$	$E_{c,1}$	$E_{c,2}$	a'_{min}	e'_{min}	$E'_{e,1}$	$E_{e,2}$
1	0.205	157.38	202.62	9.332	0.750	—	—
2	0.481	131.81	228 19	0 339	0 500	137.79	222.21
3	0.224	155 38	204.62	2.662	0 700	—	—
4	0 348	143.13	216 87	2 634	0 250	152.73	207 27

Lastly, we took into account a very drastic mass loss by supernova explosion, $m = 0.2$. Table 7 lists the numerical results for the four binary systems. The columns of the table are the same as those of Table 6 (and the units, too), and a supplementary column, $P(0\ 2, e)$ was added

Examining Tables 4–7, one can point out some characteristics of the post-explosion motion. Firstly, we see that the four considered systems have great chances to survive (as binaries) an explosion with $m \geqslant 0\ 8$ Even for a great mass loss the survival is relatively probable

If such a couple survives a mass loss with $m = 0.9$ or $m = 0\ 8$, the new relative orbit will be larger than the initial one. If $E_{e,1} < E < E_{e,2}$, the new orbit will be less eccentric than the initial one, and more eccentric in the opposite case. As to Table 7, one sees that for $m = 0\ 2$ critical values of E for which $e' = e$ do exist only for the stars 2 and 4 (great initial eccentricities) For the binaries 1 and 3, the new orbit will be more eccentric than the initial one, whatever E is (of course, between the critical values $E_{c,1}$ and $E_{c,2}$).

REFERENCES

1. A. H. Batten, J. M. Fletcher, D. G. MacCarthy, *Publ. Dominion Obs.* **17**, 1 (1989).
2. I. Giurgiu, V. Mioc, *Studia Univ. Babeş—Bolyai, Physica*, **33**, No 2, 94 (1988).
3. I. N. Minin, *Astrofizika*, **29**, 208 (1988).
4. V. Mioc, *Studia Univ Babeş—Bolyai, Physica*, **34** (1989) (to appear)
5. V. Mioc, *Babeş—Bolyai Univ, Fac Math. Phys Res Sem*, Preprint 5 (1989) (to appear)
6. V. Mioc, Á. Pál, I. Giurgiu, *Babeş—Bolyai Univ, Fac Math Phys Res Sem*, Preprint 10, 3 (1988)
7. M. P. Savedoff, *Astron J*, **71**, 369 (1966).
8. M. P. Savedoff, S. Vila, *Astron J*, **69**, 242 (1964).

INSTANTON EFFECTS IN THE PURE SUPERSYMMETRIC G_2-MODEL

E. VINŢELER*

ABSTRACT. This work is an attempt to understand the supersymmetric breaking in the models with exceptional gauge groups. We show by explicit calculations that we really have dinamical supersymmetry breaking in the G_2-model.

1. Introduction. We remind some aspects of the theory which is contained in [1]

If the vacuum expectation value of arbitrary scalar field $\langle X \rangle \neq 0$, then we have an internal symmetry breaking For the supersymmetry (SUSY) breaking we need $\langle \{Q, X\} \rangle \neq 0$, where Q is the supersymmetric charge. In quantum chromodinamics (QCD) we have the Ward identity

$$\partial_\mu(\bar\psi\gamma_\mu\gamma_5\psi) = 2im\bar\psi\gamma_5\psi + (C_2(G)/32\pi^2)F_{\mu\nu}\tilde F^{\mu\nu}$$

where $C_2(G)$ — the second Casimir eigenvalue in the adjoint representation. Analogously, in the supersymmetric case we have the so-called Konishi identity [2]

$$\{\bar Q_{\dot\alpha}, \bar\psi^{\dot\alpha}\Phi\}/2\sqrt{2} = -m\bar\Phi\Phi + (C_2(G)/32\pi^2)\lambda\lambda \quad (1)$$

where $W^\alpha W_\alpha = (\lambda\lambda + \quad)$, W^α — the intensity of vector superfield

$$W^\alpha = \lambda^\alpha + (F^{\mu\nu}\sigma^{\alpha\beta}_{\mu\nu} - D\delta^{\alpha\beta})\theta_\beta + \theta\theta D^\alpha_{\dot\alpha}\bar\lambda^{\dot\alpha}$$

Φ, $\bar\Phi$ are the chiral superfields in the N, respectively $\bar N$ representation

$$\Phi_i = \Phi_i + \sqrt{2}\psi_{\alpha i}\theta^\alpha + F_i\theta\theta$$

Although in the QCD at the clasical level there is an exact symmetry ($m = 0$) from the renormalisation we can have $m \neq 0$ and the symmetry breaking at the quantum level In supersymmetric QCD is diferent, from the non-renormalisation theorem [3] it results that if $m = 0$ at the clasical level, then $m = 0$ in all orders of the perturbation theory We can have a SUSY breaking (called dynamical) only from the non-perturbative effects (instantons)

As in QCD we have the vacuum expectation value $\langle F\tilde F \rangle$, the control parameter for the SUSY breaking is $\langle \lambda\lambda \rangle$ (we denote $\lambda\lambda = \varepsilon^{\alpha\beta}\lambda_\alpha\lambda_\beta$) The diference is that $\langle \lambda\lambda \rangle$ is infrared convergent (we do not need the cutoff on the instanton size). This results from the fact that Green's functions, which contain only the lowest components of the chiral superfields, are constant

The vacuum expectation value $\langle \lambda\lambda \rangle$ can be computed from the Green's function [4]

* University of Cluj-Napoca, Faculty of Mathematics and Physics, 3400 Cluj-Napoca, Romania

$$G_N^M(x_1, \ldots x_N) = \langle \lambda\lambda(x_1) \ldots \lambda\lambda(x_{N-M})\Phi^{\prime 1}\Phi_{,1}(x^{N-M=1}) \ldots \Phi^{\prime M}\Phi_{,M}(x_M)\rangle \quad (2)$$

i when $|x_i - x_j| < \Lambda^{-1}$, G_N^M is computed at short distances through a uni-instanton calculation

ii when $|x_i - x_j| \to \infty$, using clustering, we have $G_N^M = \langle\lambda\lambda(x_1)\rangle \ldots \langle\lambda\lambda$ $\langle\lambda\lambda(x_{M-N})\rangle\langle\Phi^{\prime 1}\Phi_{,1}(x^{N=M+1})\rangle \ldots \langle\Phi^{\prime M}\Phi_{,M}(x_N)\rangle$

2 **The method of SU(2)-Embedding.** The question is that the instanton contribution at the short distances can be partially or totally anihilated by contributions at large distances Hence we must study the mass dependence of the Green's function But in the pure Yang-Mills theories we have not explicit mass dependence, thus we introduce two matter superfields S, T and obtain the intermediate theory When $m \to \infty$ the matter superfields stand out from the spectrum and we reobtained the pure Yang-Mills theory [5]

Besides the SUSY breaking, we can have an internal symmetry breaking, in our case $G_2 \to SU(3)$ We choose S, T in the fundamental representation of G_2 (it is real and $S = T$), $\{7\} = \{1\} + \{3\} + \{3\}$ The nonsinglet SU(3) components $\{3\}$, $\{\bar{3}\}$ of the massless superfield S become the longitudinal components of the massive vectorial bosons $\{3\}$, $\{\bar{3}\}$, on $S = G_2/SU(3)$ Bosons are in the adjoint representation $\{14\} = \{8\} + \{3\} + \{\bar{3}\}$

Then the G_2-model with matter is reduced to the SU(3)-model with matter ·
i the massive particles — the vectorial bosons $\{3\}$, $\{\bar{3}\}$ with the mass m_V.
ii the massless particles — the matter singlet $\{1\}$ s, — the vectorial bosons $\{8\}$ When $m_V \ll \Lambda$ only the massless particles ascertain the dynamics of the SU(3)-model

3 **The G_2-model.** We want to compute $\langle\lambda\lambda\rangle_{G2}$ for the pure G_2-model. Instead to compute $\langle\lambda\lambda\rangle_{G_2 m}$ for the G_2-model with matter from

$$G_4^1(x_1, x_2, x_3, x_4) = \langle\lambda\lambda(x_1)\,\lambda\lambda(x_2)\,\lambda\lambda(x_3)\,\Phi^{\prime}\Phi_{,j}(y_1)\rangle \quad (3)$$

(we have a singular behaviour in $m = 0$), we will find the connection between $\langle\lambda\lambda\rangle_{G2m}$ and $\langle\lambda\lambda\rangle_{SU(3)}$ $\langle\lambda\lambda\rangle_{G2m}$ is a function of m and $\langle\lambda\lambda\rangle_{SU(3)}$

3 1 *The reduced model* We compute $\langle\lambda\lambda\rangle_{SU(3)}$ for the SU(3)-model with matter (SU(3)-singlet s) from

$$G_3^1(x_1, x_2, x_3) = \langle\lambda\lambda(x_1)\lambda\lambda(x_2)\tilde{s}s(x_3)\rangle \quad (4)$$

Through the instanton calculation

$$G_3^1(x_1, x_2, x_3) = C\mu^8 \exp(-8\pi^2/g^2) \int \frac{d^4 a d\rho}{\rho^5}(\rho^2)^6 \frac{\delta}{\delta\bar{\eta}(x_1)}\frac{\delta}{\delta\eta(x_1)}\frac{\delta}{\delta\bar{\eta}(x_2)}\frac{\delta}{\delta\eta(x_2)}\frac{\delta}{\delta\bar{\eta}(x_3)}$$
$$\frac{\delta}{\delta\eta(x_3)}\left(\prod_{k=1}^{4}\int d^4x\eta\lambda_0^{(k)}\right)\left(\int d^4xK\psi_0\right)\int\left(d^4x\bar{\psi}_0\tilde{K}\right)\exp\left[-\int d^4x(\eta\Sigma\bar{\eta} + K\bar{S}\bar{K} +\right.$$
$$\left.\left.K\tilde{S}\tilde{K}\right)\right]\Big|_{\eta=\bar{\eta}=K=\bar{K}=0} = C\Lambda'^8\int\frac{d^4 a d\rho}{\rho^5}\left(\rho^2\right)^6\sum_{i}(-1)^P\lambda_0^{(k_1)}\lambda_0^{(k_2)}(x_1)\lambda_0^{(k_3)}\lambda_0^{(k_4)}(x_2)\tilde{s}_0^{(k_5)}s_0^{(k_6)}(x_3) \quad (5)$$

where $\Lambda' = \mu\exp(-8\pi^2/\beta_1 g^2)$, for SU(3) with matter $\beta_1 = 8$, P — the parity ;

Σ — the gluon propagator, S — the quark propagator; $C \neq 0$.
λ_0 — gluino in the instanton field

$$D\lambda_0 = 0 \tag{6}$$

s_0 — scalar (singlet zero mode) in the instanton field.

$$D^2 s_0 = -i\sqrt{2}\lambda_0\psi_0 \tag{7}$$

The instanton solution is:

$$A_\mu = 2f(x)x_\nu\sigma_{\nu\mu}$$

where $f(x) = ((x-a)^2 + \rho^2)^{-1}$

From [4] we have

$$\sum_{\text{dublet}} \lambda_0\lambda_0(x) = (4/\pi^2)\rho^2 f^3(x) \tag{9}$$

$$\sum_{\text{triplet}} \lambda\lambda_0\lambda\lambda_0(x) = (72/\pi^4)\rho^6(f(x)f(y))^4(x-y)^2$$

For $s_0 s_0(x)$ we have similar result as for $\lambda_0\lambda_0$ apart from a factor of 1/6 For (5) keeping in mind (9)

$$G_3^1 = (24/\pi^6)\Lambda'^8 \int d^4a\,d(\rho^2)(\rho^2)^7\,[f(x_1)f(x_2)f(x_3)]^4 \times \left[\frac{(x_1-x_2)^2}{f(x_3)} + \frac{(x_2-x_3)^2}{f(x_1)} + \frac{(x_3-x_1)^2}{f(x_2)}\right] \tag{10}$$

From (A1)

$$G_3^1 = (24 \quad 11!/3^2 \quad 2^3\pi^6)\Lambda'^8 \int_0^1 \prod_{k=1}^{3} d\alpha_i\delta(1-\Sigma\alpha_k)\int d^4a\,d(\rho^2)(\rho^2)^7 \times$$

$$\prod_{i=1}^{3}\alpha_i^2 \sum_{j\neq k}(x_j - x_k)^2\alpha_j\alpha_k)\,[a^2+\rho^2+\Sigma(\alpha_i x_i^2) - 2a\Sigma(\alpha_i x_i)]^{-11} \tag{11}$$

From (A2), (A3)

$$G_3^1 = (77i/3\pi^4)\Lambda'^8 \int_0^1 \prod_{i=1}^{3} d\alpha_j\delta(1-\Sigma\alpha_k)\prod_{=1}^{3}\alpha_i^2\left[\sum_{j\neq k}(x_j - x_k)^2\alpha_j\alpha_k\right] \times$$

$$\times\,[\Sigma(\alpha_i x_i^2) - (\Sigma\alpha_i x_i)^2] = (154i/3\pi^4)\Lambda'^8 \tag{12}$$

From (12) and the Konishi identity

$$-m\langle\tilde{S}\,S\rangle + (6/32\pi^2)\langle\lambda\lambda\rangle_{SU(3)} = 0 \tag{13}$$

we have

$$\langle\lambda\lambda\rangle_{SU(3)} = K_{SU(3)}\Lambda^2_{SU(3)}e^{\pi ik}, \quad k = 0, 1, 2 \,. \tag{14}$$

$$K_{SU(3)} \neq 0 \text{ and } \Lambda^9_{SU(3)} = m\Lambda'^8$$

3.2. *The symmetry breaking* $G_2 \to SU(3)$. We find the connection between Λ_{G_2} and $\Lambda_{SU(3)}$.

In the point $\mu = v$ (we denote $v^2 = \langle \bar{s} s \rangle$ the coupling constants $g_{G_2} = g_{SU(3)}$. Then

$$g^{-2}_{SU(3)}(\mu) = g^{-2}_{SU(3)}(v) + (9/8\pi^2)\ln(\mu/v) = g^{-2}_{G_2} + (9/8\pi^2)\ln(\mu/v) = g^{-2}_{G_2}(\mu) - (2/8\pi^2)\ln(\mu/v) \tag{15}$$

In addition:

$$g^{-2}_{SU(3)} = (9/8^2)\ \ln\ (\mu/\Lambda_{SU(3)})\ g^{-2}_{G_2}(\mu) = (11/8^2)\ln(\mu/\Lambda) \tag{16}$$

From 15), (16):

$$\Lambda^3_{SU(3)} = v^3(\Lambda/v)^{11/3} \tag{17}$$

$$\text{or}:\ \Lambda^3_{SU(3)} = (32\pi^2/6)^{1/3}\, K^{1/3}_{SU(3)}\Lambda^3_{G_2} \tag{18}$$

From (14), (18)

$$\langle\lambda\lambda\rangle_{SU(3)} = (32\pi^2/6)^{1/3}\, K^{4/3}_{SU(3)}\Lambda^3_{G_2} \tag{19}$$

Defining:

$$\langle\lambda\lambda\rangle_{G_2} = K_{G_2}\Lambda^3_{G_2} e^{\pi i k},\quad k = 0,\ 1,\ 2,\ 3 \tag{20}$$

we see that

$$K^{1/4}_{G_2} \sim K^{1/3}_{SU(3)} \tag{21}$$

4 and 3 are half of the second Casimir eigenvalue $C_2(G_2)$, respectivelly $C_2(SU(3))$.

3.3 *The supersymmetry breaking* To relate domain $m \to 0$ to $m \to \infty$ (the pure G_2-model) we use the non-anomalous mass Ward identity

$$m\frac{\partial}{\partial m}\langle\lambda\lambda\rangle_{G_2m} = -(1/2)\langle\lambda\lambda\rangle_{G_2m}\ \chi(\lambda) = (1/4)\langle\lambda\lambda\rangle_{G_2m} \tag{22}$$

where χ is the $U^{(k)}_A$ -charge

Knowing the dimensions of Green's function in (3) $G^1_4 \sim \Lambda d(G) = \Lambda^{11}$ and from the Konishi identity we have $\langle\lambda\lambda\rangle_{G_2m} \sim \Lambda^{11/4}$. Thus

$$\langle\lambda\lambda\rangle_{G_2m} = K_{G_2m}\ m^{1/4}\Lambda^{11/4}e^{\pi i k} \tag{23}$$

for diferent vacua labelled by index $k = 0, 1, 2, 3$

Fixing

$$\Lambda = m\exp\left(-8\pi^2/\beta_1 g_0^2\right)$$

where β_1 — the first coefficient in the Gell-Mann function $\beta_1 = 11$ in presence of matter and $\beta_1 = 12$ in absence of matter, for the group G_2, we obtain:

$$m\cdot\Lambda^{11} = \Lambda^{12}_{G_2} \tag{24}$$

When $m \to \infty$, $\langle\lambda\lambda\rangle_{G_2m} \to \langle\lambda\lambda\rangle_{G_2}$ and .

$$\langle\lambda\lambda\rangle_{G_2} = K_{G_2}\Lambda^3_{G_2}\, e^{i\pi k/2}, \quad k = 0, 1, 2, 3 \tag{25}$$

We show that $K_{G_2} \neq 0$, and we have a supersymmetry dinamical breaking in the pure G_2-model

4 **Conclusions** In case of the G_2 grup was possible to calculate explicitly K_{G_2} because we had a single invariant S^aS^a, $a = 1, \ldots 7$ For other exceptional groups, in particulary of great interest in the Great Unification Theory E_6 and E_8, we have few invariants and hence we do not know how to write a formula like (5)

APPENDIX

We denote $a_i = f^{-1}(x_i)$, $b_i = \delta_i^{jk}(x_j - x_k)^2$, $i, j, k = 1, 2, 3$. Using the Feynman integral

$$\frac{1}{a_1 a_2 a_3} = 2\int_0^1 \prod d\alpha_i\, \delta(1 - \Sigma\alpha_i)\, (\Sigma\alpha_i a_i)^{-3}$$

Differentiating after a_i

$$3^2 2^3 (a_1 a_2 a_3)^{-4} \Sigma(b_i a_i) = 11! \int_0^1 \prod d\alpha_i\, \delta(1 - \Sigma\alpha_i) \prod \alpha_i^3 \sum_{j\neq k} (b_i\alpha_i)(\Sigma\alpha_i a_i)^{-11} \tag{A1}$$

Wse ue the notations $\rho^2 = k$, $m = a^2 + \Sigma(\alpha x^2) - 2a\Sigma(\alpha x)$

$$\int_0^\infty dk\, k^n (k + m)^{-11} = \frac{n!(10-n)!}{10!} m^{n-10} \tag{A2}$$

We denote $p = \Sigma(\alpha_i x_i)$, $\alpha = \Sigma(\alpha_i x_i^2)$

$$\int \frac{d^4 a}{(a^2 - 2ap + \alpha)^3} = \frac{\pi^2}{2}\frac{1}{\alpha - p^2} \tag{A3}$$

REFERENCES

1. D. Amati, K. Konishi, Y. Meurice, G. C. Rossi, G. Veneziano, *Phys Rept.* 162 (1988) 171
2. K. Konishi, *Phys Lett B* 135 (1984) 439
T. E. Clark, O. Piguet, K. Sibold, *Nucl Phys B* 159 (1979) 1
3. M. T. Grisaru, M. Rocek, W. Siegel, *Nucl Phys B* 159 (1979) 429
4. D. Amati, G. C. Rossi, G. Veneziano, *Nucl Phys B* 249 (1985) 1
5. A. Iu Morozov, M. A. Olisanetki, M. A. Schifman, *ZETP* 94 (1988) 18
M. A. Schifman, A. I. Vainshtein, *Nucl Phys B* 296 (1988) 445.

STUDIA UNIV BABEŞ—BOLYAI, PHYSICA, XXXIV, 2, 1989

TRANSPORT IN TOKAMAK PLASMAS

T. A. BEU* and M. VASIU*

Received September 29, 1989

ABSTRACT. — In high temperature-low density tokamak plasmas, radiation cooling by impurity atoms can be an important energy loss mechanism, since radiation is not reabsorbed. The coupled set of time-dependent diffusion equations for ionized tokamak plasma impurities is solved in conjunction with a simple model for neutral impurities, on the assumption of a cylindrical symmetry The resultant density distributions are used in the subsequent computation of the related power losses.

1. **Introduction**. The radiation losses from a plasma column directly dissipate electron energy and influence electron temperature and power balance in tokamak discharges [1—3]. They are also associated with instabilities through an influence on the radial profile of electron temperature [4—5]

Plasmas are contaminated by impurity atoms released from the wall of the reaction chamber and the limiters by high energy plasma particles which leak across the magnetic field configuration The radiation power is greatly enhanced by the presence of impurity atoms, especially high—Z impurities, because of their high cooling rate [6—8] Current nuclear fusion research is directed towards reduction in the high—Z contamination of the plasma In recent years, high power ICRF heating experiments up to MW level have been carried out to realize high temperature plasmas This heating technique has the advantage of efficiently heating the ions However, it has been reported that RF heating causes a relatively large impurity contamination compared to other heating techniques [9] Successful heating depends entirely on the effective reduction in the impurity contamination

A good understanding of the mechanism of impurity production and dynamics is absolutely necessary to find a method to reduce impurity contamination Several investigations on these problems have been described in the literatures [10, 11, 12].

In this paper, the stationary density distributions of impurities, such as carbon, oxygen and iron, in various states of ionization are calculated numerically using a simple MHD—model. Classical and anomalous diffusions across the magnetic field and ionization-recombination processes are taken into account. Power losses due to ionization, recombination, bremsstrahlung and excitation are also computed using the numerically obtained density distributions of impurities. The numerical results are in good agreement with ST, TFR and JIPP T—IIU experiments. The main difference between this approach and its earlier versions [13, 14] concerns the coupling of the various impurity species

* University of Cluj-Napoca, Faculty of Mathematics and Physics, 3400 Cluj-Napoca, Romania

and leads to a more realistic description of the physical processes that take place in a tokamak discharge

2 **Method of solution.** The ideal magnetically confined fusion plasma would consist only of hydrogen isotopes, helium ions and the neutralizing electrons, well separated from the material walls of the reaction chamber by suitably shaped magnetic fields In practice, high-energy plasma particles leak across the magnetic field, strike the walls and the limiters The impurity atoms thus liberated diffuse into the plasma, where they are ionized and excited.

Considering a cylindrical MHD—model, with r the radial coordinate, the neutral impurities are assumed to be flowing into the plasma at thermal velocity v_0, and their density, $n_0(r)$, decreases rapidly through ionization as impurities penetrate the plasma Using the coordinates indicated in Fig. 1, where r_p is the poloidal radius, we have

$$n_0(r) = [n_0(r_p)/4\pi] \int_0^{2\pi} d\varphi \int_{-\pi/2}^{\pi/2} d\psi \cos\psi [-(1/v_0) \int_0^{\rho} \alpha_1(\rho')n_e(\rho')d\rho'] \tag{1}$$

Here $n_0(r_p)$ is the density of the neutrals at the plasma boundary, α_1 is the ionization rate of the neutrals and n_0 is the electron density The thermal velocity is defined as $v_0 = (2kT_0/m_z)^{1/2}$, where T_0 is the temperature of the neutrals and m_z is the corresponding atomic mass

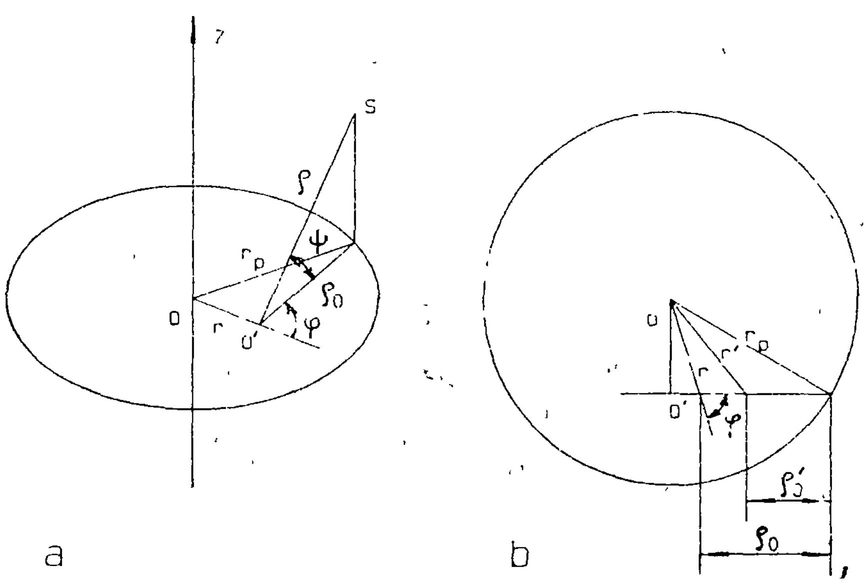

Fig 1 A polar coordinate system used in the calculation of the density distribution of the neutral impurities.

Taking into account the symmetric contributions to the inward flux of neutral impurities and making use of the Bickley function of the second kind [15]

$$Ki_2(x) = \int_0^{\pi/2} d\psi \cos\psi \exp(-x/\cos\psi)$$

we may rewrite integral (1) as follows

$$n_0(r) = [n_0(r_p)/\pi] \int_0^{\pi} d\varphi\, Ki_2\left[(1/v_0) \int_0^{\rho_0} \alpha_1(\rho_0') n_e(\rho_0') d\rho_0'\right] \qquad (2)$$

In order to evaluate $n_0(r)$ from Eq (2) one needs two further relations

$$\rho_0 = (r_p^2 - r^2 \sin^2 \varphi)^{\frac{1}{2}} - r \cos \varphi$$

$$r' = [(\rho_0' + r \cos \varphi)^2 + r^2 \sin^2 \varphi]^{1/2}$$

where r' represents the radial coordinate corresponding to the integration argument ρ_0'.

The density distributions of the ionized impurities are calculated by taking into account classical and anomalous diffusion and the ionization-recombination processes The radial density distributions are then given by the following set of coupled rate equations

$$\partial n_I/\partial t + (1/r)(\partial/\partial r)(r\Phi_I) - n_e[(1 - \delta_{I,1})\alpha_I n_{I-1} - (\alpha_{I+1} + \beta_I)n_I + \beta_{I+1}n_{I+1}] = \delta_{I,1} n_e \alpha_1 n_0 \qquad (3)$$

$$I = 1, 2, \ldots, IM$$

where n_I is the impurity ion density in the Ith ionization state, α_I is the ionization rate for the passage from the $(I - 1)$th state to the Ith state and β_I is the total recombination rate for the passage from the Ith state to the $(I - 1)$th state IM represents the total number of ionization states and δ is Kroncker's delta

The flux of impurity ions is given as [10, 16]

$$\Phi_I = -\gamma_D D_I\, \partial n_I/\partial r + \gamma_W W_I n_I$$

on the assumption that the impurity ions are in the collision-dominated (Pfirsch—Schlüter) region, but considering their density low enough for the effect of mutual collisions to be neglected The Pfirsch—Schlüter diffusion coefficient is defined by the relation

$$D_I = (1 + q^2)\rho_I^2 \nu_I$$

Here $q = (r/R_t)(B_t/B_p)$ is the safety factor, with R_t the toroidal radius, B_t the toroidal magnetic field and B_p the poloidal magnetic field Assuming a parabolic dependence of the current density on the radial coordinate and denoting the total plasma current by I_p, we have for the safety factor

$$q = 2\pi r_p^2 B_t / \mu_0 R_t I_p [2 - (r/r_p)^2]$$

The Larmor radius is given by

$$\rho_I^2 = (2m_z k T_I / e^2 B_t^2 I^2)$$

T_I being the temperature of impurity ions, while the collision frequency of impurity ions with plasma ions is defined as follows

$$\nu_I = 4(2\pi m_i)^{1/2} I^2 e^4 n_i \ln \Lambda_I / 3 m_z (4\pi\varepsilon_0)^2 (kT_i)^{3/2}$$

with n_i the plasma ion density, m_i the plasma ion mass and T_i the corresponding temperature

$$\ln \Lambda_I = \ln [3(4\pi\varepsilon_0)^{3/2} (kT_i)^{3/2} / 2\pi^{1/2} I e^3 (Z_{\text{eff}} n_e)^{1/2}]$$

is the Coulomb logarithm, where $Z_{\text{eff}} = (n_i + \Sigma I^2 n_I)/n_e$ is the effective ionic charge fo the plasma and, according to plasma neutrality, $n_e = n_i + \Sigma I n_I$. We employ a simple model for the impurity ion temperatures:

T_0 = given constant

$$T_I = \min \left[T_i, T_{I-1} + (T_i - T_{I-1}) \frac{\tau_I^{\text{ion}}}{\tau_I^{\text{equ}}} \right]$$

with the ionization time $\tau_I^{\text{ion}} = 1/(\alpha_{I+1} + \beta_I) n_e$ and the equipartition time $\tau_I^{\text{equ}} = 1/2\nu_I$.

The inward diffusion velocity due to friction with the plasma ions is defined as

$$W_I = I D_I [(1/n_i)(dn_i/dr) - (1/2T_i)(dT_i/dr)]$$

γ_D and γ_W are anomality factors.

The ionization rates employed by us were those of Lotz [17]. Taking into account the radiative recombination and the dielectronic recombination [18, 19], the approximate expression for the total recombination rate is obtained by summing the rates for these two processes [13, 14].

The rate equations (3) are solved subject to the following boundary conditions

$$n_0(r_p) = \text{given constant}$$

$$n_I(r_p) = 0, \quad I = 1, 2, \ldots IM$$

$$[\partial n_I / \partial r]_{r=0} = 0, \quad I = 1, 2, \ldots IM$$

and, considering time-dependent cases, one adds the initial conditions

$$[n_I(r)]_{t=0} = n_I^0(r), \quad I = 1, 2, \ldots IM$$

Energy losses due to the presence of impurities are one of the most serious problems in present-day tokamaks. Therefore, it is of interest to calculate the energy losses due to impurities, as the ionization loss p_i, including the radiative recombination loss p_r, the bremsstrahlung loss p_b and the excitation loss p_e They are approximately given by

$$p_i = k \sum_I n_e n_{I-1} \sigma_I (P_I + (3/2)T_e) + p_r$$

$$p_r = k \sum_I ((3/2) n_e n_I \beta_I T_e)$$

$$p_b = 1\,5 \times 10^{-38} Z_{eff} n_e^2 T^{1/2}$$

$$p_e = 1\,73 \times 10^{-31}\, T_e^{-1/2} n_e \sum_I n_I \sum_J c_{IJ} \exp\left(-P_{IJ}^{ex}/T_e\right)$$

where P_I is the ionization energy and P_{IJ}^{ex} is the excitation potential Coefficients c_{IJ} are tabulated in [10] For comparison with these energy losses we have calculated the power input by Joule heating $P_j = \eta j^2$, where j is the toroidal current density given from the total plasma current I_p assuming $j \sim 1/\eta$, and η is the Spitzer resistivity [20] $\eta = m_e \nu_e / n_e e^2 f_T$, including in f_T the effects of trapped particles and the effective ionic charge of the plasma Z_{eff}

3. Comparison with experiments. The impurity behaviour in typical experiments is as follows . impurities arrive at stationary state and also the total amount of impurities becomes fairly constant soon after the rising current phase of the discharge, though impurities are continuously produced during the whole discharge These results imply that the diffusion of impurities is not classical, since classical diffusion results in the rapid increase of impurity concentration during the discharge It is because the confinement time of fully-stripped impurity ions is several hundreds of ms, while their ionization time is of the order of several ms

In current tokamak experiments, electrons diffuse pseudo-classically or even more anomalously, since the electrons are trapped in waves caused by instabilities in the plasma, and drag the hydrogen ions and the impurity ions with them This suggests that the diffusion of impurity ions is not classical. In our calculation a set of anomality factors with $\gamma_D = 10$ and $\gamma_W = 1$ is most useful to explain all the information on the impurities, i e. impurity ion distributions, impurity fraction related to the total number of electrons, plasma one-turn voltage $V_p = 2\pi R_t I_p / \int (ds/\eta)$, and total detectable radiative power $p_{rad} = p_e + p_b + p_r + k n_e \Sigma n_I \beta_I P_I$

Calculations have been made in comparison with the experiments in the hydrogen plasma of the ST device and the hydrogen-deuterium plasma of the JIPP T—IIU device. As ST calculations have been reported elsewhere [13, 14], we will concern ourselves in this paper with the JIPP T—IIU results

The JIPP T—IIU tokamak [21] has a major radius $R_T = 0\,91$ m and a minor radius $r_p = 0\,23$ m. The hydrogen-to-ion density ratio $n_H/(n_H + n_D)$ is 10% and the toroidal magnetic field $B_T = 3T$ Our stationary calculation has been carried out for a total plasma current $I_p = 272$ kA, a mean electron temperature $T_e = 560$ eV, a mean plasma ion temperature $T_i = 220$ eV, and a mean electron density $n_e = 3.37 \times 10^{19}\ m^{-3}$ (these data correspond to the Ohmic heating phase of a typical JIPP T—IIU discharge). As confirmed by measurements, the most important impurities present in the plasma are carbon, oxygen and iron for which we considered the relative concetrations $n_0/n_e \sim \sim 1 \times 10^{-2}$, $n_0/n_e \sim 6 \times 10^{-3}$, $n_{Fe}/n_e \sim 8 \times 10^{-4}$ In Fig. 2a we have depicted our input profiles for the electron- and plasma ion temperature, while in Fig 2b, besides the input profile for the electron density, one may find our output

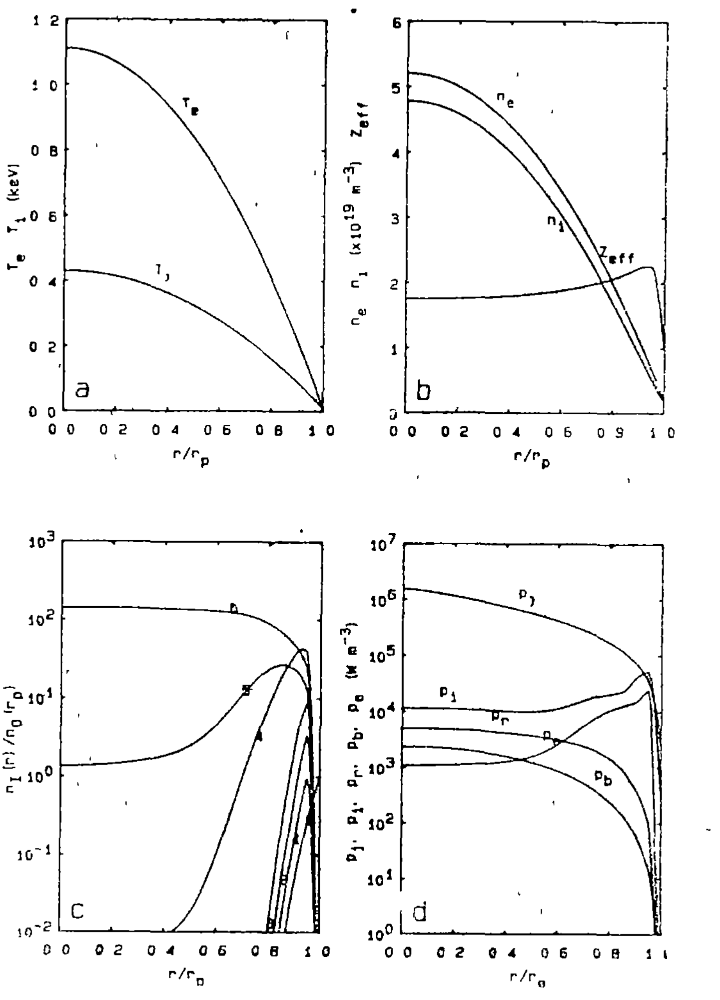

Fig 2a Input profiles for the electron- and plasma ion temperatures
Fig 2b Input profile for electron density and output profiles for plasma ion density and effective charge
Fig. 2c Density profiles for the various ionization states of carbon
Fig 2d Power losses due to ionization, recombination, bremsstrahlung and excitation for carbon, and joule input power

profiles for ion density and plasma effective ionic charge As one may observe, the value of Z_{eff} at the plasma centre is about 1 7, while in [21], using a simple model it was estimated to be 1 2. Fig. 2c, d represent the density output profiles for the various ionization states of carbon and the power losses due to the presence of the mentioned amount of carbon in the reaction chamber. For comparison, we have depicted the joule input power p_J. Our calculations yield a value of 10% for the ratio of the total radiated power to the input power, while in [21] this ratio has been reported to be about 15% The value of the plasma one-turn voltage obtained using our model was 1.33 V, slightly under the value of 1 6 V estimated in [21]

4. **Concluding remarks.** Our numerical model is in good agreement with measured macroscopic quantities in the experiments, but further — investigations are necessary to discuss its appropriateness in detail. The discrepancies may be due to the fact that the used atomic data may be affected by errors up to 30% and the calculated data reported in [21] have been obtained using a semi-quantitative model.

REFERENCES

1 H. Hsuan, K Bol and R A Ellis, *Nucl. Fusion*, **15** (1975) 657.
2 K Odajima, H Maeda, M Shiho, H Kimura, S Yamamoto, M Nagami, S Sengoku, T. Sugie, S. Kasai, M Azumi and Y. Shimomura, *Nucl. Fusion*, **18** (1978) 1337.
3 L S Scatuiro and M M Pickrell, *Nucl. Fusion*, **20** (1980) 527.
4 R A Jacobsen, *Plasma Phys*, **17** (1975) 547.
5. L R Grisham and K Bol, *Nucl Fusion*, **18** (1978) 315.
6 C Breton, C De Michelis and M. Mattioli, *J Quan Spectrosc. Radiat. Transfer*, **19** (1978) 367.
7 H W Drawin, *Phys Rep*, **37** (1978) 125
8 H W Drawin, *Phys Scripta*, **24** (1981) 622.
9 S Suckewar, E Hinnov, D Hwang, J. Shivell, G L Schmidt, K. Bol. N Bretz, P L Colestock, D. Dimock, H. P Eubank, R. J. Goldston, R, J Hawryluk, J C Hosea, H. Hsuan, D. W. Johnson, E. Meservey and D. McNeill, *Nucl Fusion*, **21** (1981) 981.
10 T Tazima, Y Nakamura and K. Inoue, *Nucl. Fusion*, **17** (1977) 914.
11 Equipe TFR, EUR—CEA—FC—1206 (1983)
12 K H. Behringer, B Denne, M J Forrest, N. C. Hawkes, A. Kaye, P. D. Morgan, N. J Peacock, M F. Stamp, H P Summers and G. Tallents, *Proc. 13th Europ Conf, Controlled Fusion and Plasma Heating*, 1986 (European Physical Society, Schliersee 1986) Vol 10, p 176
13 T A Beu, F Spineanu, M Vlad, R. I. Câmpeanu and I I Popescu, *Comput Phys Commun*, **36** (1985) 161
14. T. A Beu and M Vasiu, *Studia*, **2** (1986) 35.
15 W G. Bickley and J Nayler, *Phil Mag.*, **20** (1935) 343.
16. A. Samain, EUR=CEA=FC=745 (1974).
17 W. Lotz, IPP 1/62 (1967).
18 S. von Goeler, W. Stôdiek, H Eubank, H Fishma, S Grebenshchikov and E. Hinnov, *Nucl Fusion*, **15** (1975) 301
19. EUR—CEA, MAKOKOT — Code d'évolution (August 1977)
20. L Spitzer, "Physics of Fully Ionized Gases", Intersci. Publ (N Y), (1956).
21. I. Ogawa, IPPJ—826 (Apr. 1987)

STUDIA UNIV. BABEŞ—BOLYAI, PHYSICA, XXXIV, 2, 1989

Gd^{3+} AND Cu^{2+} EPR OF HIGH TEMPERATURE SUPERCONDUCTOR $Y_{1-x}Gd_xBa_2Cu_3O_7$

Al. NICULA*, A. V. POP*, L. V. GIURGIU** and Al. DARABONT*

Received October 18, 1989

ABSTRACT. — EPR measurements of the Gd^{3+} and Cu^{2+} were performed in the $Y_{1-x}Gd_xBa_2Cu_3O_{7-\delta}$ system The line-shape analysis for superconducting $GdBa_2Cu_3O_{7-\delta}$ was found to be Lorentzian, indicating the presence of the exchange narrowing We evidenced the possible presence of Cu^{2+} resonance in nonsuperconducting phase superimposed over the characteristic Gd^{3+} line at room temperature

Introduction. The discovery of high T_c superconductivity [1] has been followed by intensive theoretical and experimental study of this class of compounds. The pairing mechanism and the role of magnetic fluctuation of the Cu—O complex still unclear This has motivated us to investigate the magnetic properties of these compounds in general The magnetic behaviour of high T_c-superconductors can be studied with Electron Paramagnetic Resonance which provides information on the interaction of magnetic ions among themselves and between them and the crystal lattice This information is conveyed mainly by two parameters the g-factor and the linewidth H_{pp} of the resonance [2]. The experimental results obtained by EPR measurements from the superconductor ceramics are different Disagreements arise from the different quality of these samples and especially from the thermal history The absence of the EPR signals in the single phase $YBa_2Cu_3O_7$ is generally explained by the assumption that the Cu^{2+} ions are antiferromagnetically paired via oxigens, to insure S=O for the neighbouring copper ions In $YBa_2Cu_3O_{7-\delta}$ system the EPR signal is typical for Cu^{2+} resonance center with $S=1/2$, disposed in sites of (pseudo) tetragonal symmetry with anisotropic g-values $g_{||}=2.21$, $g_{\perp}=2.05$ characteristic of Cu^{2+} in impurity phases [3]. The Gd^{3+} in superconducting $GdBa_2Cu_3O_7$ does have a strong EPR signal at the field position corresponding to nearly $g = 1.97$ [4]

In this paper, we wish to report the EPR measurements in $Y_{1-x}Gd_xBa_2Cu_3O_{7-\delta}$ function of thermal history of samples, concentration x of Gd and temperature.

Experimental procedure. The samples $Y_{1-x}Gd_xBa_2Cu_3O_{7-\delta}$ were prepared by the solid phase reaction method by reacting the mixtures of Y_2O_3, Gd_2O_3, CuO and Ba_2O_3, where the concentration of the substitution of nonmagnetic yttrium with gadolinium is x = 1, 5, 10, 45, 25 and 100%. The oxides were mixed with absolut alchool in an agate mortar, pressed into pellets and firing slowly in air until 850°C The samples were sinterized at 850°C for 10 hours in air, and cooled slowly in air atmosphere down to 200°C with a rate of 1°/minute Samples with x = 100% were

* *University of Cluj-Napoca, Faculty of Matematics and Physics, 3400 Cluj-Napoca, Romania*
** *ITIM Cluj-Napoca, 3400 Cluj-Napoca 5, P O Box 700, Romania*

crushed again and recalcinated at the same temperature for 10 hours The presence of a superconducting phase with $T_c > 77$ K in the preparated samples was established by testing the Meissner—Ochesenfeld effect of an inhomogeneous magnetic field on the samples cooled under liquid nitrogen temperature

The Electron Paramagnetic Resonance measuremets were carried out by means of a RADIOPAN spectrometer SE—x/2543 at room and liquid nitrogen temperature in X band.

Results and discussion. The observed EPR line-shape from sample by $x = 1\%$, 5%, 10% and 25% Gd is presented in Fig 1. and for $x = 100\%$ in Fig 2a.

The EPR spectrum indicated at room temperature the overlapping over the characteristic Gd^{3+} line of a signal with $g = 2.06$, typical for Cu^{2+} resonance center in green phase Y_2BaCuO_5, Gd_2BaCuO_5 or $BaCuO_2$

The signal with strong intensity typical for Gd^{3+} ions and the Cu^{2+} overlapping signal disappeares at liquid nitrogen temperture. Similar results down to T_c were reported by H Kikuchi et al [4] for superconducting system $GdBa_2Cu_3O_{7-\delta}$. In Fig 2b we plotted the line shape for sample by $x = 100\%$ at room temperature. In case of Lorentzian shape

$$g(H) = \frac{1}{\pi \Delta H_l} \cdot \frac{1}{1 + \left(\frac{H - H_0}{\Delta H_l}\right)^2} \text{ for absorption curve, and}$$

$$\frac{dg(H)}{dH} = I(H) = \frac{1}{\pi \Delta H_l^2} \cdot 2(H_0 - H)\left[1 + \left(\frac{H - H_0}{\Delta H_l}\right)^2\right]^{-2}$$

for derivative curve The quantity $[(H - H_0)/I(H)]^{1/2} = \frac{\pi \Delta H_l}{\sqrt{2}}\left[1 + \left(\frac{H - H_0}{\Delta H_l}\right)^2\right]$

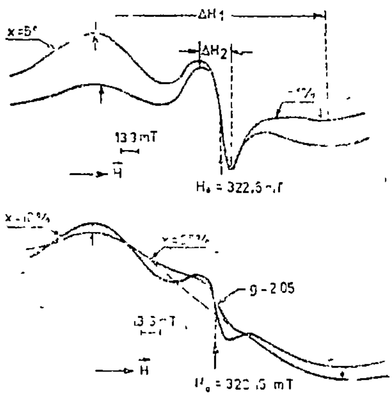

Fig. 1.

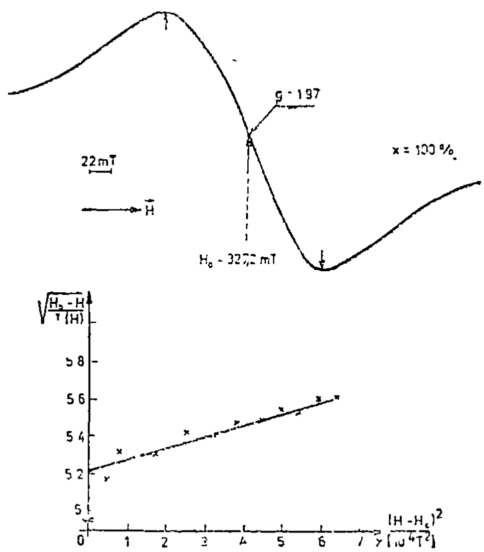

Fig 2.

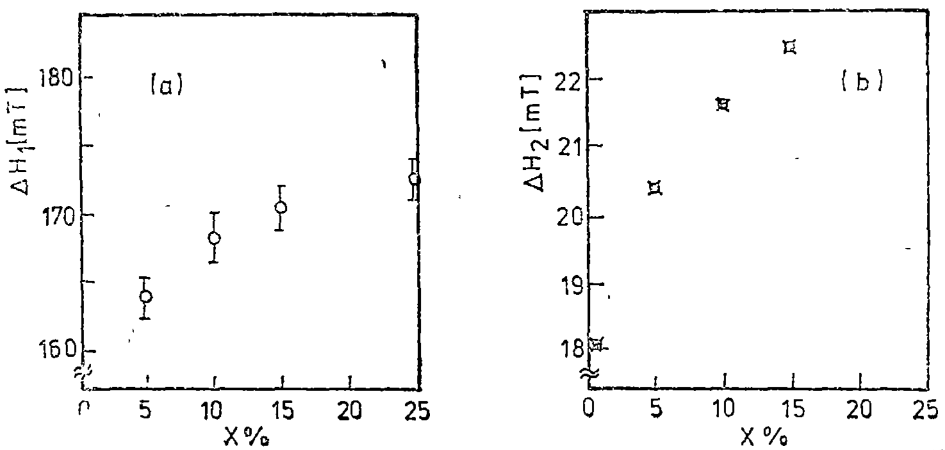

Fig 3.

(where $I(H)$ is the height of the absorption derivative at the field H and H_0 is the resonance field), is a straight line when plotted versus $(H - H_0)^2$

In Fig 3 the dependence $[(H - H_0)/I(H)]^{1/2}$ versus $(H - H_0)^2$ within experimental error evidenced a Lorentzian shape at the center of the line According to the Anderson model for magnetic resonance [6], an exchange narrowed line shape should be Lorentzian in the center

The EPR linewidth ΔH_1 for Gd^{3+} signal and ΔH_2 for Cu^{2+} signal versus x, as shown in Fig. 3a, b

This almost liniar dependence is no texpected in magnetic systems where the exchange interactions are dominant [5] The linewidth dependence ΔH_1 with the concentration of Gd^{3+} ions indicated the importance of dipolar coupling The moment of the dipolar width is determined principally by the strength of the dipolar interaction and its relative magnitude when compared with exchange coupling. The possible coupling of Gd ions to magnetic moment of Cu^{2+} in nonsuperconducting phases evidenced by evolution of lineshape function of x, is so weak bellow T_c that the presence of magnetic ions Gd^{3+} is ineffective for supressing superconductivity

Conclusions. We evidenced the possible precence of Cu^{2+} resonance in non-superconducting phase superimposed over the characteristic Gd^{3+} line in $Y_{1-x}Gd_xBa_2Cu_3O_{7-\delta}$ superconducting ceramics at room temperature for $x = 1, 5, 10, 15, 25\%$ The Lorentzian shape at the center of the Gd^{3+} line for $x = 100\%$ evidenced the exchange interactions, and the linewidth dependence ΔH_1 with the concentration x indicates the importance of dipolar coupling.

REFERENCES

1 J. G. Bednorz, K A Muller, Z Phys B, 64, (1986).
2 I Ursu, „La Resonance Paramagnetique Electronique", Ed. Dunod, Paris (1968), A I. Nicula, „Rezonanţa magnetică", Ed. Did. şi Ped. Bucureşti, 1980.

3. F Merhan, S E Barnes, T R. McGuire, W J Gallagher, R L Sandstrom, T R Dinger, D A Chance, *Phys Rev B*, **36**, 740 (1987), D Shaltiel, J Genossar, A Giagersky, Z H Kalman, B Fisher, N Kaplan, *Solid St Commun*, **63**, 987 (1987), S. Simon, I Barbur, I Ardelean, *Studia, Physica*, **32** (2), 96 (1987), J. T Lue, *Phys Rev B*, **38**, 4592 (1988)
4. F. Mehran, S E Barnes, C C Tsuei, T R McGuire, *Phys Rev B*, **36**, 7266 (1987), F Merhan, S E Barnes, E A Giess, T R McGuire, *Solid St Commun.*, **67**, 1, 55 (1988), H Kikuchi, Y Ajiro, Y Ueda, K Kosuge, M Takano, Y Takeda, M. Sato, *Journ of Phys Soc of Jap*, **57**, 406, 1887 (1988), Al Nicula, A V Pop, Al Darabont, L V Giurgiu, *Studia—Physica*, 32 (2), 1988), Al Nicula, A V Pop, L V. Giurgiu, Al Darabont, *Proceeding of the Conference on radio and microwave spectroscopy RAMIS*—89, Poznan, Poland 1989
5. M T Causa, C Fainstein, Z Fisk, S B Oseroff, R D Sanchez, L B Steren, M Tovar, R D Zysler, *Journal de Physique*, Colloque C8, Supplement an nr 12, Tome 49, (1988), W M Walsh, R J Birgeneau, L W Rupp Jr, M J Guggenheim, *Phys Rev*, *B* **20**, 4645 (1979)
6 P W Anderson, P R Weiss, *Rev Mod Phys*, **25**, 269 (1953)

ÎNTREPRINDEREA POLIGRAFICĂ CLUJ,
Municipiul Cluj-Napoca, Cd nr 550/1989

În cel de al XXXIV-lea an (1989), *Studia Universitatis Babeş—Bolyai* apare în specialităţile:

matematică

fizică

chimie

geologie-geografie

biologie

filosofie

ştiinţe economice

ştiinţe juridice

istorie

filologie

In the XXXIV-th year of its publication (1989), *Studia Universitatis Babeş—Bolyai* is issued as follows:

mathematics

physics

chemistry

geology-geography

biology

philosophy

economic sciences

juridical sciences

history

philology

Dans sa XXXIV-e année (1989), *Studia Universitatis Babeş—Bolyai* parait dans les spécialités:

mathématiques

physique

chimie

géologie-géographie

biologie

philosophie

sciences économiques

sciences juridiques

histoire

philologie

43 904

Abonamentele se fac la oficiile poştale, prin factorii poştali şi prin difuzorii de presă, iar pentru străinătate prin „ROMPRES-FILATELIA", sectorul export-import presă, P. O. Box 12—201, telex. 10876 prsfir, Bucureşti. Calea Griviţei nr. 64—66.

Lei 35